NEAR AND VACUUM ULTRAVIOLET STUDY OF METAL DONOR AND METAL ACCEPTOR CHARGE TRANSFER TRANSITIONS IN TRANSITION METAL DOPED FLUORIDE HOST MATERIALS

****

Joseph F. Sabatini

NEAR AND VACUUM ULTRAVIOLET STUDY OF METAL DONOR AND METAL ACCEPTOR CHARGE TRANSFER TRANSITIONS IN TRANSITION METAL DOPED FLUORIDE HOST MATERIALS

by

Joseph F. Sabatini
//

A DISSERTATION

Presented to the Faculty of Princeton University in

Candidacy for the Degree of

Doctor of Philosophy

Recommended for Acceptance by the

Department of Chemistry

October, 1973

ACKNOWLEDGEMENTS

For the financial and administrative support, and the time required to complete this study, I thank both the Navy's Junior Line Officer Advanced Scientific Educational (Burke) Program and the Naval Postgraduate School, Monterey, California.

My research advisor, Professor Donald S. McClure, has provided much to acknowledge, among which are initial research direction, an understanding of the problems associated with my double status as graduate student and Naval officer, an encyclopedic knowledge of chemical facts, and a rather awe-inspiring "chemical intuition".

There are three special members of "The Group" to whom special recognition is due. In alphabetical order they are Clayton Baum, Bruce Chase, and Arthur Salwin. Their combined virtues of chemical knowledge and skepticism, their physical abilities in such diverse areas as dewar lifting and flange machining, plus their genuine concern and friendship have added much to these past four years.

Finally, I must put in writing what is truly a feeble thank you to my wife Carol. Her understanding and encouragement through many of the less enjoyable periods of life as a McClure Group

graduate student have had a great effect on both the work presented in this thesis and the mental well-being of her husband.

TABLE OF CONTENTS

INTRODUCTION

The optical spectra of transition metal ions as impurities in various host materials have been vigorously investigated within the past several decades. The low energy electronic transitions correspond to excitations within the transition metal ion d orbitals and it is upon these excitations that most studies have concentrated. Those absorption bands that have not correlated with predicted d-d level transitions have been in most instances vaguely referred to as "charge transfer" in origin, implying a process in which an electron is excited from an orbital belonging predominantly to one center to an orbital of a second center. In comparison with the study of d-d transitions, the study of these many center excitations remains in its infancy.

There have been previous investigations of charge transfer transitions, but each has suffered in some way that limits the generality of its results. Jorgensen's[1] pioneering study of transition metal halides is limited to solution studies of second and third row transition metal chlorides, bromides, and iodides in the energy region below 50,000 cm^{-1}. The d-d transitions of these systems have not been completely characterized, and there

is some question as to whether several of the bands assigned as charge transfer absorptions are in fact transitions within the d levels. In addition, the ligands bromide and iodide compound the problem of interpretation by their large spin orbit constants, the result of which are band splittings.

Other inorganic systems have been studied,[2] but all studies are either limited in scope (that is, of only one of two similar systems), confined to compounds of low symmetry, or with one exception confined to the spectral region below 50,000 cm^{-1}.

We had a number of reasons for undertaking this investigation. First, we were concerned with a many center excitation, which requires a molecular orbital or band theory approach, neither of which has been demonstrated to provide numerical results of extreme reliability. The absorption spectrum of MnO_4^- which is the most frequently studied charge transfer system illustrates this statement. Day[3] has reviewed the mathematical attempts at band assignments of this system from 1952 to 1970 and he remarks that the most notable feature of these attempts is that no two interpretations are exactly the same.

Our second reason for this work is that previous data are both sparse, and as previously stated, limited in many respects.

It was therefore our intention to investigate a series of systems composed of first row transition metal ions as impurities in wide band gap host materials, and to extend the investigation to the transmission limit of these hosts. We anticipated that as we systematically varied the impurity ion in any particular host, or systematically varied the host with impurity ion constant, we would be able to correlate our absorption data with present knowledge of such factors as ionic radii, electron affinity, and d orbital transition energies.

The systems on which we report are V, Cr, Mn, Fe, Co and Ni in the $KMgF_3$ lattice, Mn, Fe, and Co in MgF_2, and Mn, Fe, and Co in CaF_2. These particular hosts were chosen for several reasons, including their highly ionic nature, well defined symmetry, extremely high bandgap, and their availability. Our choice of transition metal ions would ideally include all first row ions in all three hosts, but we are limited by the difficulties associated with the growing of high purity crystals of this type.

The conclusions of our work are that the high energy absorption bands in these systems are the result of an electron transfer from the transition metal ion d orbital to the host metal s orbital, a process which has not been previously observed in

transition metal halide systems. The single exception to this interpretation is the $KMgF_3$:Ni system in which the excitation of an electron from the fluoride p π molecular orbitals to the nickel ion e_g orbital is observed.

We encountered many difficulties in obtaining absorption measurements in the vacuum ultraviolet region. At wavelengths lower than 2000 Å, such common and experimentally useful items as pyrex, gelatin on photographic film, and water vapor and oxygen in the air exhibit intense absorption of radiation. In addition, few reproducible and intense sources of radiation exist in this high energy region. A detailed description of the experimental equipment and techniques used in this work are presented in Chapter I. These eventually evolved into a sophisticated and reliable setup, consisting of continuous mode rare gas light sources, a high resolution vacuum monochromator, a photon counting detection system, linear polarizers, and the capability of varying crystal temperature from 2°K to 300°K.

In Chapter II, the results of various experiments are presented for each transition metal fluoride system. Included are electron spin resonance, infrared, visible, near ultraviolet and vacuum ultraviolet absorption data, and the results of crystal

chemical analyses. Much of the work was done in order to obtain as complete a characterization of each crystal as possible. Once this was completed, the near and vacuum ultraviolet absorption data became the most meaningful.

In Chapter III, we present background material to aid in an interpretation of the results in terms of one of two possible processes. In one instance, the transition metal serves as an electron acceptor, and the electron is transferred to this ion from a molecular orbital composed of fluoride p π orbitals. This has been the assignment made for every transition metal halide and oxide system previously investigated. The alternative process involves the transition metal as an electron donor, with the transferred electron residing in a molecular orbital composed of host metal ion s orbitals, or in other terminology, with the electron residing in the host conduction band. Expectations based on each of these models are examined.

Finally, in Chapter IV we compare the experimental results with the expectations of Chapter III for each of the two models. As previously stated, the data of Chapter II indicate that for nearly every system, the metal to metal process is dominant. Only in the case of $KMgF_3$:Ni does the more conventional

fluoride to nickel transition occur. Based upon these assignments, explanations are offered for observed absorption bandwidths, oscillator strength temperature dependence, absolute oscillator strength, lack of polarization phenomena, number of bands, and relative band energy.

REFERENCES

1. C.K. Jorgensen, Mol. Physics 2, 309 (1959)

2. See C.K. Jorgensen, Prog. Inorg. Chem. 12, 101 (1970) for a recent review of the charge transfer literature.

3. P. Day, Czech. J. Phys. B 20, 641 (1970)

CHAPTER I

EXPERIMENTAL

A. Preliminary Remarks

Because the technology involved in vacuum ultraviolet spectroscopy is relatively unusual, and because it is anticipated that this chapter will serve as a laboratory guide for those in our research group who follow in this area, the experimental work will be described in detail.

At the origin of this project, our laboratory contained no equipment suitable for vacuum ultraviolet spectroscopy. Therefore, our technological capabilities progressed from none, to very crude, and through a series of improvements to the present level of "semi-sophistication". The original methods and improvements thereon will be described, with the hope that one who is beginning in this area might profit from the success and failure of many of our ideas.

Our present equipment consists of microwave powered rare gas light sources, a two meter vacuum monochromator, a vacuum ultraviolet sensitive photomultiplier tube, and photon

counting electronics. In addition, the ability to obtain temperature dependent spectra from $2^{o}K$ to $300^{o}K$, and the ability to take polarized absorption spectra in the vacuum ultraviolet region exist.

The specific technology will now be described in detail.

B. Light Sources

Our initial light source was a Tanaka type rare gas discharge tube, powered by a discharge excitation unit, borrowed from Professor W. Smith of Princeton University. The formal titles are Tanaka-Type Discharge Tube Model 45-202 and Rare Gas Discharge Excitation Unit Model 45-204, made by Jarrel-Ash Company, Newtonville, Massachusetts. The tube is seven inches long, forty five millimeter diameter pyrex cylinder, with various ports for entrance, exit, and pressure monitoring of a flowing gas. Vacuum tight feedthroughs permit the two one inch diameter aluminum electrodes to receive 15,000 volts AC at currents up to sixty milliamps, while immersed in the desired gas. The voltage is supplied by the excitation unit which consists simply of a large transformer and a rheostat. In theory, one should have been able to flow any rare gas, strike an initial arc between the two electrodes, and maintain a discharge by controlling the rheostat on the excitation unit. The tube is mounted in a six inch OD cylindrical aluminum container which permits the entire source to be vacuum sealed by an O-ring to a spectrometer.

In practice, several problems arose. Neither argon nor krypton gas would give a reproducible continuum in the vacuum

ultraviolet region. In addition, at gas pressures above 100 millimeters, where both continua should be maximized, the discharge tube repeatedly malfunctioned by allowing a parallel circuit through the pyrex wall to be formed. To avoid this latter problem, a new tube was made by our Chemistry Department glassblowers based on a design by Professor McClure and myself. This design incorporates removable windows and electrodes to facilitate electrode cleaning, and a double tube system to prevent voltage breakdowns. The problem of no rare gas discharge was solved by abandoning rare gases and by using hydrogen gas instead.

In this source, hydrogen molecules are electrically excited to a stable $^3\Sigma_g^+$ excited state which decays with the emission of vacuum ultraviolet radiation to a $^3\Sigma_u^+$ repulsive state. The sharp slope of the energy vs. internuclear distance curve of the $^3\Sigma_u^+$ state results in a continuum from about 1670 Å to above 2000 Å.

This source is intense and reproducible, and it contains its own emission lines which can be used as internal calibration points in conjunction with an atlas of molecular hydrogen emission lines.[1] The relatively high intensity of this source permits its use at only 30 milliamps of current flow, thus decreasing the possibility of particles being removed from the electrodes and damage occuring

to the spectrometer entrance slit. The one drawback of our hydrogen source is that its useful continuum is limited to wavelengths greater than 1670 Å.

In order to extend the continuum to higher energy, we became interested in a Carton-type flashtube. With this type of source, the radiation is produced by discharging a capacitor through a narrow evacuated capillary. By designing the system such that one obtains current densities near 30,000 amperes/cm^2, one gets a predominantly continuous emission from 1000 Å to above 2000 Å. It is believed that the discharge causes some material to be vaporized from the capillary walls, and that possibly the emission from these highly charge particles is the source of the continuum.

The literature contains descriptions of several types of flashtubes, beginning with Lyman's initial design in 1924.[2] Although improvements were made upon this design by Garton and others,[3,4,5,6,7] the fact that our laboratory contained equipment for a near ultraviolet flash-lamp led us to design our own lamp for the vacuum ultraviolet. Mr. Bruce Chase of our research group was responsible for the design and much of the actual construction of the lamp. The lamp incorporated the advantageous characteristics of previous flash tubes described in the literature such as coaxial construction and low over-

all inductance, and included several innovations in bore size and electrical insulation. The lamp was discharged manually by triggering a Signalite TG 182 spark gap using a pulse transformer. This permitted the energy stored in a five microfarad capacitor to flow through the Garton source, thus causing the discharge. The capacitor itself was charged to approximately 15,000 volts by a voltage doubler circuit of our own design and construction. The circuit is shown in Figure 1.

By using this equipment, a continuum was obtained from 1400 Å to above 2000 Å, with emission lines below 1400 Å. In order to obtain a reasonable amount of photographic darkening, tens of flashes were required, with a period of approximately 20 seconds between flashes while the five microfarad capacitor was charging. In addition, only photographic detection could be used because of the pulsed nature of the lamp. This source proved useful in extending the continuum region and in providing an overlap with the hydrogen lamp for reproducibility checks.

As our detection system became more sophisticated, a third light source was required. The need for a reproducible source that operated in a continuous rather than a pulsed mode led us to purchase a microwave powered rare gas system. From

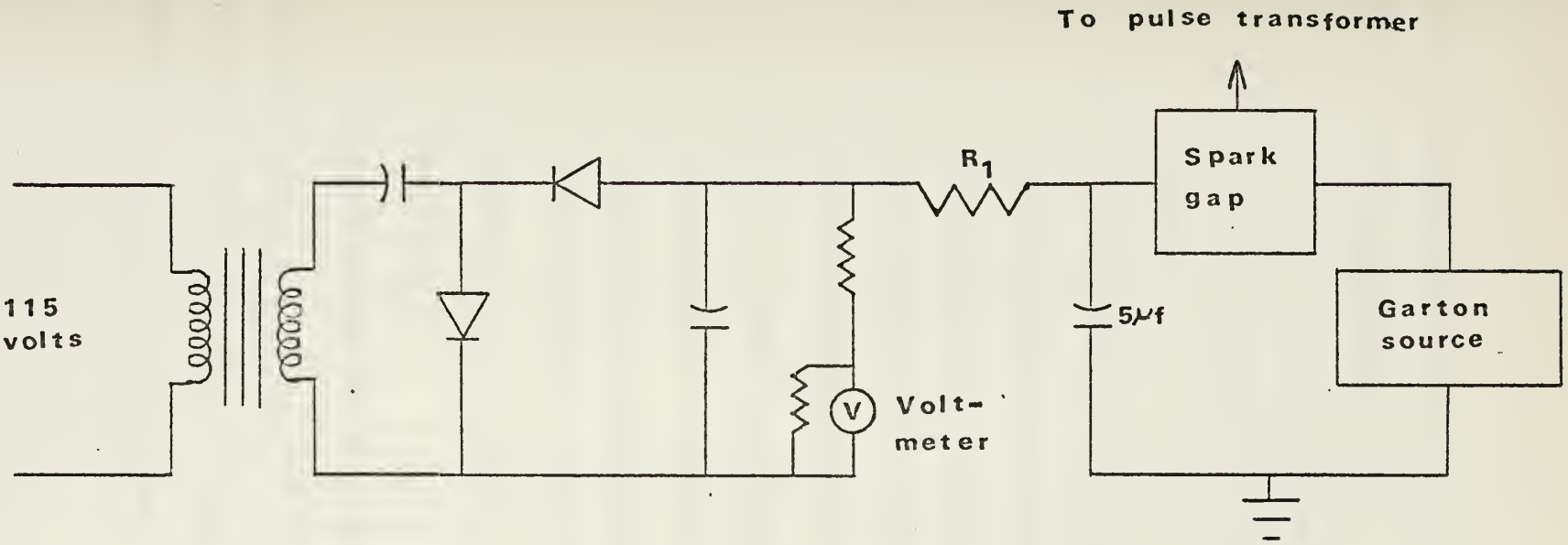

Figure 1. Electrical circuit used for the excitation of the Garton type source. Resistor R_1 is a current limiting resistor to prevent damage to the voltage doubler circuit in case of a short circuit at the Garton source. The pulse transformer is discharged manually. The 5 farad capacitor has an ultimate voltage capacity of 20,000 volts.

the OPTHOS Instrument Company, Rockville, Maryland the following equipment was purchased:

1. An MPG-3 microwave power generator which has an output of 100 watts at 2.54 GHz with less than .1% ripple.
2. A tunable Everson cavity which is used to match the impedance of the lamp to that of the generator.
3. Krypton and xenon continuum lamps which consist of quartz cylinders filled with several hundred millimeters pressure of highly purified rare gas. Each quartz tube has a side arm containing a gettering material which further purifies the lamp with use. The xenon lamp has a CaF_2 window and is usable from about 1550 Å to 2000 Å. The krypton lamp uses MgF_2 as a window material and its useful range is 1250 Å to about 1730 Å.

The details of operation have been adequately described by Wilkinson, Tanaka, and Byram.[8,9,10] It is sufficient to say that the sources are reproducible and of sufficient intensity for photographic and photon counting detection.

C. Spectrometers

In the vacuum ultraviolet region, our initial survey work was done using a Jarrel-Ash 1/2 meter Seya Namioka mount vacuum monochromator. The plate factor for this instrument is approximately 24.9 Å/mm. The monochromator is equipped with a camera attachment which holds a 2-5/8 inch length of 35 millimeter film.

The realization that interesting spectra could be obtained by this low resolution system prompted the purchase of a McPherson Model 2162 two meter vacuum monochromator from the McPherson Instrument Corporation, Acton, Massachusetts. This instrument uses a Czerny-Turner mounting with a 1200 line per millimeter grating. The plate factor is 4.16 Å/mm, resolution with 10 micron slits is .075 Å, and the f number is 17. The associated pumping system permits a working vacuum of less than 1×10^{-6} mm.

In the near ultraviolet, visible and near infrared spectral regions, a Cary Model 14R Recording Spectrometer was used.

D. Detection Systems

Vacuum ultraviolet radiation was detected at the monochromator exit slit by both photographic and photoelectric means. Each method required specialized material since photographic gelatin absorbs at wavelengths below 2055 Å and all phototube window materials with the exception of LiF and MgF_2 absorb light between 1200 and 2000 Å.

Photographically, several types of vacuum ultraviolet sensitive film and plates are available from Eastman Kodak Company. They are listed below:

1. Kodak SWR (Short Wavelength Radiation) film and SWR plate, which are of medium speed and grain.
2. Kodak Special Film, Type 104-01 which uses the SWR emulsion but has rails along the film edges to prevent abrasions on the film surface.
3. Kodak Pathe SC-5 Film which has a sensitivity of eight to ten times that of SWR but which is avilable in strips only and which is manufactured in France.
4. Kodak Special Film, Type 101-01 which has a sensitivity about ten times that of SWR and is provided with edge rails.

5. Kodak Special Plate, Type 101-05 which is similar to Type 101-01 but which is a plate.
6. Kodak Pathe SC-7 Film which has a sensitivity of ten to twelve that of SWR and is manufactured in France.
7. Film coatings called sensitizing materials, which fluouresce strongly under ultraviolet radiation. The two chemicals available are Chemical No. 8269, and Chemical No. A3167, both produced by Kodak. One applies the sensitizer to the emulsion prior to use and removes it prior to development.

Our choice was SWR film, which can be purchased in rolls of 35 mm by 25-1/4 feet. This choice was dictated by the prices of items 2 through 6 above, by the intensity of our light sources, and by the successes we enjoyed in our initial period of experimentation with this product. We found that a developing solution of D-19 and water in a 1:1 ratio gave satisfactory results, and that a Wratten series 1 (red) safelight could be used in darkroom work.

Several items must be noted when using this film, however. Occasionally the film's diffuse density in an unexposed region is higher than normal. This "fogging" is a nuisance at times, but

can be minimized by bathing the emulsion in distilled water for two minutes at 20°C prior to development. In addition, the film is very susceptible to abrasion because of the low gelatin content. The gelatin layer is so thin that the silver halide crystals actually protrude from it. Kodak does offer a gelatin coating for use after the film has been exposed, (No. 1099 gelatin) but abrasions can be minimized by careful handling of the film throughout the entire process of film cutting, camera loading, development, and storage. A third and more troublesome deficiency of SWR film is its limited straight line portion of the characteristic curve. That curve is shown in Figure 2. In order to obtain a reliable bandshape of an absorption band of optical density 2 to 3, it was necessary to take repeated exposures and to piece together those portions of the absorption band that were on the linear region of the characteristic curve.

It became apparent that a photoelectric detection system would be necessary to obviate SWR film's inconveniences and limitations that were described above. In addition, because photon counting electronics were available for our use and because of the low light levels found at our point of measurement, a photomultiplier tube was purchased which was compatible with photon

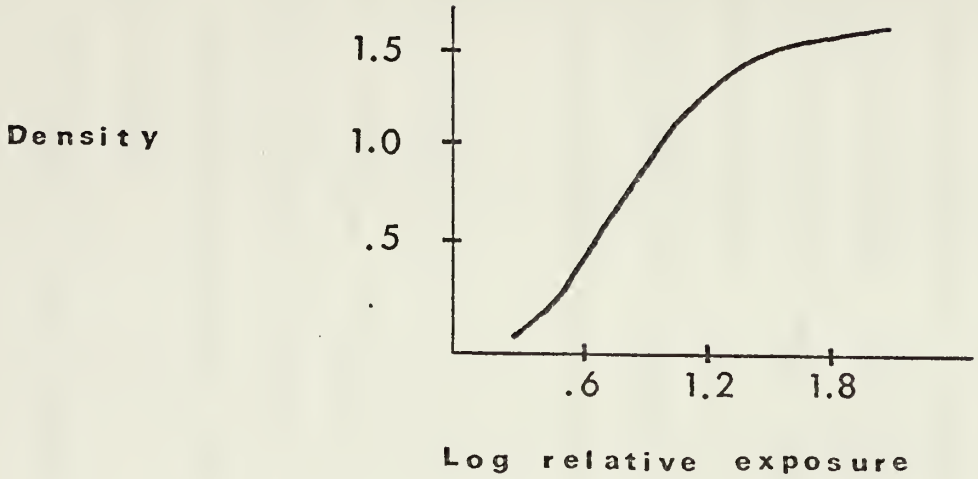

Figure 2. The Characteristic Curve for Kodak SWR film. Density= LOG 1/Transmission. Film was developed in a 1:1 solution of D-19 and water. Development was continued for four minutes at 68° F. Note that the linear region of the curve extends from a density of 0.2 to a density of approximately 1.3.

counting techniques. A diagram of the detection system is shown in Figure 3.

Because of the extreme sensitivity of the system, a Faraday cage was designed for the phototube, and extreme care was taken to ensure that all components were shielded and that no ground loops existed. After many design changes, the dark count of the detection system was reduced to that of Figure 4.

The phototube was an EMR Photoelectric Model 541G-08-18. It is an "extreme solar blind" 18 stage, end on tube with a LiF window and a CsI photocathode. The cathode is only 9.5 mm in diameter and is not sensitive to wavelengths longer than 2000 Å. This is why the low dark count shown in Figure 4 is possible without any requirement for tube cooling. The phototube is useful in the range 1050 Å to 2000 Å and its amplification at the operating voltage of 2300 volts is 1×10^6.

The remaining electronics in the detection system were used with the permission of Professor E.R. Bernstein and Mr. R.E. Smalley of Princeton University, and are listed below.

The power supply was a Fluke Model 415B High Voltage power supply.

The Amplifier/Discriminator was an SSR Instruments

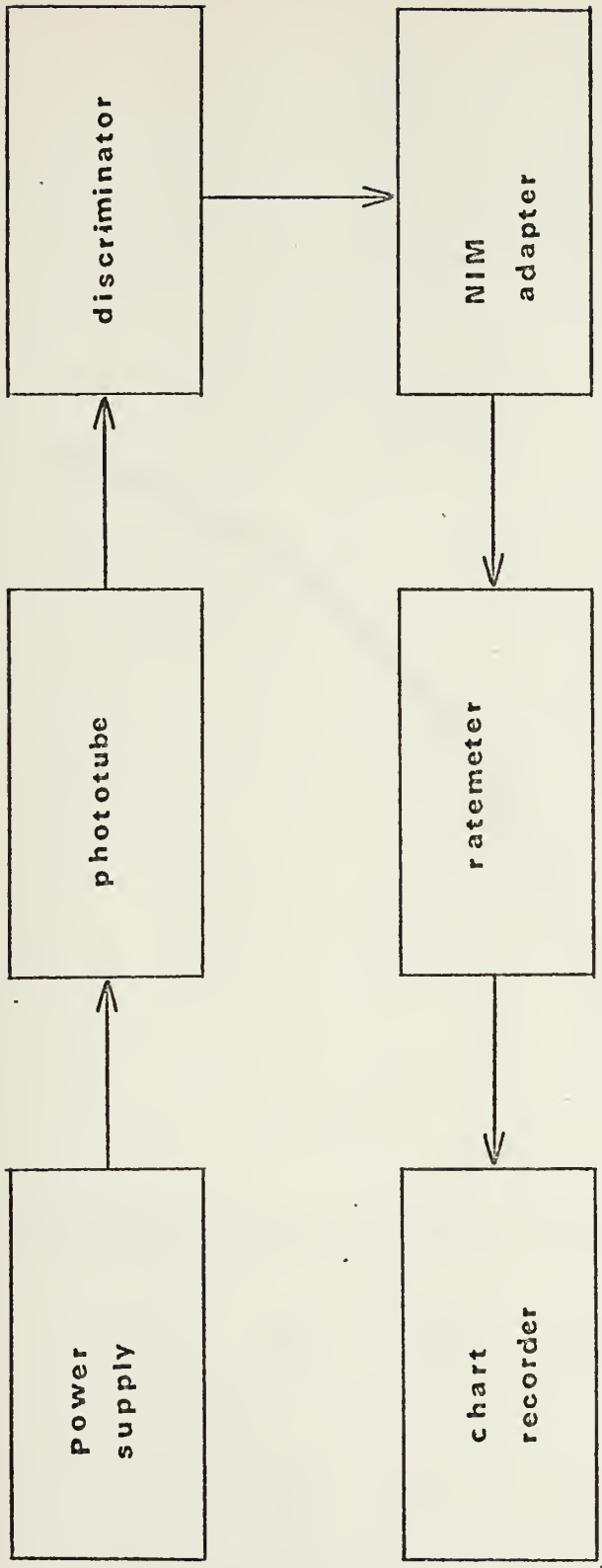

Figure 3. Block diagram of the basic components of our photon counting detection system.

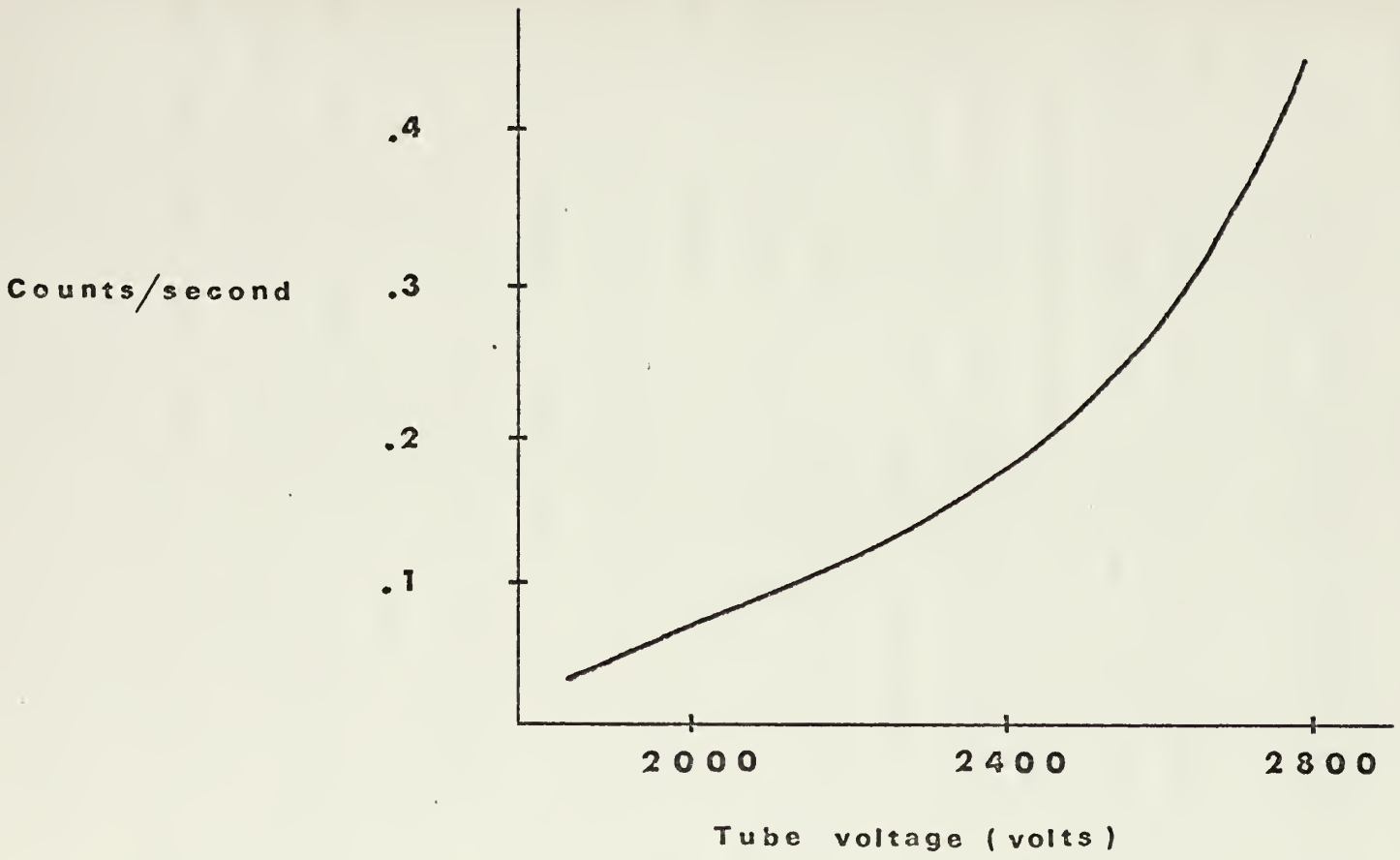

Figure 4. Dark count of photomultiplier tube vs tube voltage, as incorporated into the photon counting detection system of Figure 3. During absorption experiments, tube voltage is maintained at 2300 volts.

Company Model 1120, and the NIM Adaptor was an SSR Model 1127.

The Ratemeter was an Ortec Inc. Model 434 Digital Ratemeter.

The chart recorder used was a Hewlett Packard 7100 BM electrosensitive recorder.

Photon counting techniques have not been utilized in previously published investigations in the vacuum ultraviolet region, therefore a qualitative description of the functions of the major pieces of equipment and an explanation of the advantages over other detection techniques used in this region are appropriate.

The ultimate objective of a detection system operating under the conditions imposed by relatively weak light sources and long path length is the ability to measure low light levels with a high signal to noise ratio. In order to understand the advantages of the photon counting technique, one must first be cognizant of the various sources of noise encountered in such measurements.

One of the most common sources of noise is that caused by external disturbances. Sixty cycle noise and higher harmonics, noise created by the switching on and off of electrical equipment, and pickup from radio transmissions are examples of externally

induced noise. Particularly with components as sensitive as those previously described, these noise sources are rather troublesome.

A second source of noise is that called flicker effect noise, or more commonly 1/f noise. The 1/f terminology originates from the shape of the "power spectrum" or plot of noise intensity vs. frequency. For all electronic tubes and transistors this type of noise exhibits a curve resembling a 1/f function, where f is frequency, which is of particular concern in DC measurements.

Another problem incurred in DC measurement techniques is the unwanted signal caused by Johnson noise in resistors, which is of thermal origin and quite related to Brownian motion. By passing a current representing a measured signal, across a load resistor as one does in the DC technique, one adds this extra signal which is unrelated to that quantity being measured.

Finally, a class of noise is always present when one uses electronic elements whose functioning depends upon random single electron events. This quantized nature of such circuit elements as phototubes and diodes is responsible for what is termed "shot noise".

The photon counting method is quite successful in eliminating those noise sources listed above. First, the entire system is surrounded by a Faraday cage, which shunts external noise to ground,

causing no measurement of such signals by the detection system. It is very important that all ground loops are removed in a system as sensitive to noise as ours, and this is accomplished by connecting all grounding cables and shields to one specific point.

In order to remove the detected signal from fluctuations in the high voltage power supply, the phototube is operated in the "plateau" region, that is, at a voltage for which the tube output is nearly constant as the supply voltage is varied. By operating in this region, and by using an extremely stable power supply such as the Fluke 415 B, fluctuations in phototube output are minimized.

The amplifier/discriminator performs the function of selecting, waveshaping, and amplifying only those pulses emanating from the phototube which correspond to single photon events. This eliminates signals caused by electron emission from phototube dynodes which would be of low amplitude since they would not be multiplied by each stage of the phototube. Note that in a DC measurement, these signals would contribute to the measured signal. The true single photon pulses are then converted into well defined square waves for accurate measurement by the ratemeter. Finally these pulses are added to give a value of pulses per second, and this number is plotted vs. wavelength in a histogram presentation.

This discussion of our photon counting technique is admittedly qualitative, and more detailed presentations can be found elsewhere.[11, 12, 13, 14, 15] Little would be gained by a thorough explanation of the rationale behind such choices as type of phototube, our use of negative high voltage vice positive high voltage, or our Faraday cage design. Such decisions are properly made after a consideration of the desired ultimate response of the system, the components available, and the cost of alternate selections. It was our good fortune to have available the sophisticated electronics described above, for we were then able to invest a sizeable amount of money in the photon counting vacuum ultraviolet photomultiplier tube. This system is far superior to the standard photoelectric method of detection of vacuum ultraviolet radiation, which is the use of sodium salicylate phosphor on a plate, and measurement of its emission by DC techniques.

E. Other Equipment

In the course of experimentation in the vacuum ultraviolet region, three distinct experimental setups were used, although at times several of these were used in series. For room temperature absorption spectra, the microwave light source is vacuum sealed to a sample holder of our own design. This sample holder is bolted to the entrance slit assembly of the McPherson monochromator and thus a vacuum is maintained throughout the light path. For low temperature absorption spectra, a series of flanges are used to seal the light source to a cold finger liquid helium dewar, which in turn is attached to the entrance slit assembly. The dewar is a Model LT-3-110 Liquid Transfer Cryo-Tip Refrigerator which was purchased from Air Products and Chemicals Inc., Allentown, Pa. The sample is attached to a copper holder with a special sealant which facilitates heat transfer from the sample to the copper. By use of the technique of pumping on the liquid helium in the dewar, or by making use of a 20 watt heater on the cold finger, the temperature range of $2^{o}K$ - $300^{o}K$ is possible. The temperature is determined by a chromel vs. gold .07 atomic iron thermocouple attached to the cold finger. For polarized absorption spectra, a MgF_2 ultraviolet Rochon polarizer was purchased from Karl

Lambrecht Corporation and vacuum mounted in a holder of home-made design. A double O-ring design permits rotation of the polarizer without breaking the vacuum seal. This polarizer can be used from 1260 Å to wavelengths above 2000 Å.[16,17]

When windows were used with the above equipment, they consisted of ultraviolet quality LiF, and were purchased from the Harshaw Chemical Company.

Unless otherwise indicated, the experimental data that will be presented later were all obtained with the microwave light sources, the two meter McPherson monochromator, and the photon counting detection system. All data obtained by the use of the earlier versions of equipment described previously were reproduced with this more sophisticated system. Agreement among various combinations of sources, monochromators, and detection systems was good, however, the final experimental procedure was by far the superior one, and in fact, many more details were observed in several samples.

In practice, the final raw data were corrected to give absolute optical density. This was done by determining the intensity of light transmitted through the system both with and without the sample in the sample holder. The light intensity vs. wavelength

was digitized for both cases and stored on paper tape. By overlapping the absorption spectrum, determined with the McPherson, with the Cary 14R spectrum, and by correcting the percent transmittance of the McPherson data to that determined by using the Cary 14R, accurate values of optical density vs. energy were obtained. This is possible because the Cary 14R is a double beam instrument. The overlap region used was 1900 Å to 1970 Å. A Hewlett Packard Model 2116A computer was used for the point by point computation of optical density.

The electron spin resonance spectra were obtained with a Varian E-13 X band spectrometer. The sample was fastened to a quartz rod and was immersed in liquid nitrogen.

REFERENCES TO CHAPTER I

1. K.E. Schubert and R.D. Hudson, A Photoelectric Atlas of the Intense Lines of the Hydrogen Molecular Emission Spectrum from 1025 to 1650 Å at a Resolution of 0.10 Å AEROSPACE CORPORATION REPORT No. ATN-64 (9233)-2, (1963)

2. T. Lyman, Astrophys. J. 60, 1 (1924)

3. W.R.S. Garton, J. Sci. Instr 36, 11 (1959)

4. W.R.S. Garton, I.W. Celnick, H. Hessberg, and J.E.G. Wheaton, Proc. 4th Intern. Conf. on Ioniz. Phenomena in Gases (North-Holland, Amsterdam, 1960)

5. J.E.G. Wheaton, Appl. Optics 3, 1247 (1964)

6. M. Morlais and S. Robin, Compt. rend. 258, 862 (1964)

7. R. Goldstein and F. Mastrup, J. Opt. Soc. Am. 56, 765 (1966)

8. P.G. Wilkinson, J. Opt. Soc. Am. 45, 1044 (1955)

9. P.G. Wilkinson and Y. Tanaka, J. Opt. Soc. Am. 45, 344 (1955)

10. P.G. Wilkinson and E.T. Byram, Appl. Optics 4 , 581 (1965)

11. G.A. Morton, Appl. Optics 1 , 1 (1968)

12. R. J. Keyes and R. H. Kingston, Physics Today 48, (March 1972)

13. M. L. Frenklin et al., Anal. Chem. 41, 2 (1969)

14. J. F. James, Royal Astronomical Society 137, 15 (1967)

15. M. R. Zatzick, Research/Development, (1970)

16. W. C. Johnson, Rev. Sci. Instr. 35, 1375 (1964)

17. V. Chandrasekharan and H. Damany, Appl. Optics 8, 671 (1969)

CHAPTER II

PRESENTATION OF DATA

A. Preliminary Remarks

Prior to the presentation of specific experimental results, a number of preliminary remarks concerning the materials studied are appropriate.

In order to extend the study of electron transfer spectra into the vacuum ultraviolet spectral region, the initial requirement was that of wide band gap host materials. For several reasons, $KMgF_3$, CaF_2 and MgF_2 were chosen as the hosts.

The fluorides represent some of the more ionic compounds available. Therefore, in one widely used description of the charge transfer process in terms of a Born Haber type of cycle, we can realistically treat the system as that of interacting ions. In other words, we can consider energy terms of electrostatic origin only.

The structure of these hosts, and the site symmetry of transition metal ions doped into these hosts are well known. The materials $KMgF_3$ and CaF_2 provide sites of cubic symmetry, while MgF_2 allows the possibility of polarization data due to D_{2h} sym-

metry at the impurity ion site.

All three of these hosts can be readily polished with diamond polishing compound and the crystal polishing equipment available in our laboratory. This permits a relatively expeditious change in crystal thickness when desired, and a highly polished crystal surface which minimizes light scattering.

None of the three materials used as hosts were subject to shattering upon cooling from room temperature to 4.2°K at rates of up to 6°K per minute, as are some other ionic host materials. This was advantageous when looking at absorption bands in the high energy region of the vacuum ultraviolet. Even in a dewar evacuated to 1×10^{-6} mm, some condensation of residual vapor onto the crystal surface occurred as the temperature was lowered. By cooling the sample rapidly with no fear of its shattering, the scattering background caused by this condensation was minimized.

These materials could be grown in crystal growing ovens which were designed for continuous use at temperatures under 1400°C. This temperature requirement is not an extreme constraint in oven design and manufacture.

None of these hosts are sensitive to moisture as are LiF and NaF, and none are damaged by such standard fastening materials

as quartz cement, rubber cement, etc.

Once the initial requirement of an appropriate host material was satisfied, obtaining a variety of transition metal ions doped into the host in low concentrations became the goal. This proved to be a rather difficult and time consuming task.

Ideally, the system would be a first row transition metal ion doped at a concentration of approximately .1 to .01 mole percent. In addition, other metal ions, and such nuisances as impurity oxide ions and lattice defects would be many orders of magnitude lower in concentration.

In practice, this "ideal" system was difficult to obtain, primarily because the hosts were rather nonselective as to which of the many elements they permitted to dissolve in them. For example, the host CaF_2 is notorious for being such a good solvent.

More specifically, more than twenty five different crystals of CaF_2 doped with various transition metal ions were subjected to esr, infrared, visible, near and far ultraviolet studies. Twenty three were determined to be of no value to us because these samples contained so many different metal ions of varying oxidation states that an unambiguous assignment of high energy absorption bands was impossible. They provided us with much experimental

experience, but no data. However many of these same samples had previously been used in the study of various aspects of d-d transitions. This was possible because, by analogy to similar dopants in other hosts and by the use of crystal field calculations one could be certain that a specific absorption band was due to one specific transition metal ion. Such parallel data and accepted methods of calculation do not presently exist for charge transfer absorption bands.

A final and quite striking illustration of the difficulty of obtaining a single transition metal ion impurity is provided by the following quotation by Weakliem:[1]

> "A good crystal of $CaF_2:M^{+3}$ (M = Ti, V, or Cr) can be grown by the following procedure. A melt of CaF_2 plus 1-5% MF_2 or MF_3 contained in a new Mo crucible is held at 1400°C for several hours, and after cooling, the solidified melt is discarded and the crucible cleaned by sandblasting followed by etching with HCl. To the crucible is then added pure CaF_2 and a crystal is grown by pulling. The resulting crystal is good quality and contains about .1-1% of the transition ion . . ."

Because of the solubility problem described above, and be-

cause of the relatively small demand for extremely high purity samples, we experienced a rather low rate of return. It is estimated that our ratio of unsatisfactory crystals to satisfactory ones was about 10:1. Therefore much written credit will be given to those from whom we received samples.

Since this possibility of the host containing several dissolved ions instead of just one dissolved ion existed, we actively searched for a number of independent sources of crystals, in addition to improving our own crystal growing capabilities. We eventually obtained samples from at least twelve different locations, and because of this we found ourselves in the fortunate position of having duplicates and triplicates of many systems. Therefore, we were able to satisfy ourselves that the spectra obtained were indeed reproducible. This is important since much of the work presented here is an initial study of Laporte forbidden charge transfer transitions. Because we fully expected to find allowed transitions with oscillator strengths of nearly unity, yet did not, the fact that we could reproduce many of these unexpected and previously unstudied absorption bands gave us added confidence in our data.

As a check on crystal purity, we obtained esr, absorption, and emission spectra in our laboratory, and forwarded many of the

samples to a commercial analytical laboratory (Schwartzkopf Micro-analytical Laboratory, Woodside, New York) for further analysis.

Because our best samples contained a transition metal at about .1 mole percent concentration, it was found that a thickness of between .4 and 2 mm gave reasonable values (0-4) of optical density. Slight differences in OD values were obtained when the light was incident on different areas of the crystal face, indicating a concentration gradient. These values always differed by less than 10%, and normally were within a few percent.

Unusual looking spectra were repeated on different occasions with differing combinations of light sources and detectors, and the results presented here are indeed reproducible.

Most spectra were quite broad, even at 4.2°K. This permitted the use of large slits for a greater photon flux at the photo-tube, when using the vacuum ultraviolet instrument. The resolution was 4 Å which is about 175 cm^{-1} at 1500 Å. In order to determine whether structure was present at 4.2°K, approximately 1/3 of the vacuum ultraviolet absorption spectra were reproduced using 10 micron slits and photographic detection. Resolution with this slit width was .075 Å, which was equivalent to 2-4 cm^{-1} over the wavelength range of interest. No structure was found, and in retro-

spect none was expected.

B. $KMgF_3$

Potassium magnesium fluoride possesses the cubic perovskite structure, which can be visualized as a series of cubes, the corners of which are K^+ ions, the face centers are F^- ions, and the body centers are Mg^{+2} ions. This structure is pictured in Figure 1.

When iron group impurity ions are introduced into the $KMgF_3$ lattice, they enter in the divalent state and replace the Mg^{+2} ions, thus retaining pure O_h symmetry.[2,3]

Pure $KMgF_3$ serves as an excellent "window" for high energy radiation, and therefore as an excellent host for transition metal ions. The absorption spectrum in the vacuum ultraviolet region of a sample of undoped $KMgF_3$ grown by D. Hukin of Clarendon Laboratory, Oxford, England is shown in Figure 2.

A sample of undoped $KMgF_3$ grown by Optovac, Inc., North Brookfield, Massachusetts did not transmit as far into the vacuum ultraviolet as did the sample of Figure 2. Specifically it showed a high energy cutoff near 1400 Å. However, this sample contained many entrapped bubbles which may have contributed to the high optical density in this wavelength region. The spectrum of Optovac's $KMgF_3$ is noteworthy because several of the transition metal doped

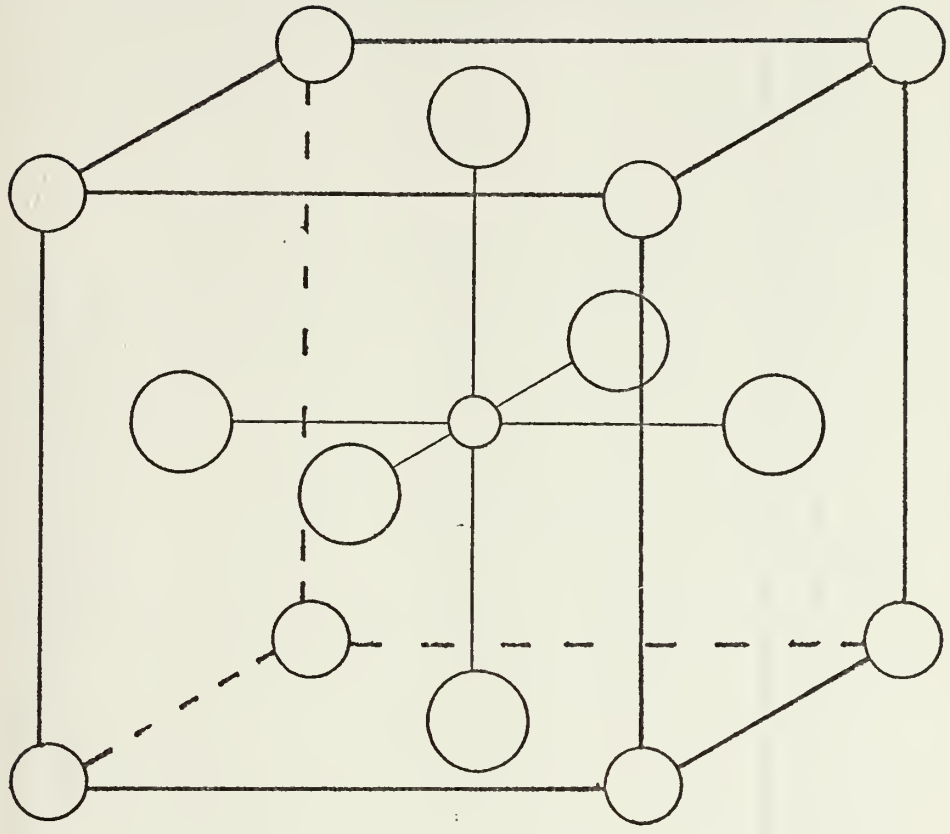

Figure 1. Perovskite structure of $KMgF_3$. Cube corners are K^+, face centers are F^-, and body centers are Mg^{++}. Cube edge is 3.973 Angstroms.

Figure 2. Room temperature absorption spectrum of undoped $KMgF_3$. Crystal thickness is .85 mm.

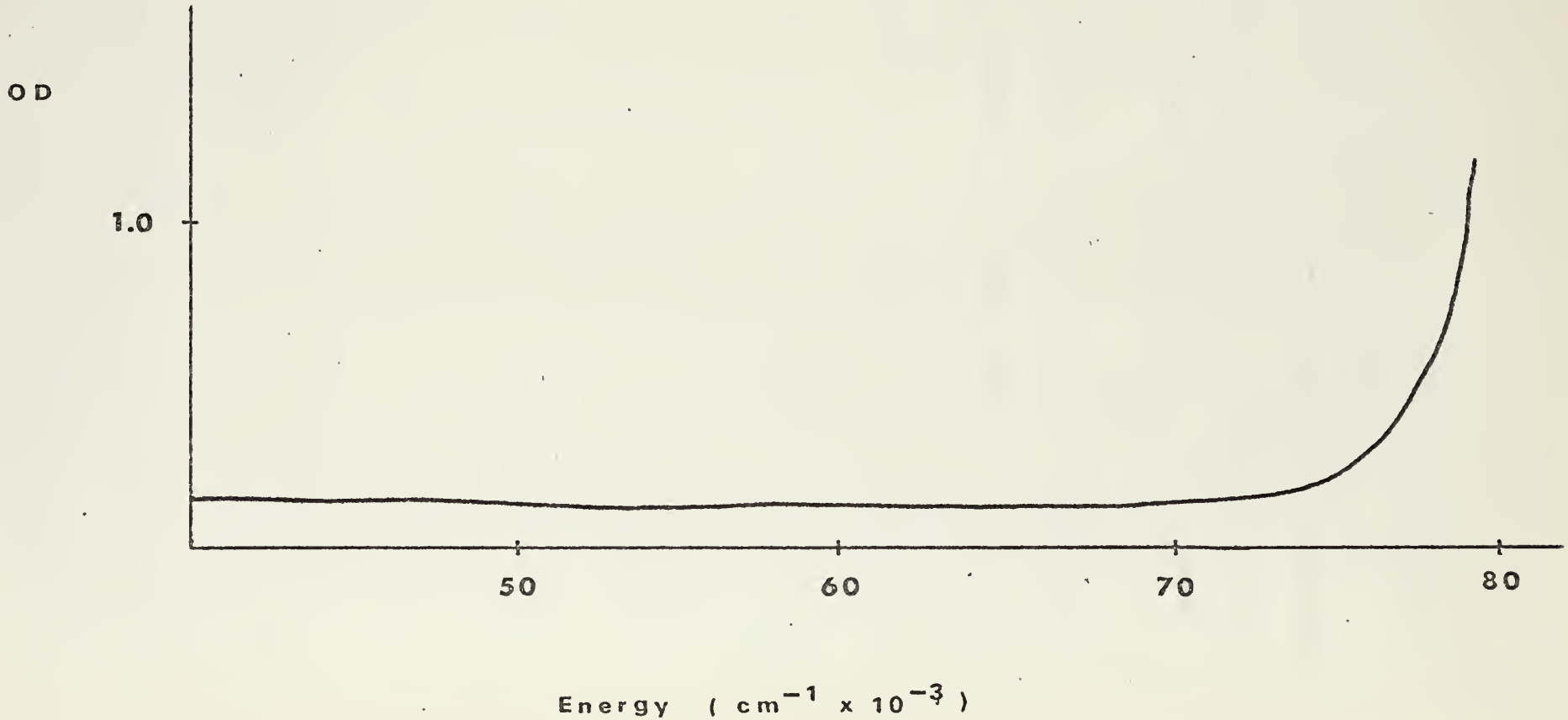

samples also cut off near 1400 Å, and this might possibly be attributed to a less than perfectly pure host material.

In order not to impugn Optovac's crystal growing capabilities, we must in all fairness relate the following. This piece of $KMgF_3$ was the last undoped sample in their possession, since they have not grown such crystals in several years. In addition, many of the doped $KMgF_3$ crystals purchased from them were found to be quite free from unwanted impurities and of high quality.

C. $KMgF_3$:V

Two samples of $KMgF_3$:V were studied and both were virtually identical. One crystal was grown by H. Guggenheim and loaned to us by M. Sturge, both of Bell Laboratories, Murray Hill, New Jersey. The second crystal was grown by D. Hukin of the Clarendon Laboratory, Oxford, England.

The d-d absorption bands of this system have recently been reported[4] in a study done at 2°K. The cubic terms and their calculated and observed energies are summarized in Table I.

TABLE I.

$KMgF_3$:V data from reference 4.

Cubic Term	Observed Energy (cm^{-1})	Calculated Energy (cm^{-1})
$^4T_2$ (t_2^2e)	12150	12150
$^4T_1{}^a$ (t_2^2e)	18400	18500
$^4T_1{}^b$ (t_2e^2)	---	28800
^2E (t_2^3)	12670	12660
$^2T_1$ (t_2^3)	13350	13420
$^2T_2$ (t_2^3)	18430	18370

$$10\ D_q = 12,150\ cm^{-1}$$

Our Cary 14 absorption data are in agreement with the results of reference 4, furthermore we find three additional absorption bands, one near 2700 Å, one near 2150 Å, and one near 1530 Å. Sturge has informed us[5] that the windows of the dewar used in the work of reference 4 did not transmit through the entire near ultraviolet spectral region. Therefore, the two lower energy bands could not be observed.

As mentioned previously, the crystal given to us by D. Hukin also exhibited those d-d bands reported plus the three new bands.

With respect to the purity of these samples, no V^{+3} was present. VF_6^{3-} exhibits very strong absorption[6] near 15,000 cm^{-1} and none was found in our samples. In addition, no other optical absorption bands than those detailed above were observed. Finally, an esr study was undertaken at 77°K, which showed only a textbook signal in the Guggenheim sample, but which showed an additional very weak signal to higher g value than the V^{+2} signal in the Hukin sample. This value did not coincide with any known first row transition metal ion.

Optically, this extra esr signal in the Hukin group sample probably contributed to the more rapidly rising cutoff above 70,000 cm^{-1}. Superimposed on this cutoff was the band at 1530 Å as in the Guggenheim sample.

Because of its simplicity, and because the strength of the V^{+2} signal compared to the lack of esr signal at other values of B (swept at higher gain) provides a striking indication of the purity of Guggenheim's sample, this spectrum is reproduced in Figure 3.

The near and far ultraviolet absorption spectra of the crystal loaned by Sturge are shown in Figures 4 and 5. The Hukin crystal is shown in Figure 6. Note that in Figure 4, the near ultraviolet bands are quite weak. In fact, the 2700 Å band is not observed at all at this crystal thickness. In Figure 6, the Hukin crystal (which is more concentrated and of greater thickness than the Sturge crystal) clearly shows the two near ultraviolet bands. As previously stated, the Sturge crystal also exhibits both bands, although the 2700 Å band is not quite as well defined as that of Figure 6. A close look at the 2100-2200 Å band shows that although the intensity changes drastically upon cooling to 77°K, the band width remains essentially the same.

Based on esr spectra and the intensity of the no phonon line[7] the sample of $V:KMgF_3$ grown by Guggenheim contains .2% V^{+2}. By comparison with the d-d absorption bands, the sample grown by Hukin contains .69%.

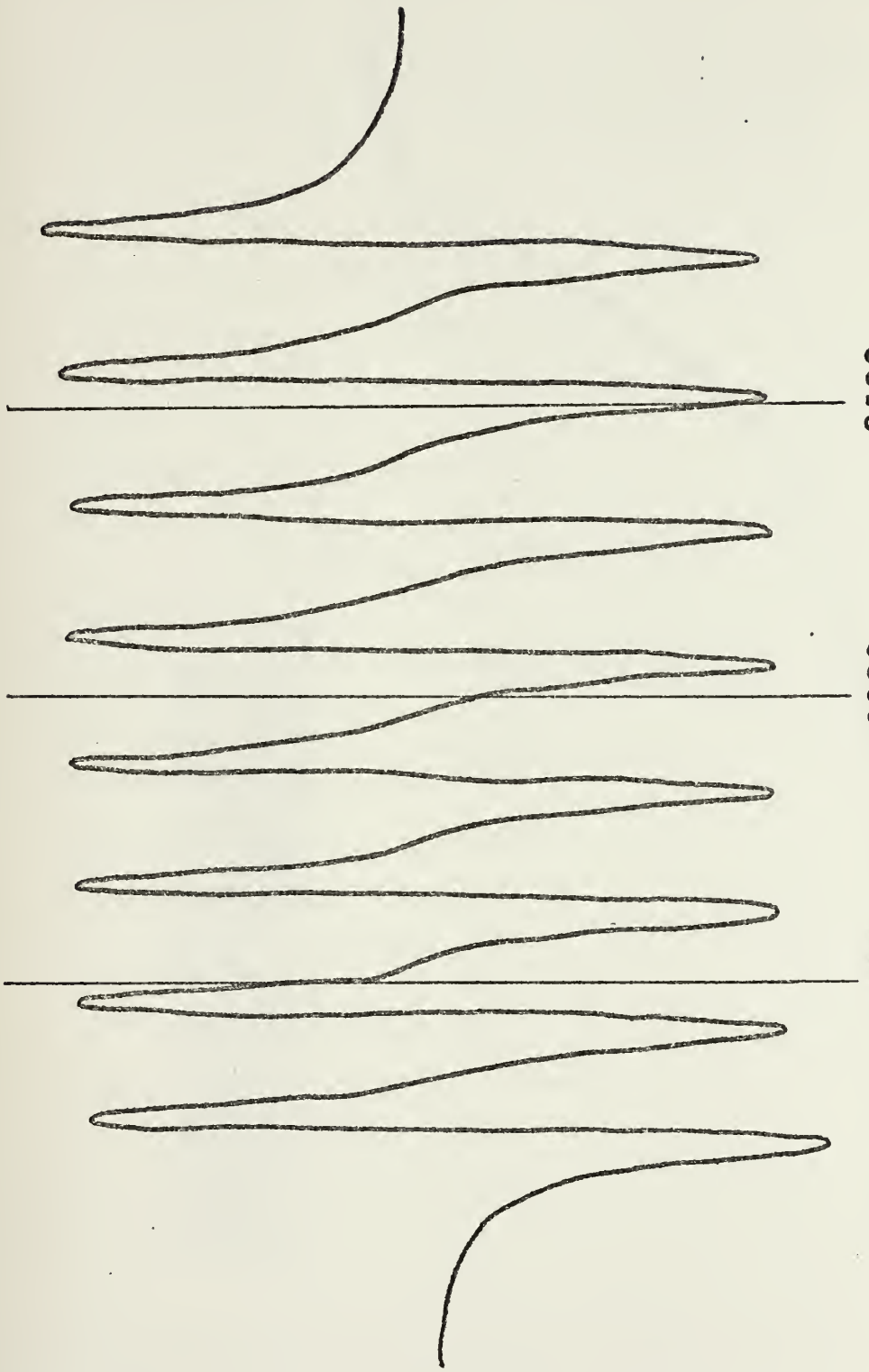

Figure 3. Esr derivative spectrum of $KMgF_3:V$ at 77^0K. Microwave frequency is 9.132 gHz.

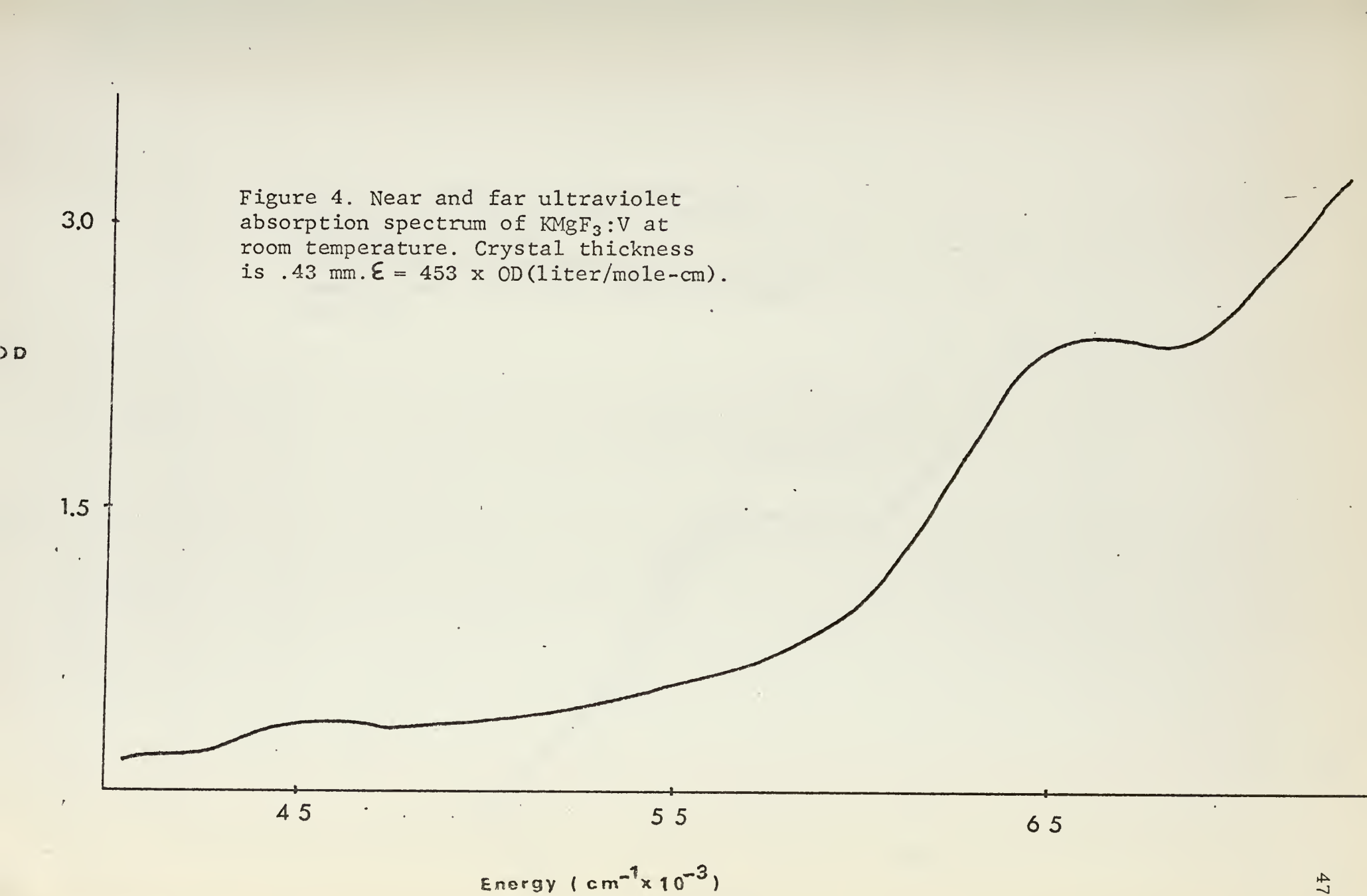

Figure 4. Near and far ultraviolet absorption spectrum of $KMgF_3$:V at room temperature. Crystal thickness is .43 mm. ε = 453 x OD(liter/mole-cm).

Figure 5. Temperature dependence of 65,000 cm^{-1} band of $KMgF_3$:V. Crystal thickness is .43 mm.
Solid line- room temperature
Dashed line- 4.2° K. ϵ = 453 x OD(liter/mole-cm).

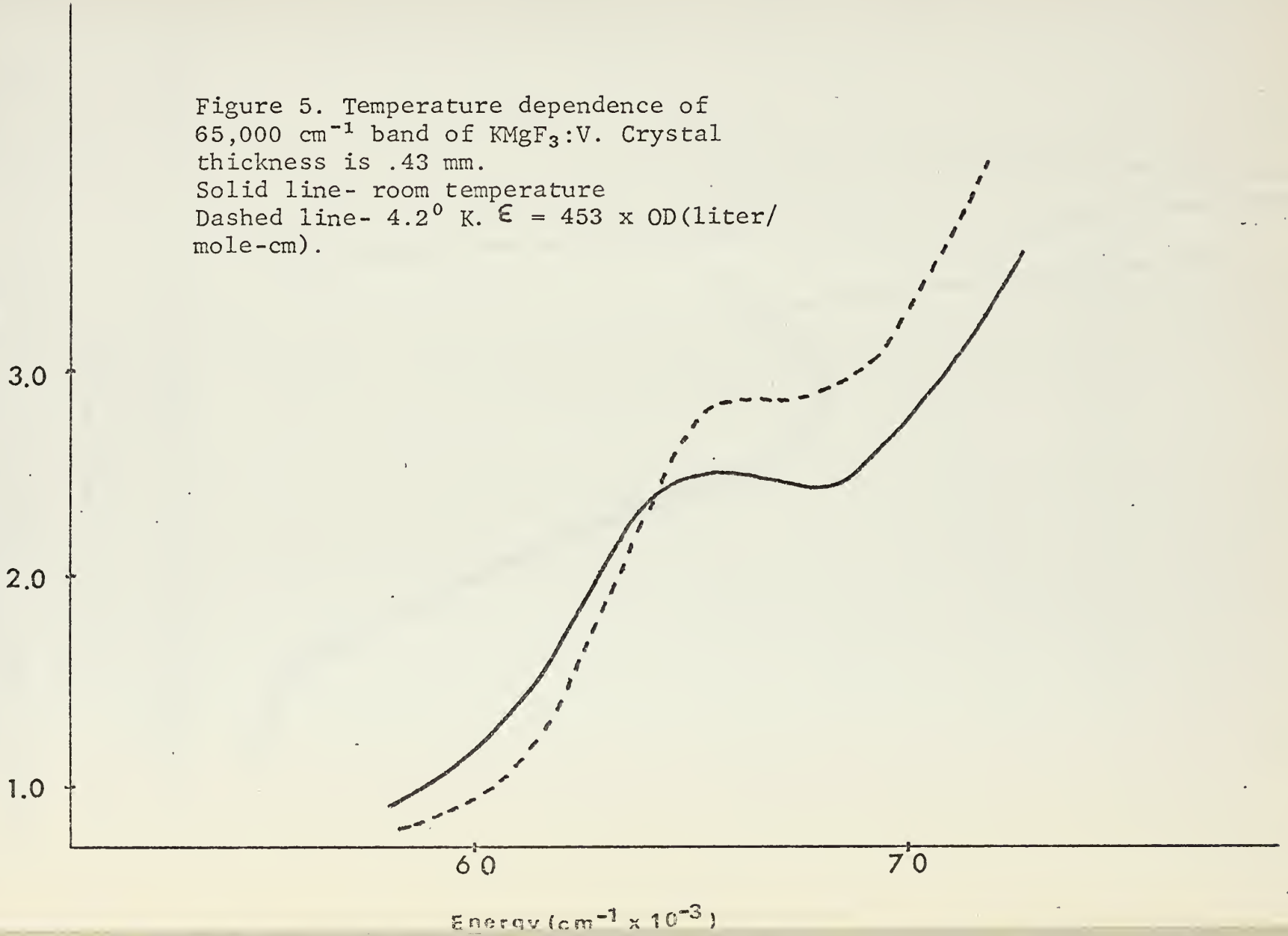

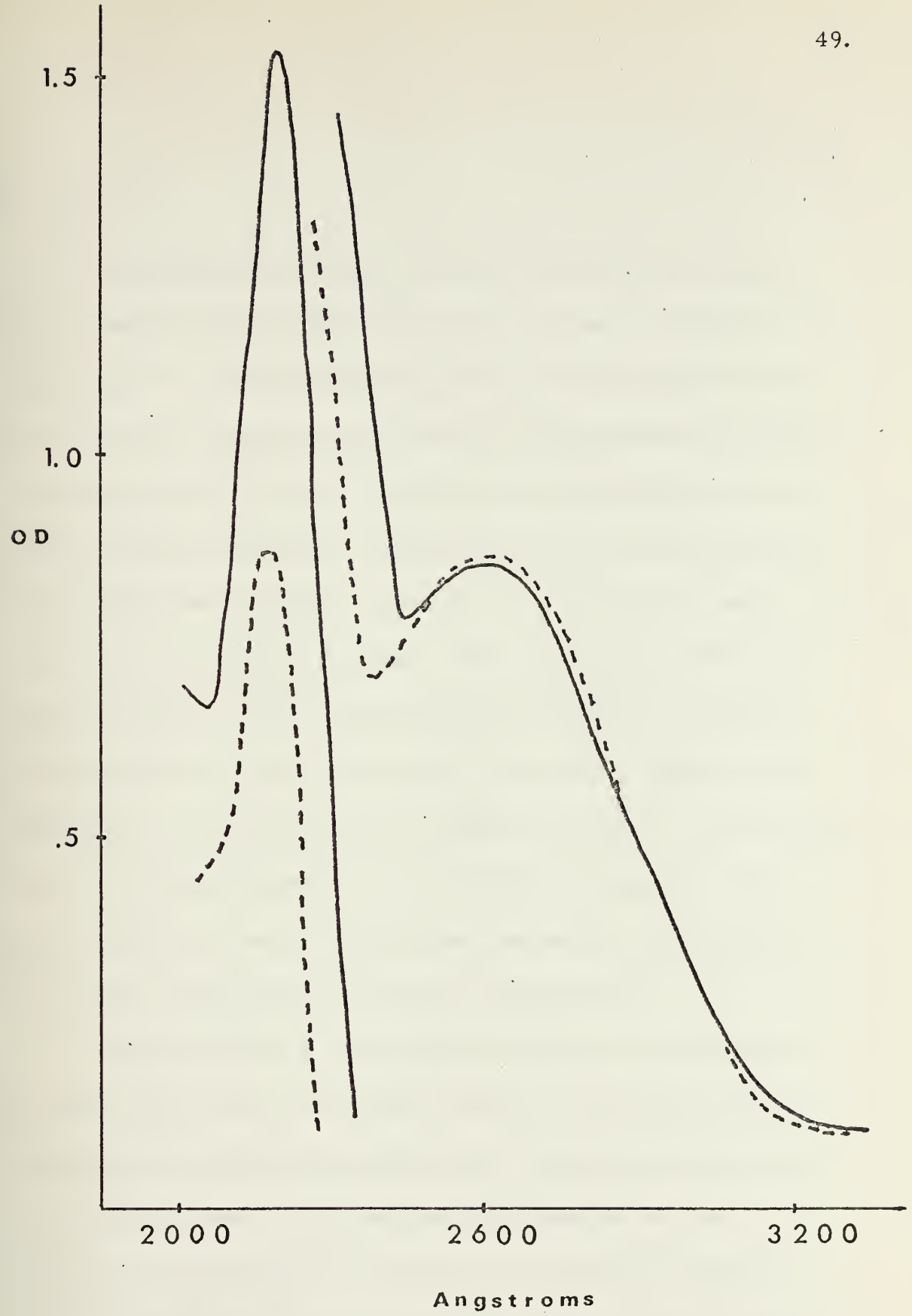

Figure 6. Near ultraviolet absorption spectrum of $KMgF_3$:V(Hukin). Crystal thickness is 3.13 mm. Solid line- room temperature Dashed line- 77^0 K. ε = 18.1 x OD (liter/mole-cm).

D. $KMgF_3$:Cr

In octahedral symmetry, one would expect to see a ^5E_g to $^5T_{2g}$ absorption band in this high spin d^4 system. In addition, one would expect a Jahn Teller splitting of this, the only spin allowed d-d transition. Experimentally, most Cr (II) compounds do exhibit a broad band near 15,000 cm^{-1}, and it is normally composed of at least three separate bands. One explanation for this large number of transitions that are seen, is that, in the ground state, these systems are tetragonally distorted. This distortion, which is an elongation along one axis, causes both the ^5E_g and $^5T_{2g}$ states to each split into two terms, which gives rise to three spin allowed transitions. In some Cr systems, such as $Cr(H_2O)_6^{+2}$ for example, there is evidence of distortion to even lower symmetry.[8] We present these facts here, because they lead us to anticipate that our system, $KMgF_3$:Cr, may also be a distorted one.

We have studied a crystal which has been grown for us by D. Hukin of Clarendon Laboratory, Oxford. A chemical analysis of the sample shows that the predominant impurity ion is chromium, at .14 weight percent. The analysis also shows the existence of iron, at .027 weight percent, but tests for vanadium, manganese, and nickel show that none of these are impurities in this particular

crystal.

The Jahn Teller split band in the near infrared region is not observed in this sample, because of the low chromium concentration. However, we do observe two broad structureless absorption bands, one of which is in the vacuum ultraviolet region near 58,000 cm^{-1} and is shown in Figure 7. The second band is near 2700 Å, and is shown in Figure 8. Neither band becomes well resolved at low temperatures.

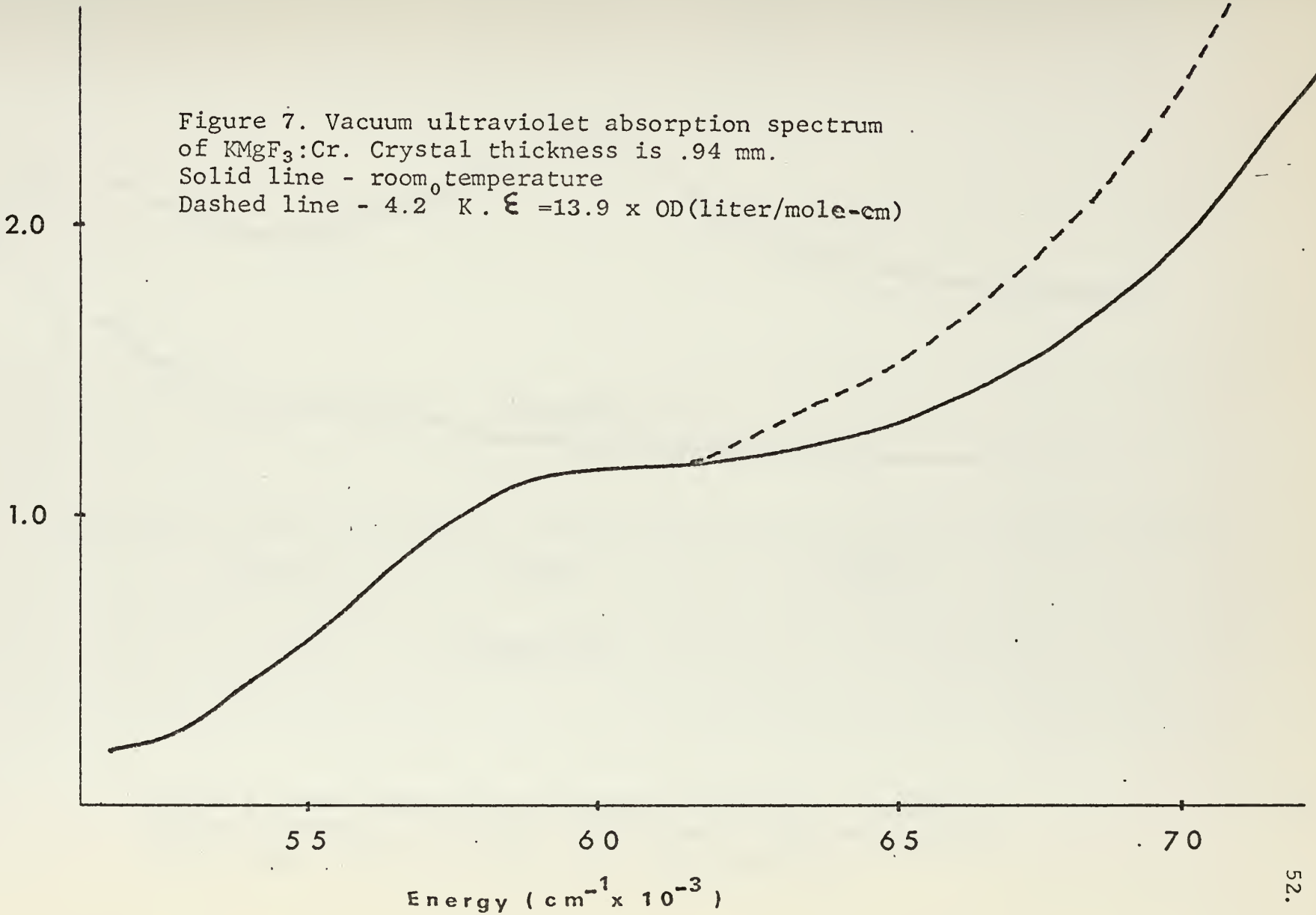

Figure 7. Vacuum ultraviolet absorption spectrum of $KMgF_3$:Cr. Crystal thickness is .94 mm.
Solid line - room temperature
Dashed line - 4.2 K. ε =13.9 x OD(liter/mole-cm)

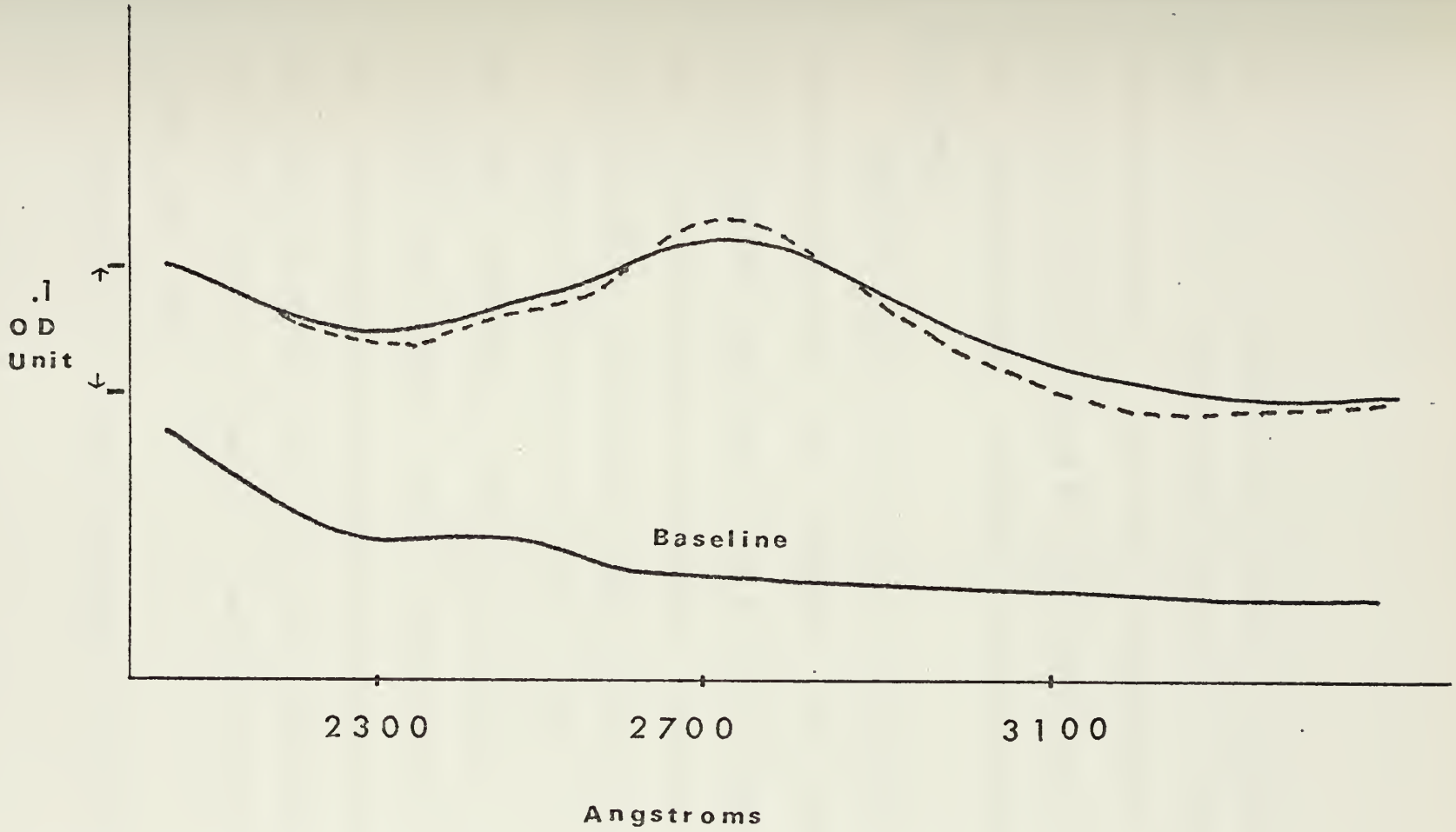

Figure 8. Near ultraviolet absorption spectrum of $KMgF_3$:Cr. Crystal thickness is .89 mm. Solid line - room temperature Dashed line - 77° K. ε =134 x OD (liter/mole-cm)

E. $KMgF_3$:Mn

We have investigated three samples of $KMgF_3$:Mn, kindly loaned to us by M. Sturge of Bell Laboratories, D. Hukin of Clarendon Laboratory, and W. Sibley of Oklahoma State University. These three samples exhibited the same spectra, and the spectra of the sample grown by H. Guggenheim and given by Sturge will be presented.

The ground state of Mn (II) in an octahedral field is ^6S. Because of the absence of other sextet terms, all d-d bands will be of low intensity, being both Laporte and spin forbidden. The studies of these low intensity transitions are numerous,[9] but all have been confined to the spectral region below 50,000 cm^{-1}.

Two esr studies are of interest to our work, however, since their results have aided us in verifying the existence of Mn ions in an otherwise clear crystal. Ogawa[10] demonstrated that Mn in $KMgF_3$ is indeed at a site of perfect octahedral symmetry and that six hyperfine groups of Mn^{55} were observable in the esr spectrum of this system. Hall *et al.*[2] repeated the experiment and found the same results.

The $KMgF_3$:Mn sample from Sturge contained 3% Mn^{+2},

as determined by spin resonance.[11] For reasons of completeness and in order to detect any other impurity ions, we obtained the esr spectrum of this sample at 77°K. As expected, the six groups mentioned above were easily observed, and a careful search at high gain revealed no additional signals. A search of the infrared, visible, and near ultraviolet regions produced no absorption bands. It can be assumed that this crystal contains predominantly Mn (II) as an impurity.

The vacuum ultraviolet absorption experiment disclosed a single broad featureless band near 60,000 cm^{-1}. Its intensity decreased with temperature upon cooling to 4.2°K, and this is reproduced in Figure 9. Note the facts that the crystal is rather thin (.46 mm) and that the background increases at high energy. This OD increase was determined to be reproducible when the crystal was repolished and the spectrum obtained several days later.

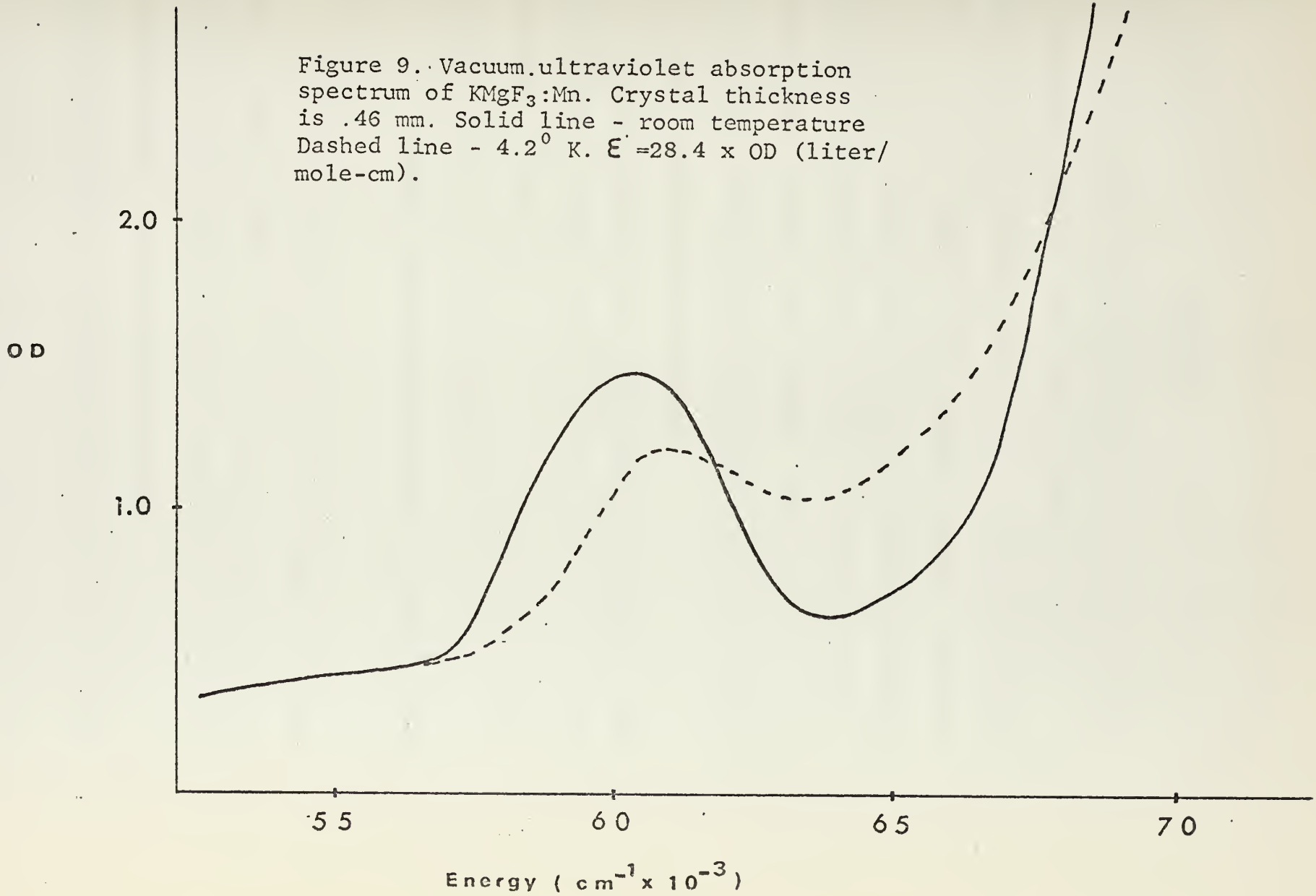

Figure 9. Vacuum ultraviolet absorption spectrum of $KMgF_3$:Mn. Crystal thickness is .46 mm. Solid line - room temperature Dashed line - 4.2° K. ε =28.4 x OD (liter/mole-cm).

F. $KMgF_3$:Fe $KMgF_3$:Ni

Unfortunately, the systems $KMgF_3$:Fe and $KMgF_3$:Ni must be presented together, in spite of the possibility of confusion. The reason is that most of the samples which we have studied contain both iron and nickel ions to varying degrees. In fact, one of the great problems associated with this study has been the assignment of absorption bands to their ion of origin, and these two systems are quite representative of that problem. The presentation of both systems at one time will provide for a more lucid understanding of the rationale behind our final assignment.

In the infrared spectral region, $KMgF_3$:Fe displays a Jahn Teller split $^5T_{2g}$ to ^5E_g absorption which consists of one broad structureless double humped band.[12] At 20°K, the mean absorption band is at 9500 cm^{-1} and the splitting of the two bands is 1350 cm^{-1}. No further spin allowed transitions are permitted within the d shell.

The optical absorptions in $KMgF_3$:Ni and $KNiF_3$ have been rather thoroughly studied,[13, 14, 15, 16] and one would expect to be able to easily characterize a sample as being $KMgF_3$:Ni based on this published data. In these octahedral systems, three spin allowed bands are observed belonging to the $^3T_{2g}$, $^3T_{1g}$ (F), and

$^3T_{1g}$ (P) levels of the d^8 configuration, with the higher $^3T_{1g}$ being the most intense and occurring near 24,000 cm^{-1}.

Due to the low doping levels of most of our samples however, only this 24,000 cm^{-1} band was observable, and only in one or two samples. A concentration that permitted us to easily observe these low energy transitions caused the vacuum ultraviolet transitions to be of higher absorbance than is readily measurable. In many samples, none of these d-d transitions were found using the Cary 14 instrument, yet a chemical analysis showed that nickel was indeed present. As a result of the low concentration required for the observation of vacuum ultraviolet bands, these highly studied and well characterized low energy d-d bands were of little aid to us. Several crystals containing nickel and iron were studied, and they will be listed here.

1. $KMgF_3$:Ni (A) which was grown by H. Guggenheim of Bell Laboratories, and given to us by him.
2. $KMgF_3$:Ni (Dietz) which was given to us by R. E. Dietz, also of Bell Laboratories.
3. $KMgF_3$:Ni (Hukin) which was grown by D. Hukin of Clarendon Laboratory, Oxford, and given to us by him.
4. $KMgF_3$:Fe (A) which was purchased from Optovac, Inc.

5. $KMgF_3$:Fe (Optovac) which was a second crystal purchased from Optovac, Inc., and which was from a different boule than $KMgF_3$:Fe (A).
6. $KMgF_3$:Fe (Hukin) which was grown by D. Hukin and given to us by him.

Some of the more important characteristics of the spectra will now be presented.

The sample $KMgF_3$:Fe (Hukin) does not exhibit the low energy $^5T_{2g}$ to ^5E_g absorption band reported by Jones.[12] It does, however, show a series of bands in the near ultraviolet region, one of which is near 2800 Å at room temperature and which shows that it is actually composed of two bands at 77°K. The second room temperature band remains single and unstructured at 77°K. The vacuum ultraviolet spectrum consists of at least four bands, one of which contributes to the flat portion of the spectrum near 55,000 cm^{-1}. The entire ultraviolet spectrum is shown in Figure 10, and the near ultraviolet bands are shown in Figure 11.

The crystal $KMgF_3$:Fe (Optovac) also does not exhibit the Jahn Teller split $^5T_{2g}$ to ^5E_g absorption. Additionally, it does not show the two bands near 2800 Å, but it does give rise to a 2040 Å band as in the Hukin crystal. A number of bands are found

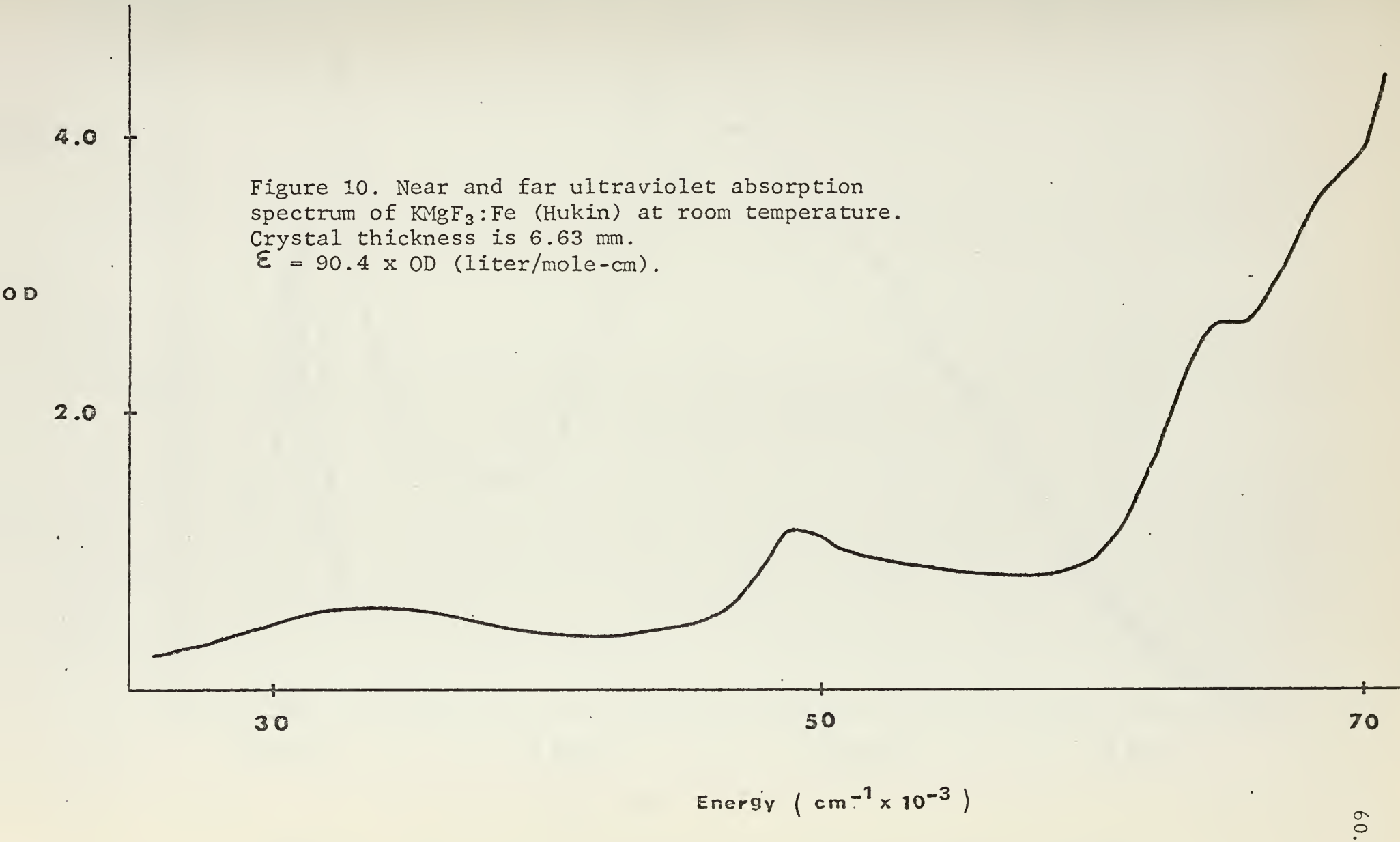

Figure 10. Near and far ultraviolet absorption spectrum of $KMgF_3$:Fe (Hukin) at room temperature. Crystal thickness is 6.63 mm.
ε = 90.4 x OD (liter/mole-cm).

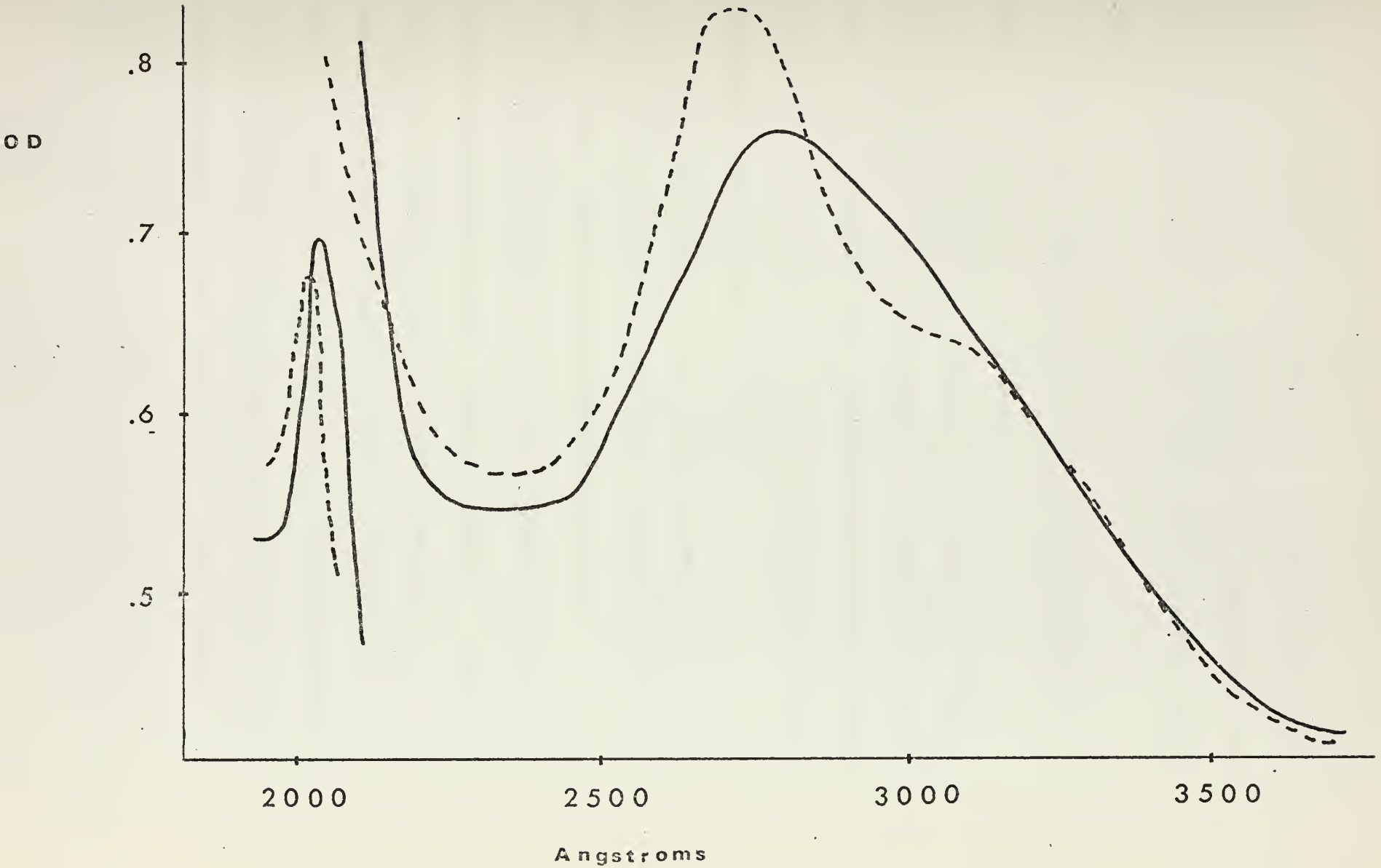

Figure 11. Near ultraviolet absorption spectrum of $KMgF_3$:Fe(Hukin). Crystal thickness is 12.78 mm. Solid line- room temperature Dashed line- 77° K ϵ = 37.1 x OD(liter/mole-cm)

in the vacuum ultraviolet region and they are shown in Figure 12. Note that a small inflection at room temperature near 45,000 cm^{-1} becomes more prominant at 4.2°K. This feature is more obvious in Figure 13.

The sample $KMgF_3$:Fe (A) exhibits the same features as $KMgF_3$:Fe (Optovac).

Concerning the nickel doped crystals, the sample $KMgF_3$:Ni (Dietz) exhibited a series of transitions, all of which can be attributed to Ni (II). There are three d-d bands in the regions 7000 cm^{-1}, 12,000 cm^{-1}, and 23,000 cm^{-1}. In the vacuum ultraviolet region, a weak band is observed near 64,000 cm^{-1}.

The crystal $KMgF_3$:Ni (Hukin) exhibits essentially the same absorption spectrum as $KMgF_3$:Ni (Dietz) showing the three d-d bands and a much better resolved band at 64,000 cm^{-1}.

The sample $KMgF_3$:Ni (A) is quite different from the two previous nickel doped crystals. It does not exhibit the characteristic Ni (II) d orbital transitions at room temperature, but it does show the most intense of the three, the $^3T_{1g}$ (P) band at liquid helium temperature. It also shows a broad structureless band near 2040 Å and three additional absorption bands in the vacuum ultraviolet region, one near 56,000 cm^{-1}, one near 64,000 cm^{-1},

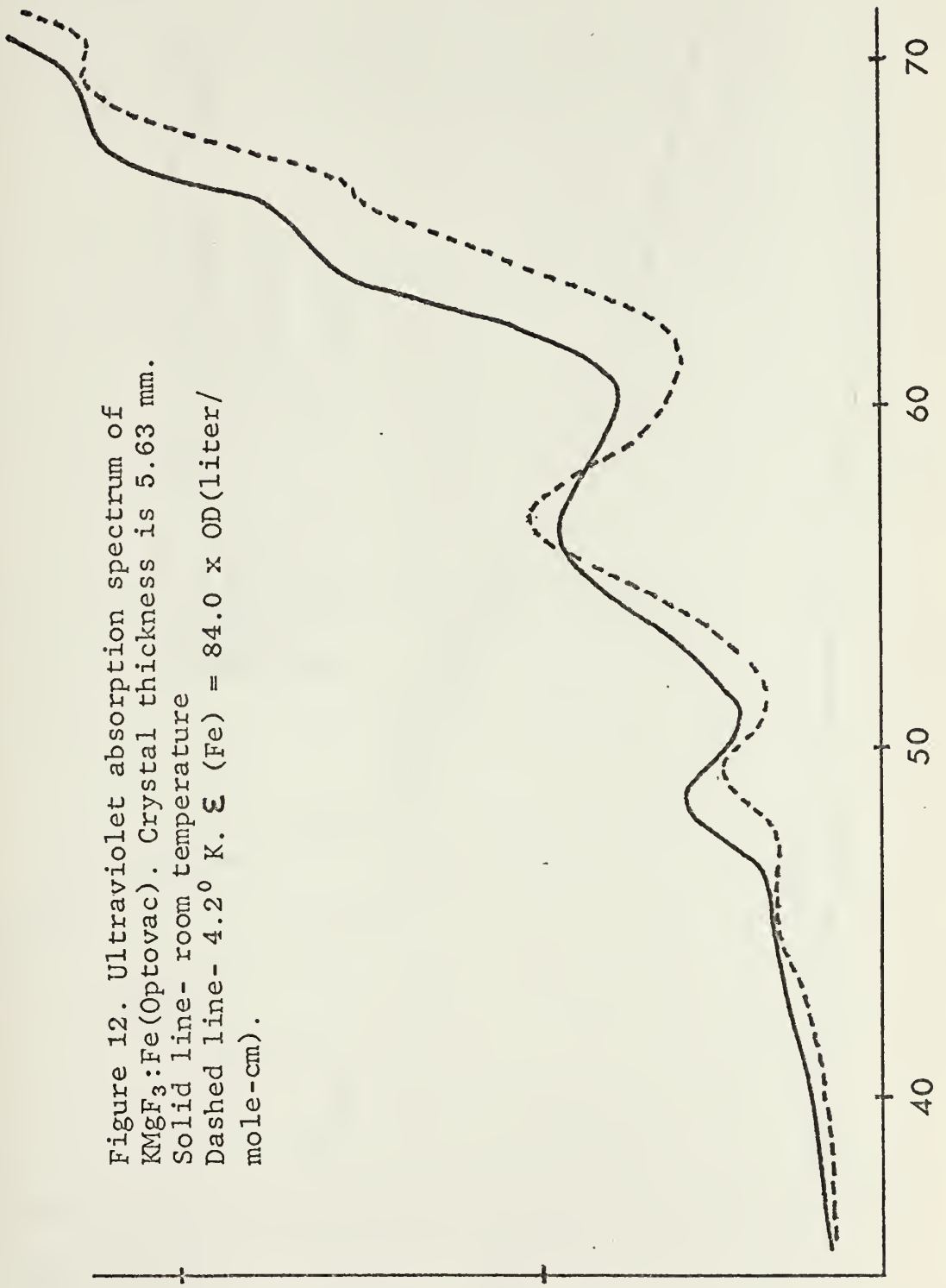

Figure 12. Ultraviolet absorption spectrum of $KMgF_3$:Fe(Optovac). Crystal thickness is 5.63 mm.
Solid line- room temperature
Dashed line- 4.2° K. $\mathcal{E}$ (Fe) = 84.0 x OD(liter/mole-cm).

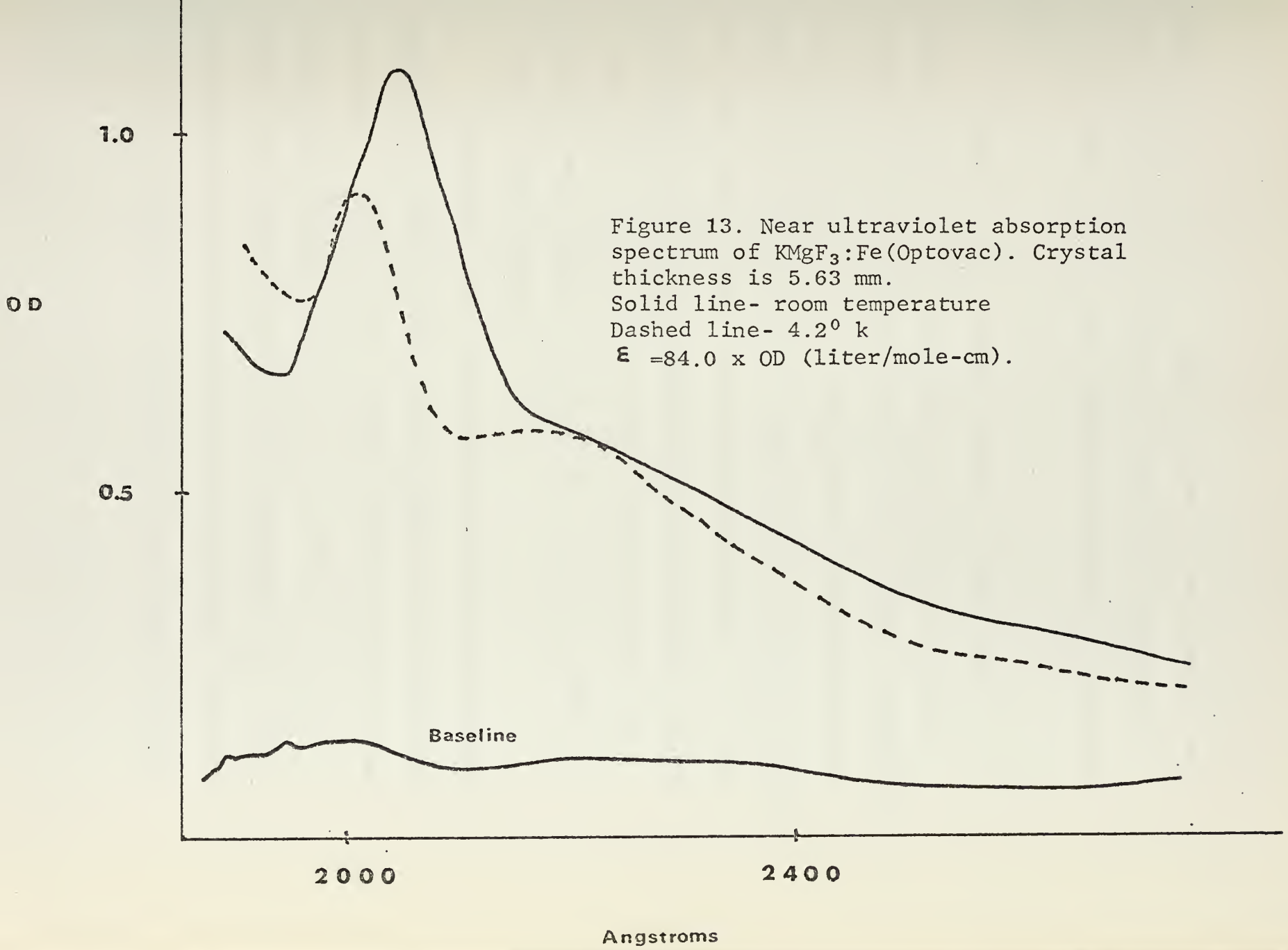

Figure 13. Near ultraviolet absorption spectrum of $KMgF_3$:Fe(Optovac). Crystal thickness is 5.63 mm.
Solid line- room temperature
Dashed line- 4.2^0 k
ε =84.0 x OD (liter/mole-cm).

and one near 68,000 cm^{-1}. These energies are the values at room temperature. There are shifts as one lowers the temperature to 4.2°K, and the spectra of this sample are shown in Figures 14 and 15.

The electron spin resonance spectra of these crystals, obtained at 77°K, provided more data but little that was conclusive. In $KMgF_3$:Ni (Dietz) only the Ni (II) signal was observed. In $KMgF_3$:Ni (A), the Ni (II) signal was again easily detected, but other signals to lower g values were also present. These signals could not be assigned to any first row transition metal ion of oxidation states one to three. The $KMgF_3$:Fe (A) sample displayed only the same unknown signals at g less than 2.2 as did $KMgF_3$:Ni (A). $KMgF_3$:Fe (Hukin) also showed the same signals as $KMgF_3$:Fe (A), but with the addition of a series of bands centered at g = 5.7.

In summary, the esr data showed that all the samples labeled $KMgF_3$:Ni did contain Ni (II). Also the $KMgF_3$:Ni (A) crystal had an esr signal very much like that of $KMgF_3$:Fe (A), and the iron doped samples did not contain detectable amounts of Fe (I) or Fe (III). In addition, none of the iron doped crystals contained Ni (II). This is quite important since we have been informed by Sibley[17] that nickel is a common impurity in the MgF_2 powder that is used as starting

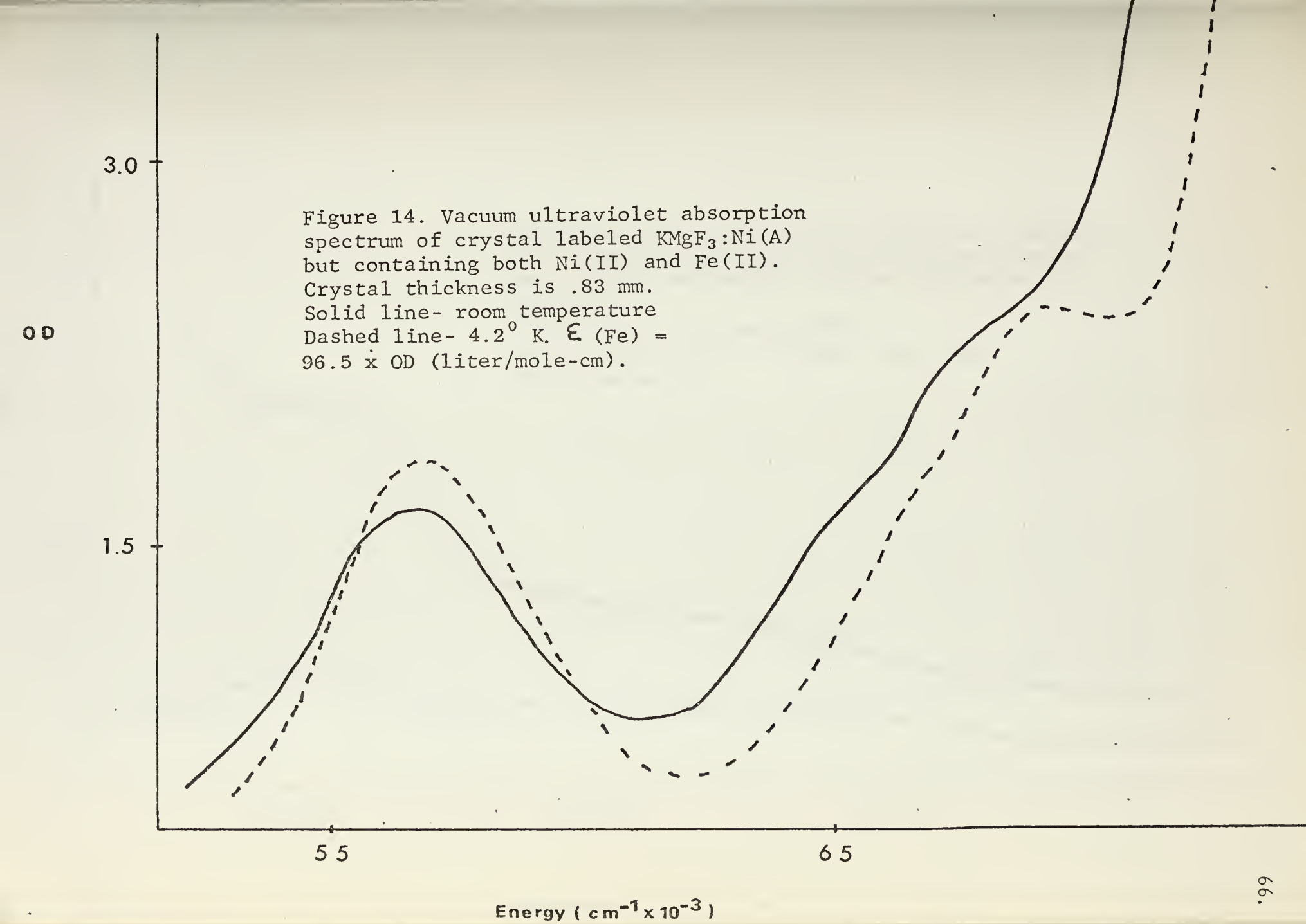

Figure 14. Vacuum ultraviolet absorption spectrum of crystal labeled $KMgF_3$:Ni(A) but containing both Ni(II) and Fe(II). Crystal thickness is .83 mm. Solid line- room temperature Dashed line- 4.2° K. ε (Fe) = 96.5 x OD (liter/mole-cm).

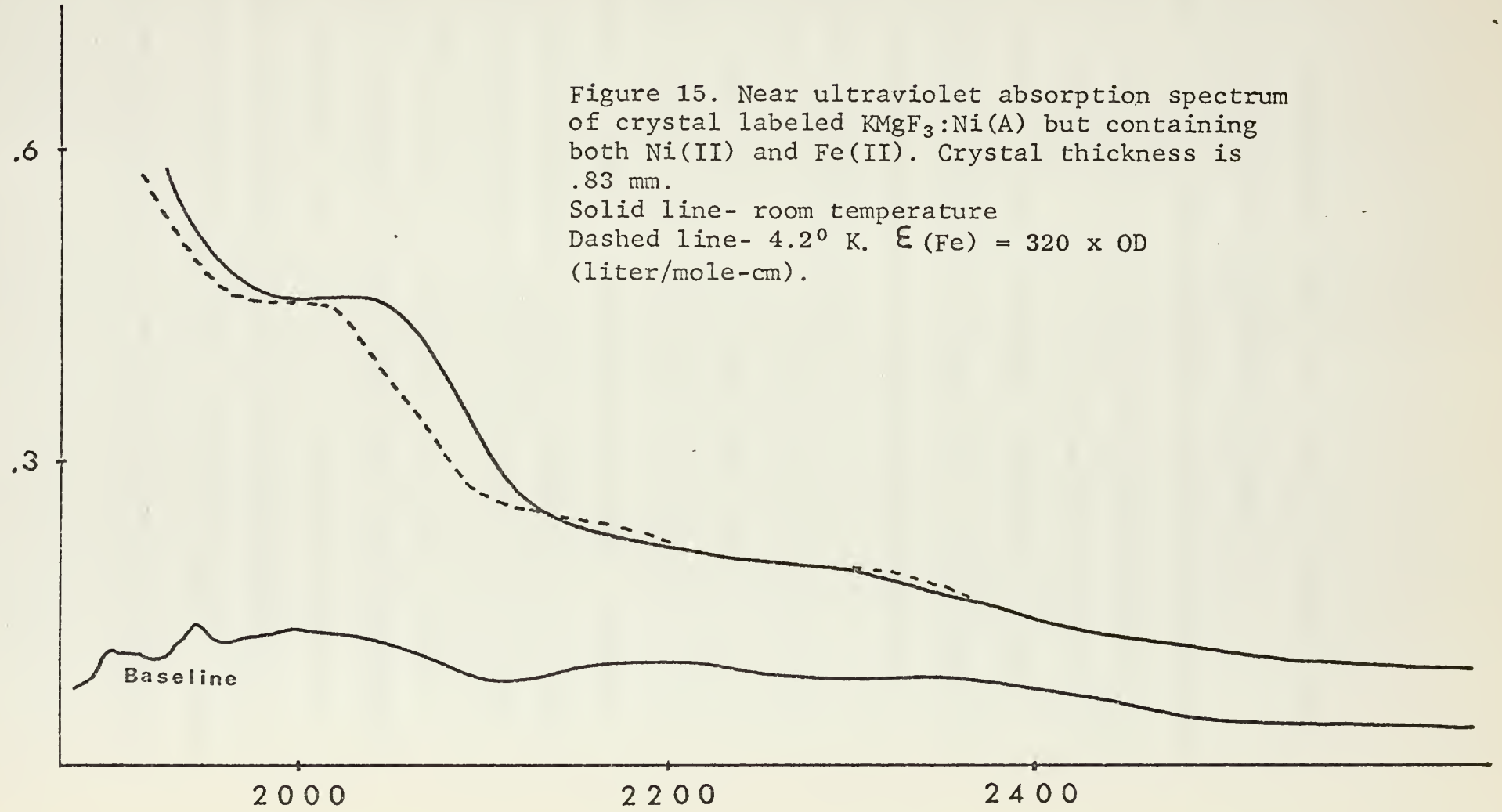

Figure 15. Near ultraviolet absorption spectrum of crystal labeled $KMgF_3$:Ni(A) but containing both Ni(II) and Fe(II). Crystal thickness is .83 mm.
Solid line- room temperature
Dashed line- 4.2° K. ε(Fe) = 320 x OD (liter/mole-cm).

material for growing $KMgF_3$. Therefore we have tested all samples, including the ones previously mentioned, for nickel ion.

Thus far in the experimental work, our data, which consisted of infrared, visible, near and far ultraviolet absorption spectra, and esr spectra, enabled us to rule out certain possible band assignments but did not permit us to make a definitive statement concerning the various optical absorption bands we had found. Our final action was to have a chemical analysis done by Schwartzkopf Laboratories on a representative number of samples.

For two reasons, every crystal studied was not chemically analyzed, nor was a test done for every metal ion that would fit into the $KMgF_3$ lattice. First, these were destructive tests, yet we wanted to retain a number of samples for future work. Secondly, the cost of this service depended upon the number of ions for which we desired analyses. Fiscal matters, then, made it desirable to limit our analyses to the most probable impurity ions. For all samples the concentration of some combination of the ions vanadium, chromium, manganese, iron, cobalt, and nickel were determined.

The results of these analyses proved quite enlightening. It was determined that the sample $KMgF_3$:Ni (Hukin) contains .6 weight percent nickel, and less than .01 weight percent each of manganese,

iron, cobalt, and vanadium. This crystal, therefore, provided a standard for determining the concentrations of nickel ion in other samples, since the $^3T_{1g}$ band intensity could be used for comparison purposes. In addition, it permitted us to assign the band at 64,000 cm^{-1} to nickel.

The results for $KMgF_3$:Ni (A) were even more interesting. They showed that this sample contains only .02 weight percent nickel, but .13 weight percent iron. For sake of continuity, this crystal will still be called $KMgF_3$:Ni (A), although it contains predominantly iron.

The sample $KMgF_3$:Fe (A) contains .038 weight percent iron, and .0014 weight percent nickel.

The sample $KMgF_3$:Fe (Hukin) contains .038 weight percent iron and .0064 weight percent nickel.

Based on the data previously presented, we make the following assignments.

Nickel---Three spin allowed d-d transitions plus one band at 64,000 cm^{-1}.

Iron-----Four bands, at 67,000 cm^{-1}, 56,000 cm^{-1}, 48,500 cm^{-1}, and 44,000 cm^{-1}. Again these energies are values of band maxima at room temperature.

As a test of these assignments, the various ion concentrations were converted to mole percent, and with the value of crystal thickness appropriate to the concentration, numbers corresponding to values of optical density were calculated. This facilitated a comparison of band intensities as a feasibility check on the above assignments. An example will make this approach clearer.

Assume that the absorption band near 64,000 cm^{-1} could be assigned to either iron or nickel. This particular band is observed in $KMgF_3$:Fe (A), $KMgF_3$:Fe (Optovac), $KMgF_3$:Ni (A), and $KMgF_3$:Ni (Hukin). To test the possibility that this transition is due to the iron ion, products of mole percent iron times crystal thickness were calculated for each crystal. The results were:

$KMgF_3$:Fe (A)	$\frac{.387 \text{ cm-mole}}{\text{liter}}$
$KMgF_3$:Fe (Optovac)	$\frac{.213 \text{ cm-mole}}{\text{liter}}$
$KMgF_3$:Ni (A)	$\frac{.107 \text{ cm-mole}}{\text{liter}}$
$KMgF_3$:Ni (Hukin)	$\frac{.0211 \text{ cm-mole}}{\text{liter}}$

A typical comparison would be that of $KMgF_3$:Ni (A) and $KMgF_3$:Ni (Hukin). The band at 64,000 cm^{-1} is barely discernible

in $KMgF_3$:Ni (A), yet if we assign this band as an iron transition, based on the numbers on the page before, it should only be one-fifth as intense in the $KMgF_3$:Ni (Hukin) crystal. To the contrary, it is more intense. Therefore the band cannot be assigned to the iron ion. Using this technique, the assignments above were shown to be feasible.

Note the extra absorption band near 2800 Å in $KMgF_3$:Fe (Hukin) Figure 11, and its resemblance to the crystal $KMgF_3$:Cr, Figure 8. Since this band is not visible in the other iron and nickel doped crystals, a very possible assignment is that it is due to the chromium ion. Unfortunately, the chemical analyses of these two samples preclude this possibility. The crystal $KMgF_3$:Fe (Hukin) contains .038 weight percent iron, .0069 weight percent nickel, and less than .0018 weight percent chromium. The sample $KMgF_3$:Cr contains .14 weight percent chromium, .0012 weight percent nickel, and .027 weight percent iron. A series of calculations of mole percent times crystal thickness and subsequent comparison with measured optical density values show that this band in $KMgF_3$:Fe (Hukin) cannot be assigned to the chromium ion, assuming that our assignment of the band in $KMgF_3$:Cr is correct. In addition, multiple comparisons among the several iron and

nickel doped crystals previously presented, and the chromium sample show no reasons why the iron and nickel assignments are not correct. At this time, we must profess our ignorance of the origin of the 2800 Å bands in $KMgF_3$:Fe (Hukin).

It is hoped that the preceeding presentation has reinforced our statement that many of the difficulties associated with this work have centered around the sorting of absorption bands and their correct assignments. Our initial lesson in this area was quite dramatic, since one of our first vacuum ultraviolet absorption bands which we found as the 56,000 cm^{-1} band in $KMgF_3$:Ni (A). We then used this "nickel" absorption, in conjunction with ideas on charge transfer energies, to plan other systems and other experiments. As stated previously, we now assign this band to the iron ion.

G. $KMgF_3$:Co

In contrast to the difficulties involved in assigning the absorption bands observed in $KMgF_3$:Ni and $KMgF_3$:Fe, the assignment of these in the system $KMgF_3$:Co is rather straightforward.

The Co (II) ion in an octahedral field gives rise to three spin allowed optical transitions, $^4T_{1g}$ to $^4T_{2g}$, $^4T_{1g}$ to $^4A_{2g}$, and $^4T_{1g}$ to $^4T_{1g}$ (P). These d-d bands and the electron spin resonance spectra of octahedral cobalt have been extensively studied,[3,18,19,20,21,22,23] and the results of these studies allow a quite easy characterization of the bands observed in our crystals.

Our esr study at 77°K shows only one resonance, which is at g = 4.37, and which corresponds to Co (II).[3] This signal is quite strong, and a search at other values of magnetic field at very high gain shows no additional absorptions, quite in contrast to the several additional resonances we find in our crystals of $KMgF_3$:Ni and $KMgF_3$:Fe. Our conclusion based on the esr study is that there is a high concentration of cobalt ion in a very pure host crystal.

Our Cary 14 spectra indicate two absorption bands, one of which is near 14,000 Å and which corresponds to the lowest spin allowed transition $^4T_{1g}$ to $^4T_{2g}$. The second, and more intense of the two bands, is found near 5000 Å and corresponds to the

$^4T_{1g}$ to $^4T_{1g}$ (P) transition, with the weak $^4T_{1g}$ to $^2T_{1g}$ transition included. The oscillator strength of this higher energy band, by comparison with the work of Ferguson, Wood, and Knox,[22] allows us to estimate our cobalt concentration as one percent. The transition $^4T_{1g}$ to $^4A_{2g}$ is not seen in this sample. Its low intensity is anticipated because, in a strong field characterization, it corresponds to a two electron transition. No further absorption bands are found within the Cary 14 instrument, again giving an indication of crystal purity. In the work of references 22 and 23, the authors state that nickel ion was an impurity in their samples, but we find no indication of this ion in our crystals. Finally, the lack of extraneous optical absorption bands indicates the presence of cobalt in the plus two oxidation state only, since Co^{+3} in an octahedral fluoride system gives rise to a broad band near 8000 Å.[24]

In the vacuum ultraviolet region, only one absorption band is found, and this is shown in Figure 16. The obvious assignment is that this band is associated with the Co (II) ion.

The spectra described above are those of a sample grown by H. Guggenheim and given to us by M. Sturge, both of Bell Laboratories. By electron spin resonance and no phonon line intensities, Sturge has estimated the cobalt concentration to be one

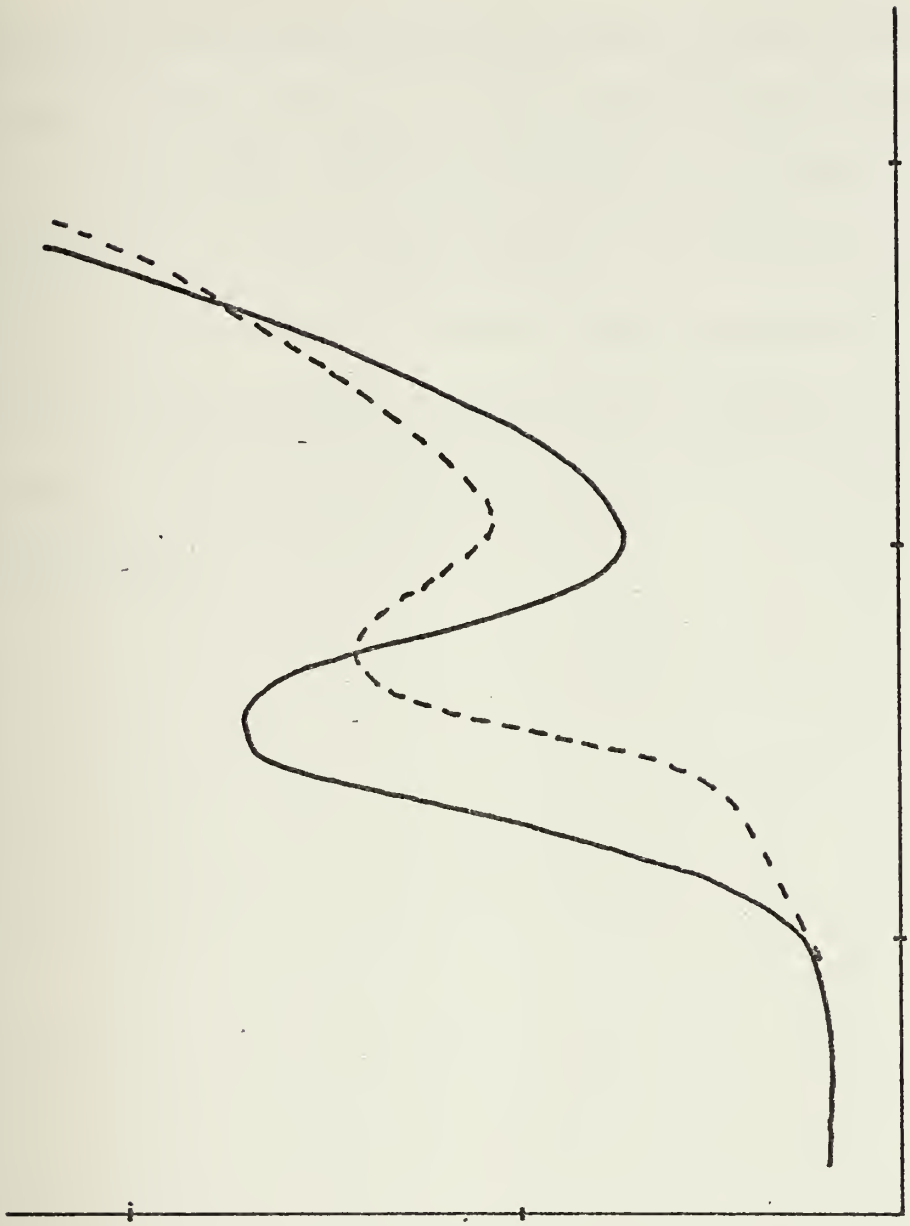

Figure 16. Vacuum ultraviolet absorption spectrum of $KMgF_3$:Co. Crystal thickness is .87 mm. Solid line - room temperature. Dashed line - 4.2° K.

percent, which agrees with our estimate which was made by comparing the $^4T_{1g}$ to $^4T_{1g}$ oscillator strength as described previously.

Last e in our work, we received several additional samples of $KMgF_3$:Co from D. Hukin of Oxford. These samples had been grown by him, and were of varying cobalt concentration. Their absorption spectra were quite identical to the spectra obtained using the crystal given by Sturge, and served to reaffirm our assignments.

H. $KMgF_3$: Lattice Defects

Two highly improbable circumstances were considered as sources of some of the broad structureless absorption bands which were not readily assignable as d-d transitions in transition metal doped $KMgF_3$.

The first possibility was that, by subjection of our crystals to vacuum ultraviolet radiation in the course of absorption experiments, lattice defects were produced. Perhaps a large concentration of such defects could be produced by a long term irradiation, and perhaps such defects were "color centers", that is, they might absorb energy in the spectral region of our studies.

A second and rather unlikely possibility was that, at some time in the history of our crystals, several had been subjected to ionizing radiation. This radiation might have been the source of color centers in our samples. The fact that the history of almost every crystal studied was thoroughly known made this possibility extremely unlikely, yet we did not want to dismiss even such an improbable eventuality without a test on our part.

Three studies that relate to the problem of radiation damage in $KMgF_3$ have been reported in the literature. The initial work was that of Hall[25] who reported the possibility of V_k centers being

formed in $KMgF_3$ that had been subjected to x irradiation. Later, Hall and Leggeat[26] used esr, optical absorption, and polarized emission techniques to study x irradiated $KMgF_3$. They assigned an optical absorption band at 2800 Å, which corresponded to an esr resonance at g = 2, to an F center, analogous to similar centers in alkali halides. In addition, a 4400 Å band was tentatively assigned to an M center, which consists of two adjacent F centers. Riley and Sibley[27] followed with a detailed study of such defects in electron or ^{60}Co gamma irradiated $KMgF_3$. Through polarized bleaching experiments and measurements of band temperature dependence, they assigned visible and near ultraviolet absorption bands to F centers, F_2 centers (M centers), F_3 centers, and V_k centers. With these studies as background material, we proceeded to test each of the rather unlikely possibilities mentioned above.

First, we subjected a crystal of undoped $KMgF_3$ to vacuum ultraviolet radiation produced by our rare gas sources. After a period corresponding to two times the normal irradiation period of a typical absorption experiment, the near and far ultraviolet absorption spectra were obtained. Several transition metal doped samples of $KMgF_3$ were also used in the same type of experiment. No changes in the absorption spectra were observed after irradia-

tion, therefore our vacuum ultraviolet sources were not the cause of any measurable color centers.

Secondly, we wanted to determine if ionizing radiation could possibly produce any of the absorption bands we had found in our samples. A comparison of the visible and near ultraviolet absorption spectra of x irradiated $KMgF_3$ published by Riley and Sibley, with our spectra of transition metal doped $KMgF_3$, showed that the near ultraviolet absorption band in our $KMgF_3$:Cr looked suspiciously like the F center absorption band.

We proceeded then to intentionally form lattice defects in our undoped $KMgF_3$ sample. The crystal of $KMgF_3$ that showed the flat spectrum of Figure 2 was x irradiated for sixty minutes, through the use of irradiation equipment of Professor B. Royce of Princeton University. The x ray tube utilized a tungsten target, the tube was operated at 90 kV and 21 milliamperes, and the sample was located three centimeters from the target. This one hour room temperature irradiation produced the spectrum of Figure 17, which is similar to the spectrum of Riley and Sibley. The vacuum ultraviolet absorption experiment showed that no additional absorption bands resulted from this irradiation. A comparison between our $KMgF_3$:Cr crystal and the x irradiated $KMgF_3$ crystal showed

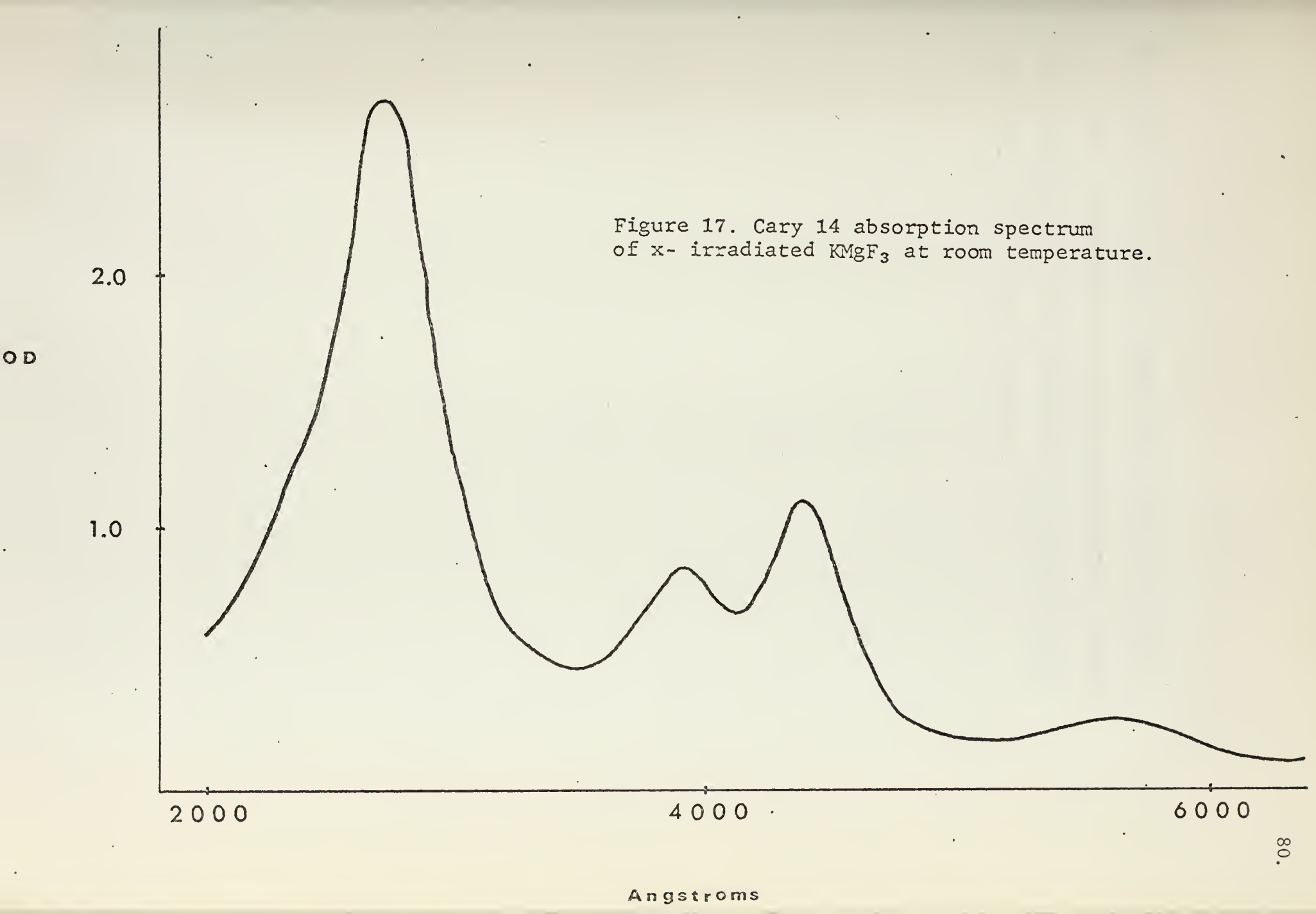

Figure 17. Cary 14 absorption spectrum of x- irradiated $KMgF_3$ at room temperature.

that the near ultraviolet absorption bands were not the same.

Our final conclusion from these experiments is that none of the absorption bands that we have found in transition metal doped $KMgF_3$ can be assigned to defect centers.

I. MgF_2

The host MgF_2 serves as an excellent window material for use in the vacuum ultraviolet region. It is second only to CaF_2 in its solubility in water, therefore its transmission properties do not deteriorate when the crystal is exposed to moisture in the air, as do the properties of lithium fluoride and sodium fluoride. MgF_2 is rugged, hard, and resists thermal and mechanical shock. For these reasons, it is often used as a window in the vacuum ultraviolet region, in the sense of performing the function of a vacuum seal while transmitting light. The transmission range is from 1100 Å through 7.5 microns.[28]

The crystal structure of MgF_2 is well known,[29] and that structure is shown in Figure 18. It is a rutile structure, with two formula units per unit cell. Because it is a uniaxial crystal, it exhibits birefringence, and this property has been well studied.[30] It is these combined properties of light transmission and birefringence that permit the construction of polarizers for the vacuum ultraviolet from MgF_2.

The final property of interest to us is that a transition metal ion impurity in a doped sample lies at a site of D_{2h} symmetry.

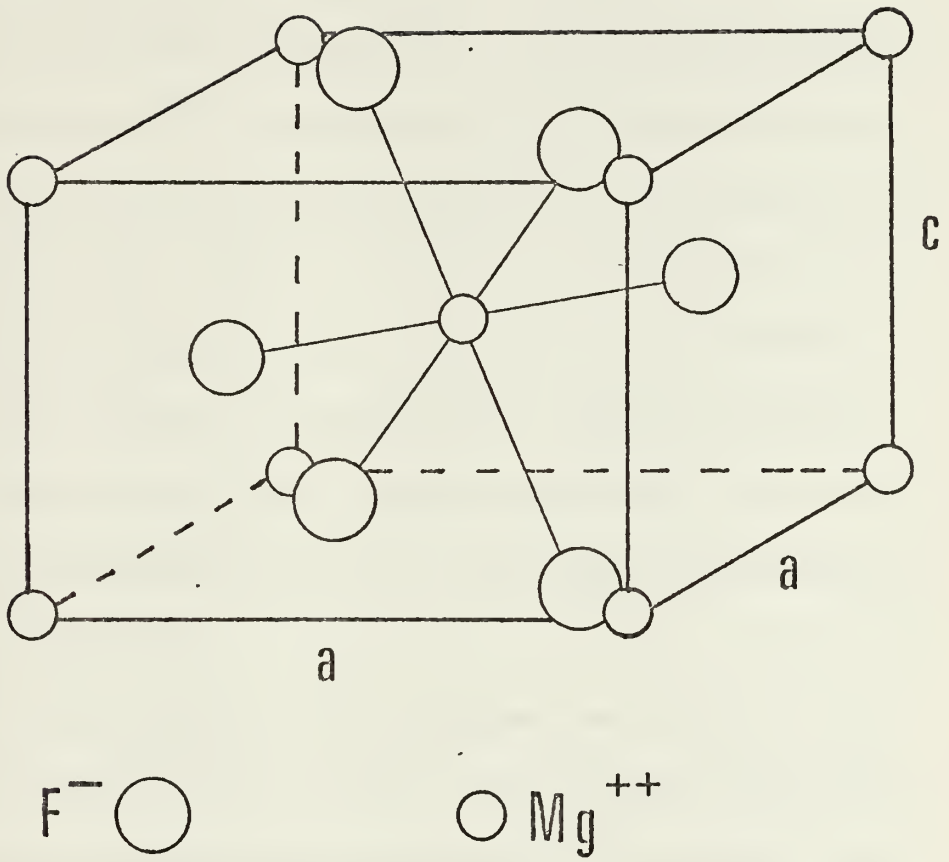

Figure 18. Crystal structure of MgF_2. Edge a is 4.625 Angstroms, edge c is 3.052 Angstroms.

J. MgF_2:Mn

In spite of the fact that it is difficult to introduce appreciable amounts of Mn (II) into the MgF_2 lattice,[31] we were able to obtain a relatively concentrated sample from R. Dietz of Bell Laboratories. This sample contains .23 weight percent Mn by wet chemical analysis. Because of the fact that all manganese d level transitions are spin forbidden in this system, no d-d absorption bands were observed in the range of the Cary 14 instrument (1950-26,000 Å). However, this manganese concentration was sufficiently high to enable us to observe one broad, structureless band in the vacuum ultraviolet region near 61,000 cm^{-1}. This single absorption band is shown in Figure 19.

Since the symmetry of the manganese ion is lowered from octahedral in $KMgF_3$ to D_{2h} in MgF_2, there existed the possibility that this absorption band might be polarized. We conducted a polarization experiment in the vacuum ultraviolet region and the results of that experiment are shown in Figure 20. The figure demonstrates clearly that no polarization effects are observable when the electric vector is either parallel or perpendicular to the MgF_2 c axis.

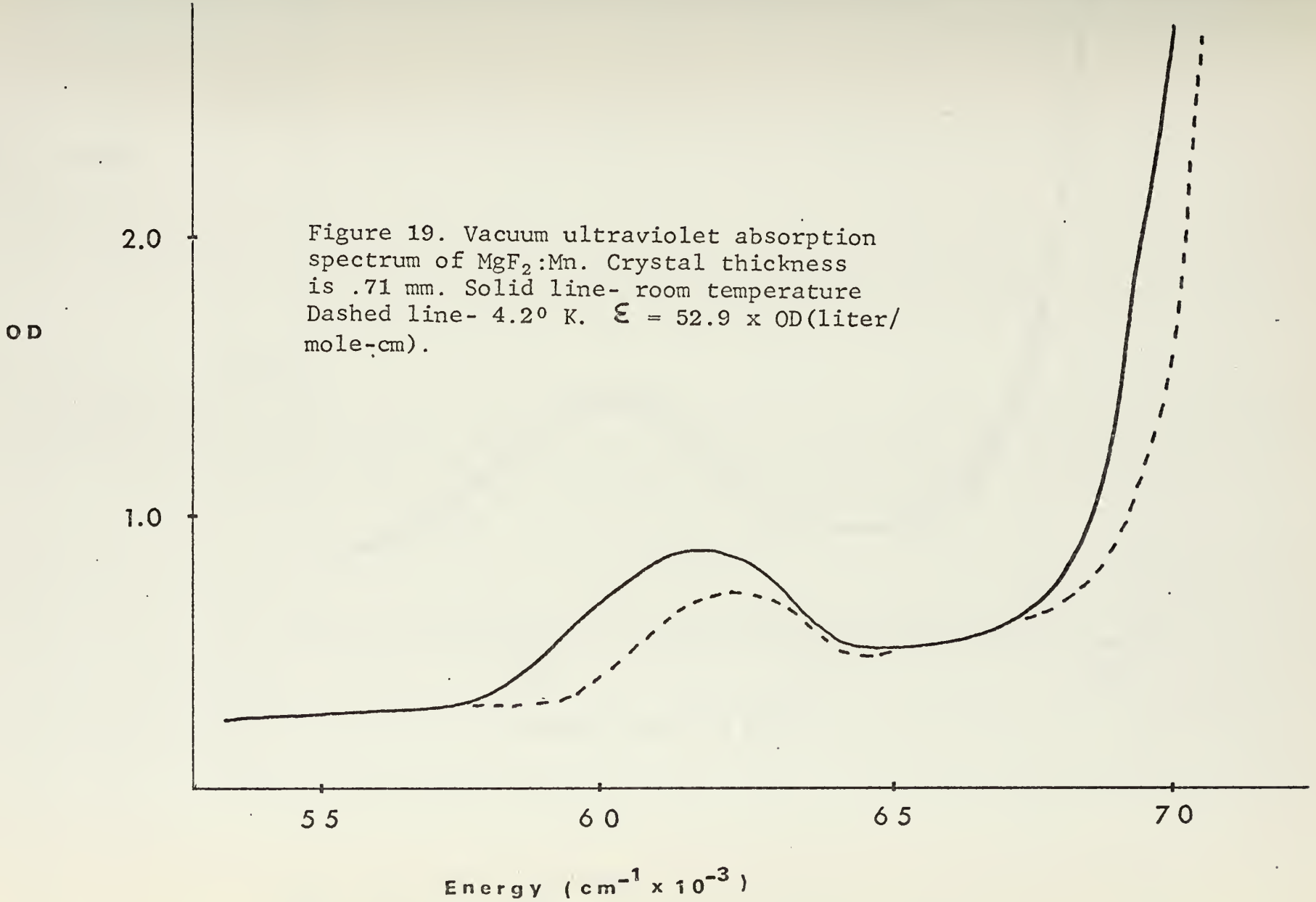

Figure 19. Vacuum ultraviolet absorption spectrum of MgF_2:Mn. Crystal thickness is .71 mm. Solid line- room temperature Dashed line- 4.2° K. ε = 52.9 x OD(liter/mole-cm).

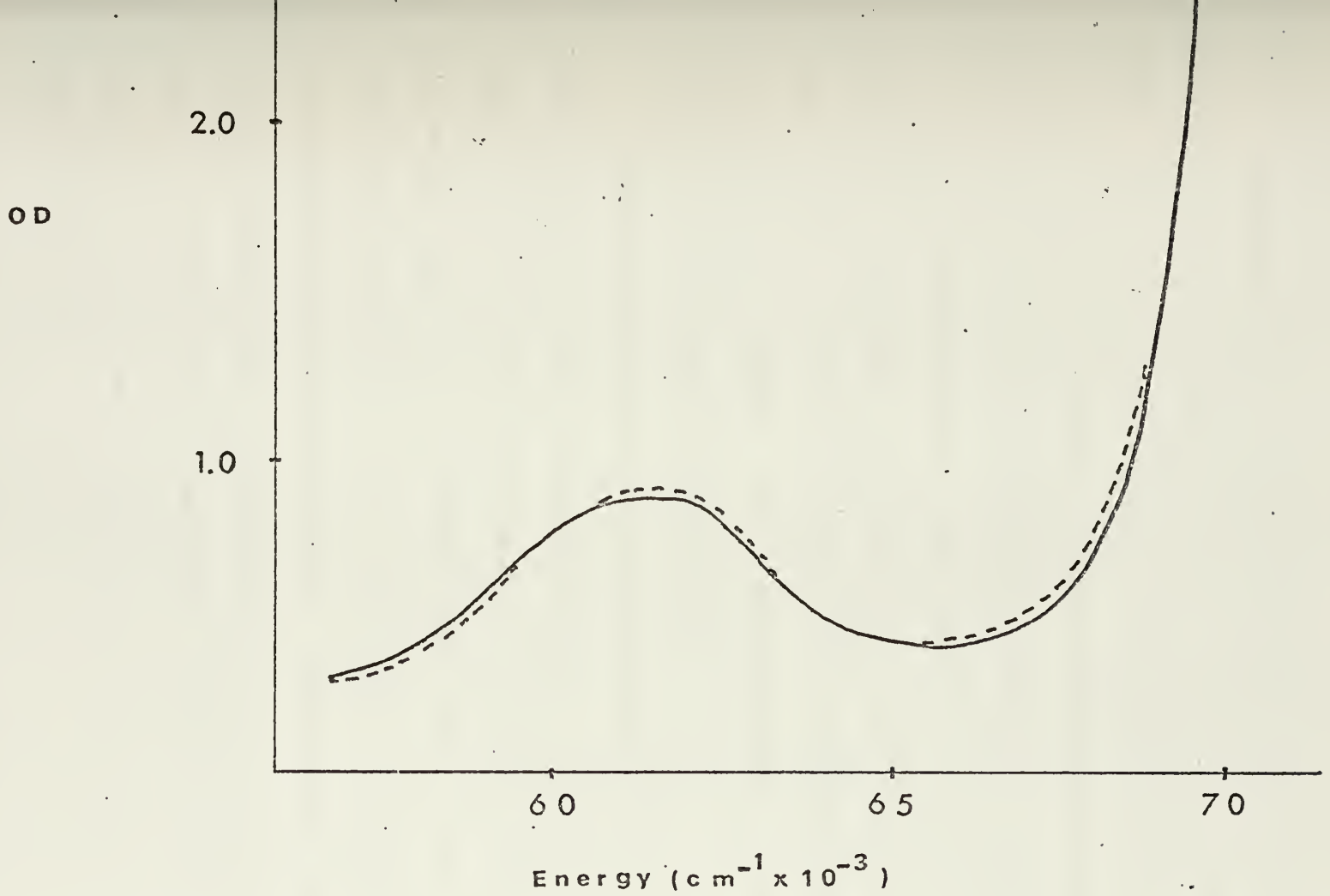

Figure 20. Room temperature absorption spectrum of MgF_2:Mn using plane polarized light. Crystal thickness is .71 mm.
Solid line E||to c axis. Dashed line E⊥ to c axis.

K. MgF_2:Fe

Analogous to the spectrum of $KMgF_3$:Fe, the near and far ultraviolet spectrum of MgF_2:Fe consists of several absorption bands. There is one major difference in the quality of the two systems, however. A chemical analysis of the MgF_2:Fe sample shows that iron is by far the predominant impurity ion, whereas the $KMgF_3$:Fe system contained a much higher ratio of iron to nickel ions. Specifically, the analysis shows that the MgF_2:Fe sample contains .56 weight percent iron and .01 weight percent each of nickel and vanadium. This crystal was kindly given to us by R.E. Dietz of Bell Laboratoratories.

As a first approximation, we can assume that the iron impurity ion sits at a site of octahedral symmetry. Therefore, this system, which has the configuration $t_{2g}^4 e_g^2$, should exhibit a low energy $^5T_{2g}$ to ^5E_g Jahn Teller split absorption band. No such band was found in our crystal, due to the combination of iron concentration and crystal thickness. All absorption bands that were observed were at energies greater than 22,000 cm^{-1}, which is much higher than the anticipated spin allowed d level transition. The near and far ultraviolet absorption bands are shown in Figure 21.

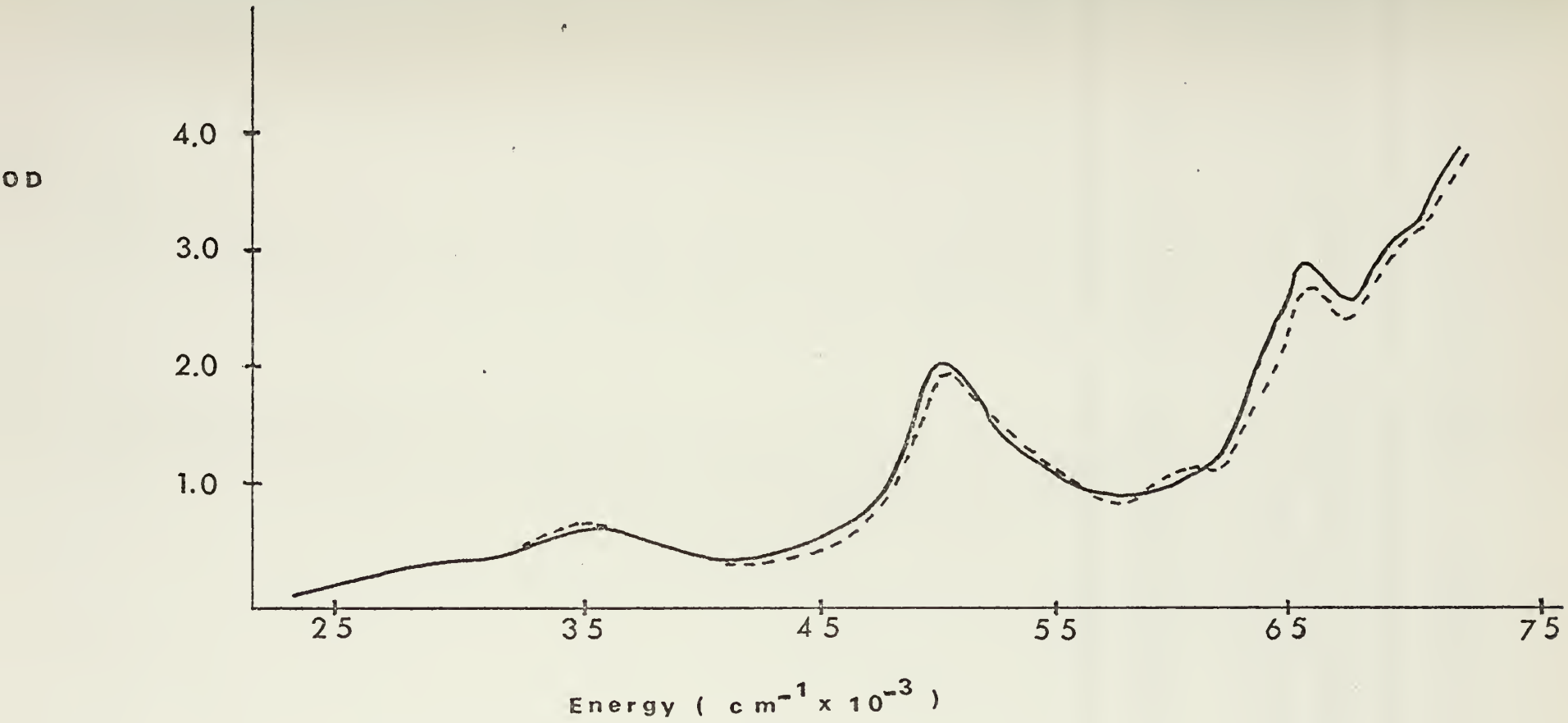

Figure 21. Near and far ultraviolet absorption spectrum of MgF_2:Fe. Crystal thickness is .57 mm. Solid line - room temperature. Dashed line - 4.2°K.

As with the MgF_2:Mn sample, an experiment to determine the polarization properties of these bands was attempted, since the actual site symmetry is D_{2h} and not O_h. We directed the electric vector of our plane polarized light parallel and perpendicular to the crystal c axis.

None of the absorption bands showed any preference for absorbing light polarized in the parallel or perpendicular direction.

L. MgF_2:Co

Two crystals of cobalt doped into the magnesium fluoride lattice were studied. One was given to us by R. E. Dietz of Bell Laboratories, and one by W. A. Sibley of Oklahoma State University. Both samples showed identical spectra, and the work on MgF_2:Co (Sibley) will be shown here. This particular sample came to us as a highly polished and well characterized one, with a known concentration of 2.0 mole percent cobalt.

The d-d transitions in MgF_2:Co have been widely studied,[31,32,33,34] and are sufficiently separated in energy from the vacuum ultraviolet band which we found to be of no problem in band assignment. That absorption band is shown in Figure 22.

An absorption experiment with plane polarized light showed no polarization effects in this band.

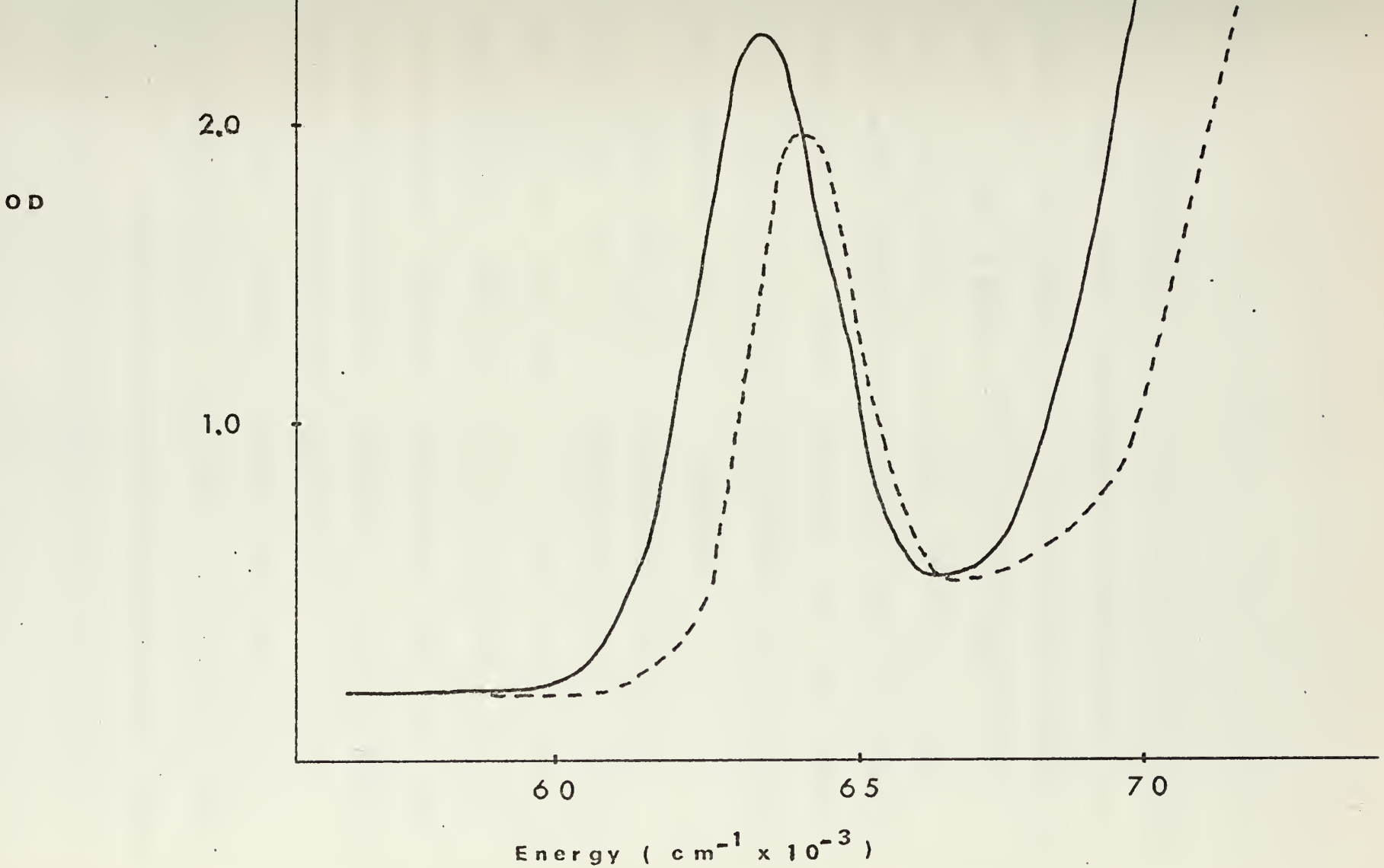

Figure 22. Vacuum ultraviolet absorption spectrum of MgF_2:Co (Sibley). Crystal thickness is .68 mm. Solid line- room temperature. Dashed line- 4.2° K
ε = 14.45 x OD (liter/mole-cm)

M. CaF_2

Calcium fluoride meets the requirements of a host material for a vacuum ultraviolet study of impurity transition metal ions quite well. It has a hardness of 4.0 on the Moh scale, which means that one can obtain a highly polished surface through the use of diamond polishing grit. Once polished, it will retain an optical quality surface indefinitely when subjected to the normal laboratory environment of water, vacuum grease, tape, etc. Also, calcium fluoride is the second best high energy window material commonly used, transmitting from 1250 Å to 9 microns.

The structure of this host can be easily visualized as a series of cubes, the corners of which are fluoride ions. At every other body center is the calcium ion, at a site of cubic (eight coordinated) symmetry. With this structure, the fluoride ions are at a site of tetrahedral symmetry. When an impurity ion of +2 charge is introduced into the lattice, it displaces a calcium ion, and therefore it too is subjected to cubic (O_h) symmetry.

In the case of titanium, vanadium, and chromium ions as impurities in this host, the more stable oxidation state is found to be +3.[1] To compensate for an ion of +3 charge replacing a calcium ion of +2 charge, an extra fluoride ion becomes situated at an

adjacent, formerly empty, body center position. This charge compensating fluoride ion then adds a tetragonal component to the cubic crystal field. For the ions in the second half of the first row transition series (including manganese), the +2 state is the more stable one, thus there is no requirement for the interstitial fluoride charge compensator.

One interesting aspect of CaF_2 is that it cleaves easily, along a (1 1 1) plane. Unfortunately, it has been found that thermal shock can initiate this cleavage, thus introducing the possibility of destruction of a sample while cooling from room temperature to liquid helium temperature prior to obtaining the low temperature absorption spectrum. Through trial and error, we determined that we could cool our samples of approximately one millimeter thickness by 10 millimeter diameter dimensions at a cooling rate of up to $6^{\circ}K$ per minute without shattering. This figure is a lower limit, that is, we did not shatter (cleave) any samples at cooling rates at or below this value, nor did we attempt a more rapid cooling rate.

This point is emphasized because Optovac, in its description of optical crystals available for purchase from that company, goes to great lengths to warn one of the possible effects of thermal

shock on calcium fluoride.[28] We found no such effects under the conditions cited previously.

Finally, calcium fluoride does have one disadvantage in a study of this type. It is both indiscriminate and voracious as a solvent for metal ions. Of approximately twenty transition metal doped samples obtained from H.A. Weakliem of RCA Laboratories, Princeton, New Jersey, and Optovac, Inc., only two were of high enough purity to present in this work.

N. CaF_2:Mn

Under the influence of the crystal field brought about by the fluoride ions in the calcium fluoride lattice, the d orbitals split into two degenerate sets t_{2g} and e_g. In contrast to the results in an octahedral field, the e_g orbitals are the lower orbitals in energy in this eight coordinated system. In a high spin system such as CaF_2:Mn then, the five electrons of the d shell fill first the e_g orbitals with two electrons of parallel spin, and then the t_{2g} orbitals with parallel spin giving the $e_g^2\ t_{2g}^3$ configuration and a $^6A_{1g}$ ground state. Since there are no spin allowed d-d transitions, the CaF_2:Mn crystal is transparent to the eye, and, at manganese concentrations appropriate for our work, transparent throughout the spectral regions of the Cary 14 instrument.

We purchased a sample of CaF_2:Mn from Optovac, Inc., and because of the transparency described above, we obtained the esr spectrum at 77°K in order to determine whether the manganese ion was indeed present. Our results were quite similar to those published by Baker, Bleany and Hayes,[35] indicating that our crystal does contain manganese in the plus two oxidation state. We then obtained the vacuum ultraviolet absorption spectrum at room temperature and liquid helium temperature, and the results are shown

in Figure 23. Upon completion of these experiments, we forwarded the crystal to Schwartzkopf Microanalytical Laboratory for analysis. The results show that this is a double doped system. There is .065 weight percent manganese and .020 weight percent iron. Because of the low iron concentration, no iron d-d bands were detectable on the Cary 14.

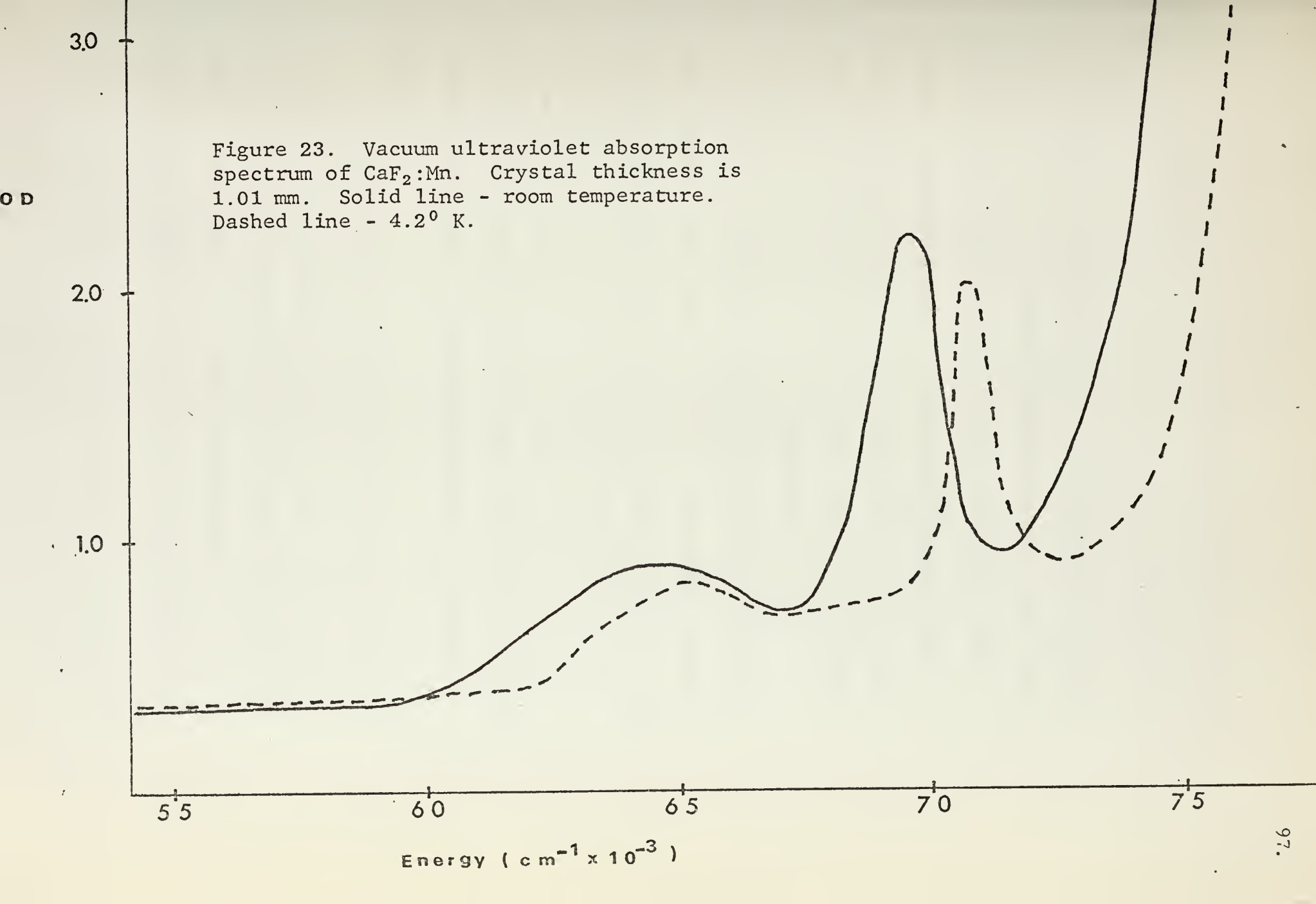

Figure 23. Vacuum ultraviolet absorption spectrum of CaF_2:Mn. Crystal thickness is 1.01 mm. Solid line - room temperature. Dashed line - 4.2° K.

O. CaF_2:Co

The optical absorption spectrum of cobalt doped calcium fluoride was originally reported by Stahl-Brada and Low,[36] who assigned the absorption bands to d orbital transitions. Later, Weakliem repeated this work and also concluded that the data could be well understood within the framework of a crystal field acting on the d orbitals.[1] However, both of these investigations were limited to the spectral region below 50,000 cm^{-1}.

We were fortunate to receive from Weakliem for our use a very attractive pink crystal of CaF_2:Co. The cobalt concentration of the bulk of this sample was much too high for our use, however, a rather large concentration gradient existed. From the most weakly doped portion, we were able to cleave a thin slice that showed both the most intense d level transition and a vacuum ultraviolet transition. The high energy transition is shown in Figure 24.

At the completion of our absorption experiments, we split the crystal, retained one piece for future work, and forwarded the second piece to Schwartzkopf Microanalytical Laboratory for analysis. They reported the cobalt ion concentration at .077 weight percent. This value must be met with some skepticism

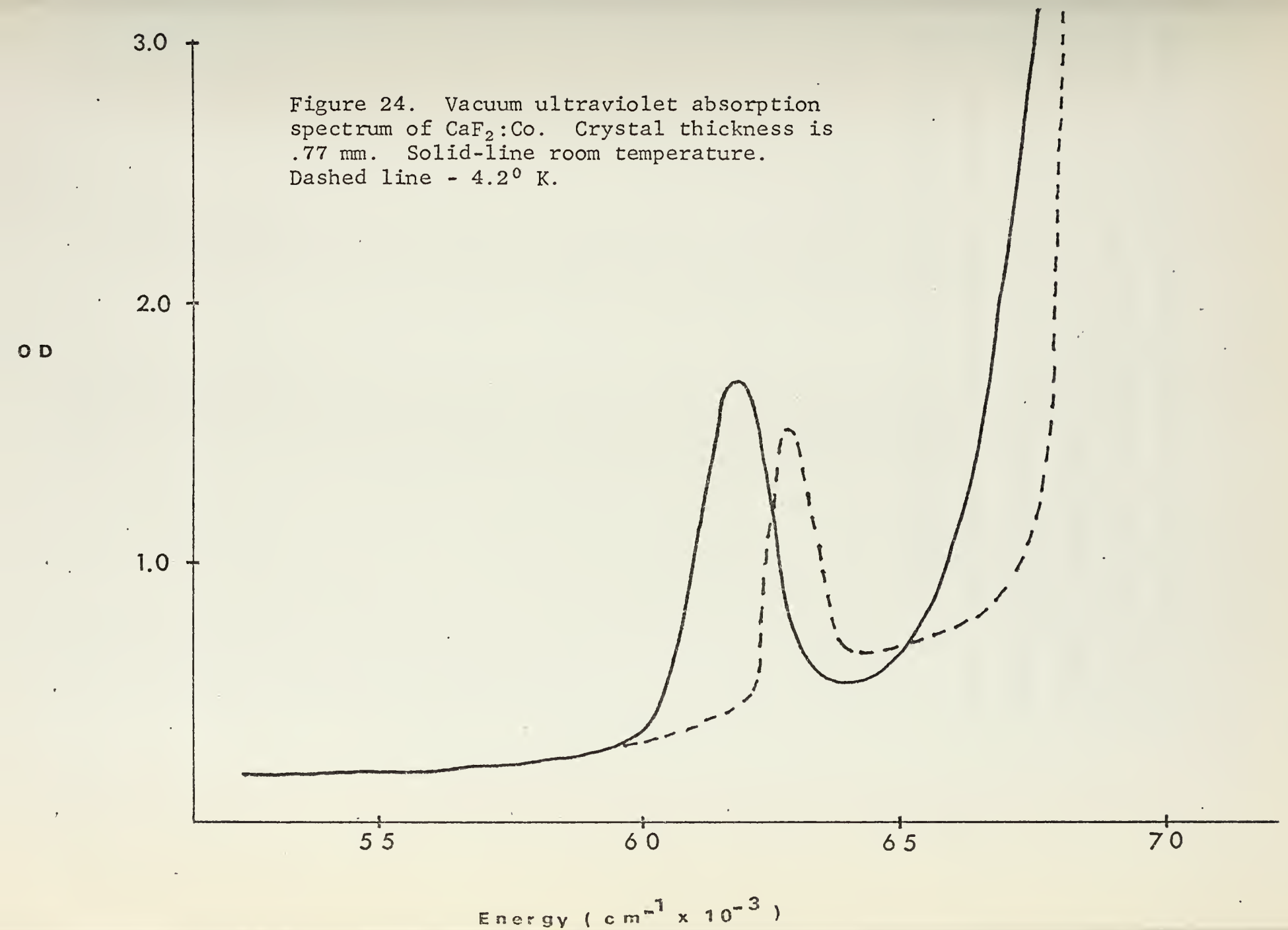

Figure 24. Vacuum ultraviolet absorption spectrum of CaF_2:Co. Crystal thickness is .77 mm. Solid-line room temperature. Dashed line - 4.2° K.

because of the large concentration gradient of the original sample. However, since approximately half of the crystal whose spectrum is shown in Figure 24 was utilized in this analysis, and since the crystal was split along a direction perpendicular to the gradient, it is reasonable to assume that the .077 percent cobalt concentration represents fairly accurately the entire crystal.

P. Temperature Dependence

A method of determining whether an electronic transition is allowed or forbidden in the first approximation is to monitor the total integrated intensity as a function of temperature. For an allowed transition, as the temperature is lowered, the oscillator strength remains the same. This is so, because as the ground state vibrational level becomes more highly populated at the expense of higher energy vibrational levels, the transition from n = 0 vibrational level to the excited state n = 0 vibrational level makes up for the loss in oscillator strength from the n = 1 to n = 1 and n = 2 to n = 2 transitions.

However, for a forbidden transition, we must invoke a perturbation theory approach to explain the associated temperature dependence. We assume that some perturbing vibrational mode mixes electronic states of parity differing from the ground electronic state into the ground electronic state. This serves to give an odd (ungerade) ground state some even (gerade) character and vice versa. Therefore, although the pure electronic transition which is of g to g or u to u character gives a transition moment of zero, the admixed ground state allows some contributions from u to g or g to u transitions. Thus, these transitons, although

weak, are observable. In addition, as one goes from low to high temperatures, the thermal energy becomes distributed among higher energy vibrations, some of which may be the effective perturbing vibrations mentioned above. We therefore see an increase in oscillator strength as temperature increases, and the low energy portion of the band becomes more pronounced.

Speaking more quantitatively, several attempts have been made to postulate a model for the temperature dependence, and from that model deduce a mathematical description. Liehr and Ballhausen[37] have proposed that the oscillator strength is proportional to $\coth \frac{h\nu}{2kT}$ where $h\nu$ is the energy of the perturbing vibration. Although the approximations made in this approach seem too restrictive to permit this function to accurately represent the oscillator strength over a large temperature range,[38] we can expect reasonable agreement over a more limited range, perhaps from liquid nitrogen temperature to room temperature.

As an attempt to determine if we could associate a perturbing vibration as obtained from a hyperbolic cotangent function with a measured lattice vibration, we obtained the absorption spectra for $KMgF_3$:Co over the temperature range 65-300°K. $KMgF_3$:Co was picked for this experiment because the vacuum

ultraviolet absorption band in this system is isolated from other bands. In contrast with many of the other high energy absorptions presented previously, this band is not superimposed on a rapidly rising cutoff edge. For these reasons, we felt that we could obtain accurate integrated intensities of this particular band.

The results of this experiment are presented in Figure 25. Note that the best fit is obtained for a vibrational energy of 315-325 cm^{-1}. Assuming that the transition metal d orbitals are involved in this band, and that the transition is indeed a forbidden one, we look for odd parity vibrations of the crystal. Four such vibrations are predicted for the perovskite lattice, three of which are T_{1u} and infrared active and one of which is T_{2u} and not infrared active.[39] These vibrational energies are 156, 300, $\approx$ 330, and 478 cm^{-1}.

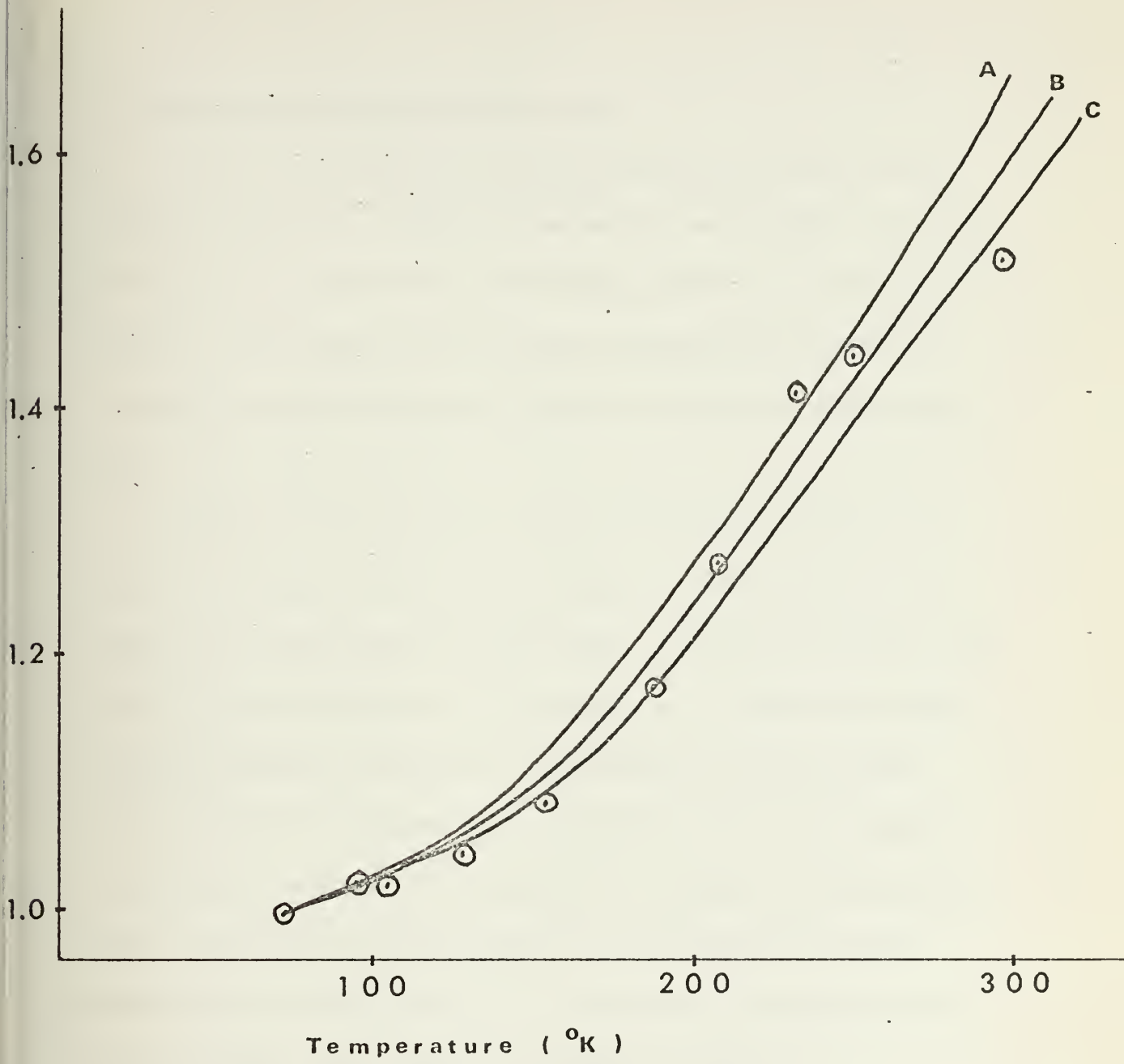

Figure 25. Ratio of oscillator strength at some temperature to oscillator strength at 65° K, vs. temperature for the vacuum ultraviolet absorption band in $KMgF_3$:Co. Circles are data points. Three curves of coth $\frac{E_{vib}}{2kT}$ are plotted. Curve A for E_{vib} = 300 cm^{-1}. Curve B for E_{vib} = 315 cm^{-1}. Curve C for E_{vib} = 330 cm^{-1}.

Q. Summary of Absorption Spectra Data

The room temperature and low temperature band maxima, maximum extinction coefficient, bandwidth, and oscillator strength for the metal ion impurities in the $KMgF_3$ lattice are presented in Table II. These data represent those absorption bands that have not been previously assigned as the d to d transitions of the metal ion.

Based on arguments that will be detailed in Chapters III and IV, we assign the two highest energy absorption bands in the $KMgF_3$:Fe samples (which contain nickel impurity) to the $KMgF_3$:Ni system, and Table II reflects this assignment. The values of extinction coefficient, bandwidth, and oscillator strength for this system are merely estimates, since we must arbitrarily subtract an absorption baseline corresponding to a steeply rising absorption edge. An arbitrary baseline must also be subtracted from the highest energy band in $KMgF_3$:Cr, and limits on the value of oscillator strength for this band are presented in Table II.

In Tables III and IV, we summarize the absorption spectra data for the impurity ions in the MgF_2 and CaF_2 hosts respectively. With respect to Table IV, there are no extinction coefficient and oscillator strength tabulations for CaF_2:Mn + Fe, because this

system has not been completely studied. This crystal, which was the only one of seven purchased from Optovac Inc. that gave rise to a resolvable vacuum ultraviolet absorption band, was subjected to a destructive test for manganese and iron ions only. In retrospect this was an error, for both ions were found to be present, and both were of relatively high concentration. It is not known which other transition metal ions are present, if any, and since our experience with Optovac grown calcium fluoride crystals indicates possible contamination, we cannot with any degree of confidence assign both of the absorption bands.

Because the data that will be most useful in the interpretation that follows are associated with the transition metal ion series in $KMgF_3$, those absorption bands are shown, for ease of comparison, in Figure 26.

Table II

Energy maxima, band width at half height, maximum extinction coefficient and oscillator strength (as $f = 4.6 \times 10^{-9} \varepsilon_{max} \times$ (half width)) for transition metal ions in $KMgF_3$.

System	Band Maxima (cm^{-1})	Width at half height (cm^{-1})	Maximum Extinction Coefficient (liters/mole-cm)	Oscillator Strength
$KMgF_3$:V	38,500 (300°K)	6360	13.25	3.9×10^{-4}
	38,500 (77°K)	6360	13.25	3.9×10^{-4}
	47,600 (300°K)	7720	45.2	1.61×10^{-3}
	47,900 (77°K)	7720	34.4	1.23×10^{-3}
	65,400 (300°K)	5300	294	8.27×10^{-3}
	65,800 (4.2°K)	5000	290	7.8×10^{-3}
$KMgF_3$:Cr	36,500 (300°K)	6000	17.1	4.74×10^{-4}
	36,500 (77°K)	5500	18.6	4.70×10^{-4}
	59,200 (300°K)	7750 - 8800	12.0 - 16.5	4.3 - 6.7×10^{-4}

Table II - continued

System	Band Maxima (cm^{-1})	Width at half height (cm^{-1})	Maximum Extinction Coefficient (liters/mole-cm)	Oscillator Strength
$KMgF_3$:Cr	59,200 (4.2°K)	7200 - 8200	12.0 - 16.5	4.0 - 6.2×10^{-4}
$KMgF_3$:Mn	60,200 (300°K)	3700	28.4	4.84×10^{-4}
	60,600 (4.2°K)	3300	14.2	2.15×10^{-4}
$KMgF_3$:Fe	45,250 (77°K)	3640	25.6	4.3×10^{-4}
(Optovac)	49,000 (300°K)	4410	58.5	1.19×10^{-3}
	49,450 (77°K)	3200	52.5	7.74×10^{-4}
	56,800 (300°K)	5960	77.9	2.14×10^{-3}
	57,000 (4.2°K)	4240	99.4	1.93×10^{-3}
$KMgF_3$:Co	62,700 (300°K)	2650	62.9	7.66×10^{-4}
	63,800 (4.2°K)	2280	52.5	5.51×10^{-4}

Table II - continued

System	Band Maxima (cm^{-1})	Width at half height (cm^{-1})	Maximum Extinction Coefficient (liters/mole-cm)	Oscillator Strength
$KMgF_3$:Ni	64,000 (300°K)	Estimated limits are 2900 - 3300	45.5 - 54.0	6.06×10^{-4} - 7.8×10^{-4}
	65,000 (4.2°K)	for both temperatures		
	68,100 (300°K)	Estimated limits are 2900 - 3500	54.0 - 65.5	7.6×10^{-4} - 1.05×10^{-3}
	68,500 (4.2°K)	for both temperatures		

Table III

Energy maxima, band width at half height, maximum extinction coefficient and oscillator strength (as $f = 4.6 \times 10^{-9} \varepsilon_{max} \times$ (half width)) for transition metal ions in MgF_2.

System	Band Maxima (cm^{-1})	Width at half height (cm^{-1})	Maximum Extinction Coefficient (liters/mole-cm)	Oscillator Strength
MgF_2:Mn	62,000 (300°K)	4130	26.4	5.02×10^{-4}
	62,500 (4.2°K)	3080	16.9	2.39×10^{-4}
MgF_2:Fe	27,500 (300°K)	4200	16.5	3.18×10^{-4}
	28,200 (4.2°K)	4000	16.7	3.08×10^{-4}
	34,800 (300°K)	7500	32.6	1.12×10^{-3}
	35,100 (4.2°K)	6500	33.2	9.9×10^{-4}
	49,900 (300°K)	5800	104	3.77×10^{-3}
	50,500 (4.2°K)	5300	99	2.41×10^{-3}
	54,300 (300°K)	(inflection)		

Table III - continued

System	Band Maxima (cm^{-1})	Width at half height (cm^{-1})	Maximum Extinction Coefficient (liters/mole-cm)	Oscillator Strength
MgF_2:Fe	54,300 (4.2°K)	(inflection)		
	60,100 (4.2°K)	est. 3500		
	65,100 (300°K)	6000	66	1.81×10^{-3}
	65,900 (4.2°K)	5500	58	1.46×10^{-3}
	68,900 (300°K)	(inflection)		
	68,900 (4.2°K)	(inflection)		
MgF_2:Co	63,400 (300°K)	2690	29	3.59×10^{-4}
	64,200 (4.2°K)	2020	23.6	2.19×10^{-4}

Table IV

Energy maxima, band width at half height, maximum extinction coefficient and oscillator strength (as $f = 4.6 \times 10^{-9} \varepsilon_{max} \times$ (half width)) for transition metal ions in CaF_2.

System	Band Maxima (cm^{-1})	Width at half height (cm^{-1})	Maximum Extinction Coefficient (liters/mole-cm)	Oscillator Strength
CaF_2:Fe+Mn	65,400 (300°K)	4230		
	65,000 (4.2°K)	3080		
	69,500 (300°K)	1630		
	70,700 (4.2°K)	980		
CaF_2:Co	61,600 (300°K)	1660	468	3.58×10^{-2}
	62,700 (4.2°K)	1200	334	1.84×10^{-2}

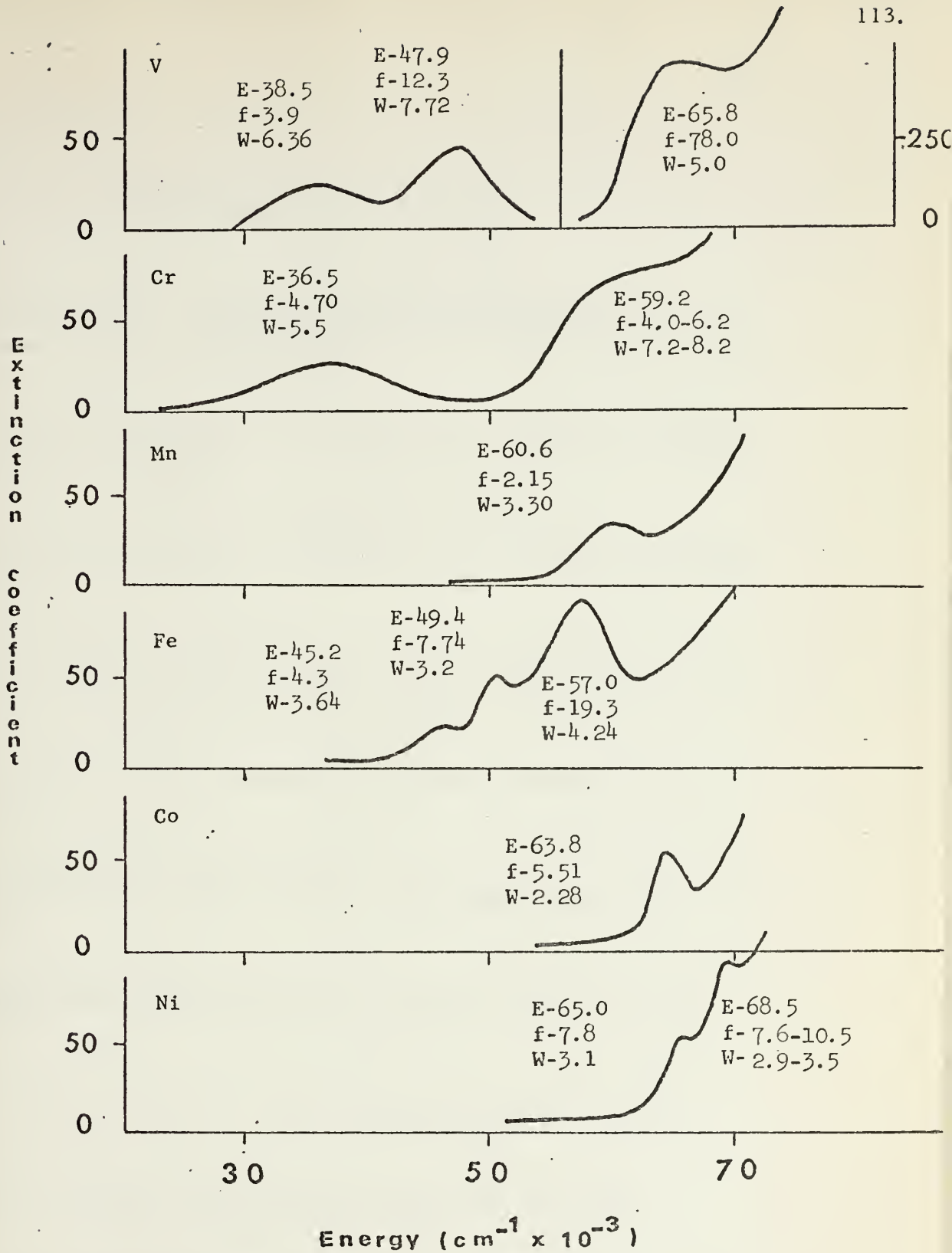

Figure 26. Low temperature (4.2°K and 77°K) absorption spectra of transition metal ions in $KMgF_3$. Refer to Table II for the actual temperatures for each specific crystal. Each band is labeled by three vertical numbers. The upper number indicates the band maximum (E- cm^{-1} x 10^{-3}). The middle number indicates the oscillator strength(f- x 10^{-4}). The lowest value is the bandwidth(W- cm^{-1} x 10^{-3}).

REFERENCES TO CHAPTER II

1. H.A. Weakliem, Systematic Study of the Crystal Field of CaF_2, ARPA Order No. 306-62 (1964)

2. T.P. Hall, W. Hayes, R. Stevenson and J. Wilkens, J. Chem. Phys. 38, 1977 (1963)

3. T.P. Hall, W. Hayes, R. Stevenson and J. Wilkens, J. Chem. Phys. 39, 35 (1963)

4. M.D. Sturge, F.R. Merritt, L.F. Johnson, H.J. Guggenheim, and J.P. van der Ziel, J. Chem. Phys. 1, 405 (1971)

5. M.D. Sturge, Bell Laboratories, personal communication (1973)

6. C.J. Ballhausen and F. Winther, Acta Chem. Scand. 13, 1729 (1959)

7. M.D. Sturge, Bell Laboratories, personal communication (1972)

8. J.P. Fackler and D.G. Holah, Inorg. Chem. 4, 954 (1956)

9. See J. Ferguson, Progr. Inorg. Chem. 12, 237 (1970)

10. S. Ogawa, J. Phys. Soc. Japan 15, 1475 (1960)

11. M.D. Sturge, Bell Laboratories, personal communication (1972)

12. G.P. Jones, Phys. Rev. 155, 259 (1967)

13. K. Knox, R.G. Shulman and S. Sugano, Phys. Rev. 130, 512 (1963)

14. J. Ferguson, H.J. Guggenheim and D.L. Wood, J. Chem. Phys. 40, 822 (1964)

15. J. Ferguson and H.J. Guggenheim, J. Chem. Phys. 44, 1095 (1966)

16. J. Ferguson, Australian J. Chem. 21, 323 (1968)

17. W.A. Sibley, Oklahoma State University, personal communication (1972)

18. J.H. Thornley, C.G. Windsor and J. Owen, Proc. Roy. Soc. (London) Ser. A 284, 252 (1964)

19. N. Nesterova, I.G. Senii, R.V. Pirasev and P.P. Syrnikov, Sov. Phys. Solid State 9, 15 (1967)

20. C.J. Ballhausen and C.K. Jorgensen, Acta Chem. Scand. 9, 397 (1955)

21. O.G. Holmes and D.S. McClure, J. Chem. Phys. 26, 1686 (1957)

22. J. Ferguson, D.L. Wood and K. Knox, J. Chem. Phys. 39, 881 (1963)

23. M.D. Sturge, Phys. Rev. B 4, 2092 (1971)

24. F.A. Cotton and M.D. Meyers, J. Am. Chem. Soc. 82, 5023 (1960)

25. T.P. Hall, Brit. J. Appl. Phys. 17, 1011 (1966)

26. T.P. Hall and A. Leggeat, Solid State Commun. 7, 1657 (1969)

27. C.A. Riley and W.A. Sibley, Phys. Rev. B 1, 2789 (1970)

28. Optovac Inc., Bulletin 50, (1969)

29. J. Ferguson, H.J. Guggenheim, H. Kamimura and Y. Tanabe, J. Chem. Phys. 42, 775 (1965)

30. V. Chandrasekharan and H. Damay, Appl. Optics 8, 671 (1969)

31. L.A. Kappers, S.I. Yun and W.A. Sibley, Phys. Rev. Letters 29, 943 (1972)

32. L.F. Johnson, R.E. Dietz and H.J. Guggenheim, Appl. Phys. Letters 5, 21 (1964)

33. H. Kamimura and Y. Tanabe, J. Appl. Phys. 34, 1239 (1963)

34. H.M. Gladney, Phys. Rev. 146, 253 (1966)

35. J.M. Baker, B. Bleany and W. Hayes, Proc. Roy. Soc. A 247, 141 (1958)

36. R. Stahl-Brada and W. Low, Phys. Rev. 113, 775 (1959)

37. A.D. Liehr and C.J. Ballhausen, Phys. Rev. 106, 1161 (1957)

38. J. Ferguson, Progr. Inorg. Chem. 12, 159 (1970)

39. G.R. Hunt, C.H. Perry and J. Ferguson, Phys. Rev. 134, 688 (1964)

CHAPTER III

BACKGROUND

A. Introduction

The high energy absorption bands which have been detailed in Chapter II are the result of a charge transfer process, which, in a first approximation, can be visualized as an excitation of an electron from an orbital belonging primarily to one center, to an orbital belonging primarily to a second center. In the fluoride systems studied here, we can be more specific in defining the charge transfer process, and two distinct possibilities exist. In one situation, the transition metal ion serves as an electron acceptor, and the electron is transferred from a molecular orbital composed primarily of fluoride p orbitals, to the transition metal d orbital. The alternate possibility is that in which the transition metal ion is the electron donor, and the electron terminates in the host crystal conduction band or in an antibonding ligand molecular orbital.

The theoretical framework for understanding these two possible processes will be presented in this chapter, as will the

resultant expectations or predictions based upon each model. In Chapter IV we will compare the experimental data with these expectations and make specific assignments of the charge transfer process in each system studied. We will find that the transition metal to conduction band process is the dominant one in our systems.

It is important to be aware of the fact that previous data on inorganic charge transfer systems are sparse, especially when compared to the great quantity of work which has been done on d to d transitions. These relatively localized transitions yield much information about the d shell and its various interactions, but they give little information on orbitals more involved in chemical bonding, such as the ligand p orbitals. Charge transfer transitions make possible a more thorough understanding of these bonding orbitals, and in some cases permit one to obtain information on higher energy antibonding orbitals.

One of the reasons for the lack of data in the area of charge transfer transitions is the difficulty in interpretation. The d-d transitions lend themselves to a well tested perturbation theory approach, which in turn permits believeable numerical calculations. On the contrary, there does not exist one such straightforward approach in the interpretation and calculation of charge

transfer transitions. In this area we are concerned with a many center excitation, which requires either a molecular orbital approach or a band theory approach, each with its concomitant mathematical complexities.

One caution in the use of the terminology "charge transfer" is in order. We do not know the detailed electronic distribution in many electron systems such as have been studied here. We also do not know specifically how such a distribution changes with a transition described above. Therefore the phrase charge transfer should be thought of as representing a type of many center transition, and not as representing the true state of electronic distribution.

B. The Transition Metal as an Electron Acceptor

The previous charge transfer data available concerning transition metal ion halide and transition metal ion oxide systems have all been interpreted as arising from fluoride or oxide 2p orbital to transition metal d orbital excitations. We can express this process as a host valence band to transition metal impurity transition, or as a transition from a molecular orbital composed of ligand p orbitals to a molecular orbital or primarily transition metal parentage. The molecular orbital viewpoint is considered the more applicable, implying that the impurity ion interacts with its nearest neighbor ligands to an extent different from the host metal ion which it replaced. This will have the effect of "de-coupling" the neighbor anion p orbitals (in the case of halides and oxides) from the valence bond. This conclusion was reached by Tippins[1] in a study of charge transfer spectra of several first row transition metal ions in the corundum (Al_2O_3) lattice, based on the fact that the observed bandwidths were much smaller than those expected from a band to impurity ion transition. With respect to our $KMgF_3$:Ni system, the absorption band of which is interpreted as a ligand to metal transition, the observed bandwidths of approximately 3100 cm^{-1} and 2500 cm^{-1} are much smaller than

expected if the band viewpoint were operative. Mattheiss[2] has calculated the valence band density of states and width for $KNiF_3$ by the Augmented Plane Wave (APW) method and, based upon this calculation, we would anticipate an absorption bandwidth of nearly 10,000 cm^{-1}. We conclude then, that a molecular orbital viewpoint should be used in the interpretation of ligand to metal excitations, and all previous data have in fact been interpreted within this framework.

A brief description of the molecular orbital approach in constructing a qualitative energy diagram will be presented here, in order to familiarize one with the nomenclature and to provide an aid in visualizing these transitions. This is equivalent to the strong field scheme in which one initially views a transition as one electron in nature, and then considers the effects of electron electron repulsion, spin orbit effects, etc. Since the majority of data presented in this study are obtained from systems of octahedral symmetry, the molecular orbital scheme of that symmetry will be presented.

Initially we consider the atomic orbitals 4s, 4p, and 3d of a first row transition metal ion and the 2p orbitals of a F^- ligand. Under octahedral symmetry we determine the transformation

properties of these orbitals in order to eventually write a molecular orbital wavefunction of the form

$$\Psi_{MO} = N (\Psi_{metal} + b \Psi_{ligand})$$

where Ψ_{metal} is the metal orbital, Ψ_{ligand} is a combination of ligand orbitals, b is a coefficient indicating the degree of covalency, and N is a normalizing constant. The normalizing condition gives

(1) $N^2 (1 + b^2 + 2bG) = 1$

where G is the "group overlap" integral.[1]

$$G = \int \Psi_{metal} \Psi_{ligand} \, d\tau$$

The function Ψ_{metal} and Ψ_{ligand} must belong to the same irreducible representation of the symmetry group in order to form a meaningful molecular orbital wavefunction.

Using the coordinate system of Figure 1 and the symmetry operations of the O_h group, we construct molecular orbital wavefunctions Ψ_{MO} from the appropriate atomic wavefunctions. The symmetry designations and the atomic orbitals are given in Table 1.

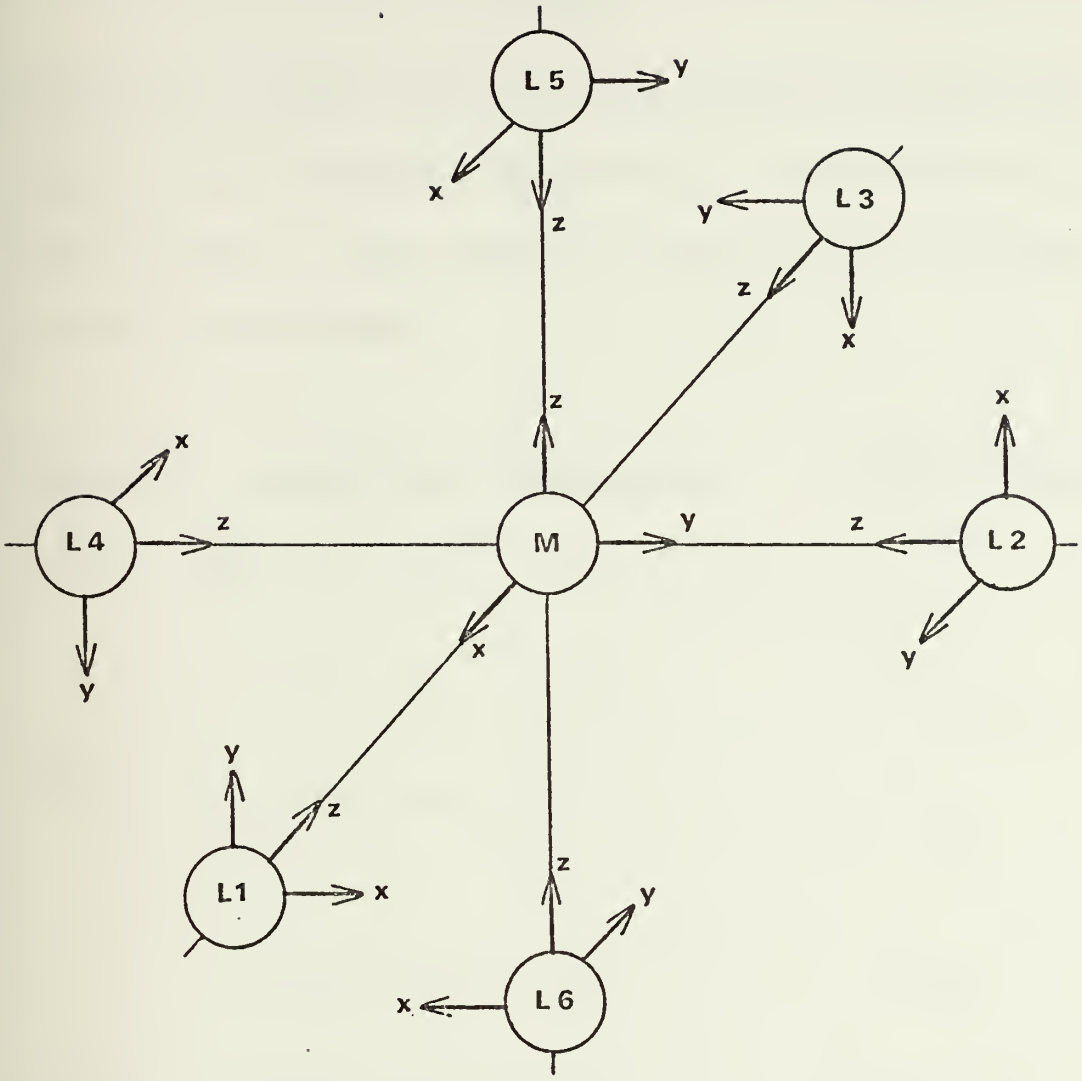

Figure 1. Coordinate system for ML_6 octahedral molecule.

Table I

Combinations of ligand orbitals and metal orbitals for appropriate symmetry representations in O_h symmetry. Coordinate system is that of Figure 1. Only metal 3d, 4s, and 4p orbitals and ligand 2p orbitals are considered.

Symmetry	Ligand Orbital Combinations	Metal Orbitals
A_{1g}	$\frac{1}{6}(Z_1 + Z_2 + Z_3 + Z_4 + Z_5 + Z_6)$	4s
E_g	$1/2\ (Z_1 - Z_2 - Z_3 - Z_4)$	$3d_{x^2-y^2}$
	$\frac{1}{12}(2Z_5 + 2Z_6 - Z_1 - Z_2 - Z_3 - Z_4)$	$3d_{z^2}$
T_{2g}	$1/2\ (y_1 + x_5 + x_3 + y_6)$	$3d_{xz}$
	$1/2\ (x_2 + y_5 + y_4 + x_6)$	$3d_{yz}$
	$1/2\ (x_1 + y_2 + y_3 + x_4)$	$3d_{xy}$

Symmetry	Ligand Orbital Combinations	Metal Orbitals
	$1/2 \quad (y_1 - x_5 + x_3 - y_6)$	
T_{1g}	$1/2 \quad (x_2 - y_5 + y_4 - y_6)$	None
	$1/2 \quad (x_1 - y_2 + y_3 - x_4)$	
	$1/2 \quad (y_1 - x_2 - x_3 + y_4)$	
T_{2u}	$1/2 \quad (y_2 - x_5 - x_4 + y_6)$	None
	$1/2 \quad (x_1 - y_5 - y_3 + x_6)$	
	$1/2 \quad (Z_1 - Z_3) \quad (\sigma)$	
	$1/2 \quad (y_2 + x_5 - x_4 - y_6) \quad (\pi)$	$4p_x$
T_{1u}	$1/2 \quad (Z_2 - Z_4) \quad (\sigma)$	
	$1/2 \quad (x_1 + y_5 - y_3 - x_6) \quad (\pi)$	$4p_y$
	$1/2 \quad (Z_5 - Z_6) \quad (\sigma)$	
	$1/2 \quad (y_1 + x_2 - x_3 - y_4) \quad (\pi)$	$4p_z$

A qualitative molecular orbital energy level diagram is shown in Figure 2.

Note that the lowest energy orbitals are σ combinations of ligand and metal orbitals, that is they are symmetrical with respect to rotation about the metal ligand axis. These orbitals are stabilized in comparison to the π combinations because the overlap with metal orbitals is greater, leading to a stronger chemical bond. The twelve ligand π combinations overlap the metal orbitals of same symmetry to different degrees, and form bonding and non bomding molecular orbitals of varying energies. In addition, ligand-ligand interactions cause a stabilization or destabilization of these π bonding and non bonding orbitals.

The energy ordering of these orbitals varies with the specific system of interest. Jorgensen,[4] in one of the important initial studies of charge transfer spectra of octahedral transition metal halides, determined the energy ordering to be $t_{1g} \rangle t_{2u} \rangle t_{1u}$ . . . McClure,[5] on the basis of nodal patterns of various ligand orbital combinations, predicted $t_{1g} \rangle t_{2u} \rangle t_{2g} \rangle t_{1u}$ . . . More recently, Modine,[6] in an MCD and optical study of V^{+3}:MgO determined that the π t_{1u} orbital is of higher energy than the π t_{2u} orbital. Also, and MCD study

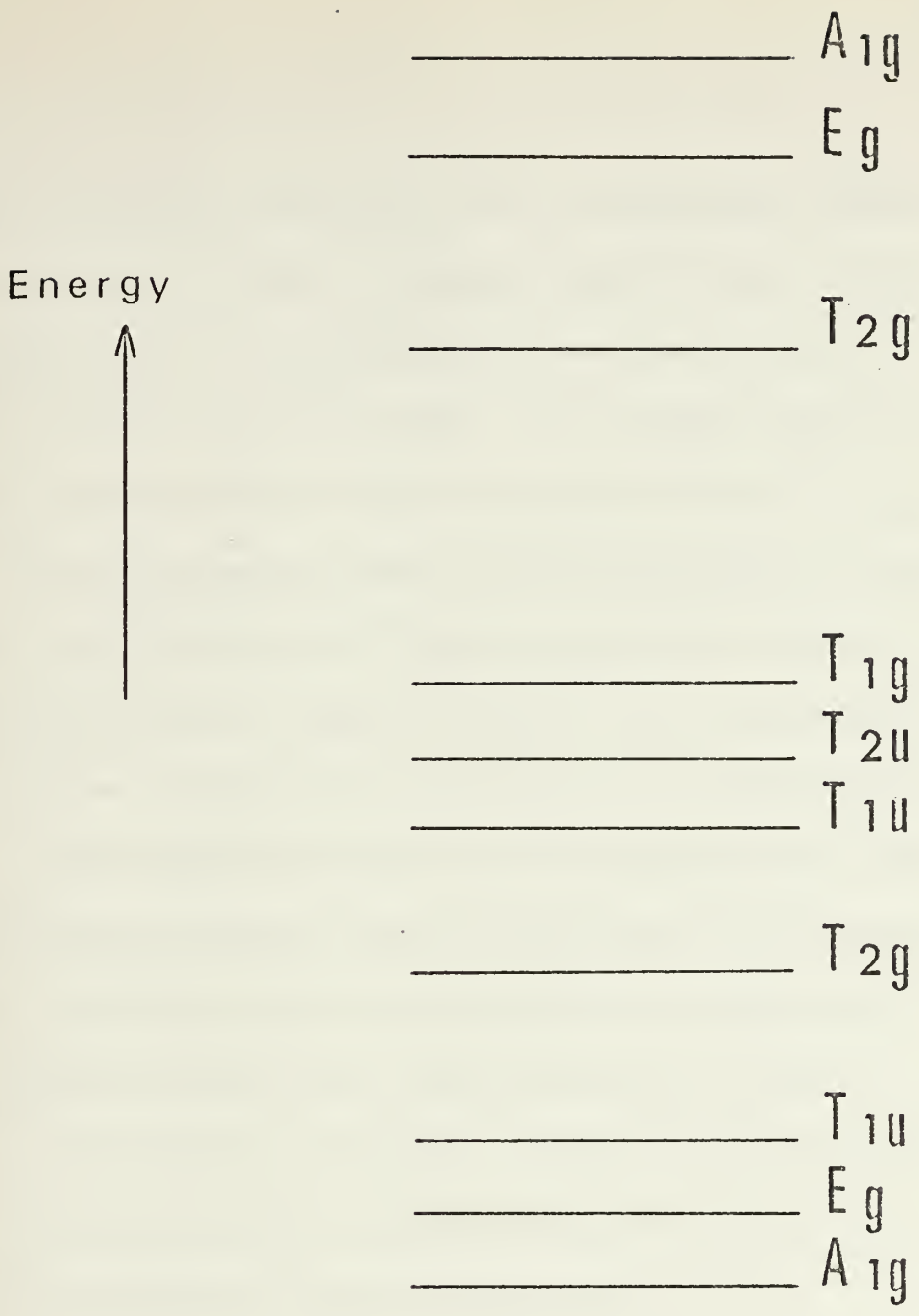

Figure 2. Qualitative energy ordering of molecular orbitals defined in Table 1. The upper three orbitals are of predominantly metal parentage, the remainder are predominantly ligand.

of $IrCl_6^{2-}$ by Henning, McCaffery, Schatz, and Stephens[7] showed that, in this system the π t_{1u} orbital is again of higher energy than the π t_{2u}. Note that the question centers on the relative ordering of the two ungerade orbitals. There is little doubt that the highest energy orbital of this set is the non bonding π t_{1g}.

The data presently available indicate that the π t_{1g} orbital is in the range 3000-6000 cm^{-1} higher in energy than the π t_{1u} which is 2000-9000 cm^{-1} higher than the π t_{2u}. These figures are for purposes of calibration only, since many of the assigned bands consist of slight inflections on a rising absorption tail, and the assignment of a specific energy to these bands is an inexact practice. In addition, these data are obtained from second and third row transition metal ions with predominantly chloride, bromide, and iodide ions as ligands. Therefore, spin orbit coupling is not always negligible, and splittings of bands occur, thus adding to the difficulty in energy assignments.

In Figure 2, the following situation exists for the octahedral fluorides and oxides presented in this study. The orbitals a_{1g}, e_g, t_{1u}, t_{2g}, t_{1u}, t_{2u}, and t_{1g} contain a total of 36 electrons, the maximum number allowed. These electrons can be thought of as primarily belonging to the ligands, since the orbitals consist pri-

marily of six ligand σ orbitals and twelve ligand π orbitals. In other words, in the wavefunction

$$\Psi_{MO} = N (\Psi_{metal} + b \Psi_{ligand})$$

the mixing parameter b is a large number.

For the antibonding t_{2g} and e_g orbitals, a different situation exists. The occupancy of these orbitals depends upon the specific transition metal ion involved, and it is by a systematic varying of this ion that one can create situations favorable to an understanding of the spectra. In this particular investigation, all systems studied are of a high spin nature. As one goes across the first row transition metals, the t_{2g} and then the e_g orbitals first become filled with electrons of parallel spin before electrons of opposite spin go into these orbitals. The reason that parallel spins are favored is quite simply that the energy required to cause a spin pairing is greater than the energy difference between the t_{2g} and e_g antibonding orbitals. If this t_{2g} - e_g energy difference were solely the result of an electrostatic field caused by the ligands, we would be in the "weak field" regime of crystal field theory.

Just as the lower lying orbitals could properly be considered as primarily ligand in nature, these orbitals can be classified as

predominantly metal. Therefore the phrase charge transfer is appropriate in describing the process in which an electron is excited from one of these orbitals to the other.

We will now concern ourselves with the application of the molecular orbital scheme and other variations and modifications to this approach that have been previously used to interpret ligand to metal charge transfer transitions.

While a reasonable quantity of work has been done on one or two specific systems, there have been few attempts to systematically vary the transition metal and/or the ligand involved, in order to make use of our existing knowledge of trends in such things as spin orbit coupling constants, ionic size, and orbital electron affinity as one does vary these ions. We shall therefore concentrate on experimental work of this type, since we are looking for a unifying explanation of what actually happens in a many electron system that exhibits charge transfer spectra.

Probably the most intensely studied and best characterized systems to date are the second and third row transition metal hexahalides. The transition metal ion is in the +3 or +4 oxidation state, the ligands are primarily chloride, bromide, and iodide ions, the local symmetry is octahedral, and the systems are low spin.

Unfortunately, much of the work on these systems has been done in solution, and because of this, very little data concerning electron lattice coupling and polarization characteristics have been obtained.

Based on the molecular orbital diagram of Figure 2, we can anticipate four different types of ligand to metal transitions in systems of this kind. At lowest energy, we expect a series of bands corresponding to p π to t_{2g} transitions. Most probably the next higher energy transitions would be from the set of p π orbitals to the e_g orbitals. At higher energy we anticipate the σ to t_{2g} and σ to e_g transitions.

We will relate these expectations to one of the initial studies of charge transfer transitions. Jorgensen[8] observed the infrared, visible, and near ultraviolet room temperature absorption spectra of Ru (III), Ru (IV), Rh (III), Pd (IV), Sn (IV), Sb (V), W(VI), Re (IV), Os (III), Os (IV), Ir (III), Ir (IV), and Pt (IV) with chloride, bromide, and iodide as ligands. He found three of the four sets of transitions listed above, arguing that the σ to t_{2g} transition should be of low intensity based on orbital overlap considerations. In addition to agreeing with the types of transitions listed above, the absorption bands he observed were broad and most were quite intense ($\varepsilon > 5,000$). Jorgensen was able to correlate the energy of

several of the absorption bands with the reducing and oxidizing character of the metal and ligand. He found that the energy of a transition decreases as one goes from a weakly to strongly oxidizing metal ion, and as one goes from a weakly to strongly reducing ligand. These observations confirmed that the absorption bands seen were in fact ligand to metal charge transfer transitions.

Since the time of Jorgensen's article, additional work on heavy metal hexahalides has been undertaken. A number of approaches to the interpretation of charge transfer spectra have resulted, some of which relate to the spectra presented in Chapter II.

One approach is to attempt to relate the measured energies of charge transfer bands to differences in energy terms derived from a one electron molecular orbital diagram.[9] In Figure 3 (a) we represent the ground state of a transition metal ion containing one d electron in an octahedral environment. We assume that the highest filled ligand orbitals are of t_{1g} symmetry. In (b) of that figure, we have completed the charge transfer process, with the transferred electron localized on the metal. We will now write the total energy for the two different situations, (a) and (b), and will equate the transition energy to the difference between the two. We will represent the one electron energies of the t_{2g} and t_{1g}

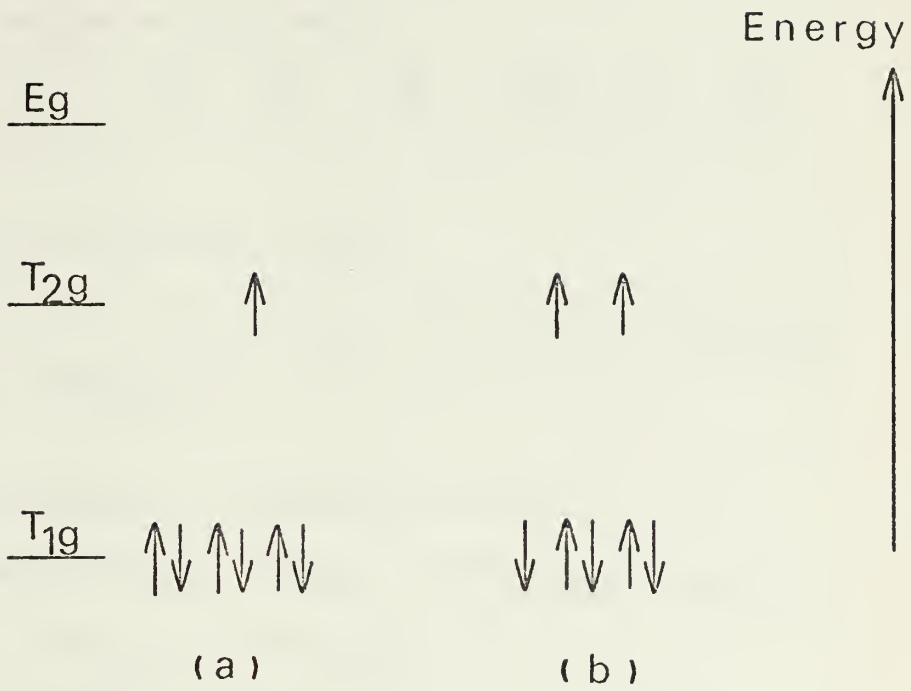

Figure 3. Qualitative energy level diagram of two highest energy filled and lowest energy unfilled molecular orbitals of octahedral MX_6 system for transition metal ion containing one d electron. (a) represents the ground state. (b) represents the state resulting from an electronic transition from the ligand T_{1g} to the metal T_{2g} orbital. The metal E_g orbital is empty.

orbitals as $E(t_{2g})$ and $E(t_{1g})$ respectively, the coulomb energies as $J(a,b)$ where

$$J(a,b) = \iint \frac{1}{r_{12}} \psi_a^2 \, d\tau_1 \psi_b^2 \, d\tau_2$$

and exchange energies as $K(a,b)$ where

$$K(a,b) = \iint \frac{1}{r_{12}} \psi_a \psi_b \, d\tau_1 \psi_a \psi_b \, d\tau_2.$$

The ground state energy is then

(2) $E(\text{ground state}) = 6E(t_{1g}) + E(t_{2g}) + 15J(t_{1g}, t_{1g}) + 6J(t_{1g}, t_{2g}) - 6K(t_{1g}, t_{1g}) - 3K(t_{2g}, t_{1g})$

After the transition is completed, we have

(3) $E(\text{excited state}) = 5E(t_{1g}) + 2E(t_{2g}) + 10J(t_{1g}, t_{1g}) + J(t_{2g}, t_{2g}) - 4K(t_{1g}, t_{1g}) - 4K(t_{1g}, t_{2g}) - K(t_{2g}, t_{2g})$

The difference between (2) and (3) gives

(4) $E(\text{transition energy}) = -E(t_{1g}) + E(t_{2g}) - 5J(t_{1g}, t_{1g}) + 4J(t_{1g}, t_{2g}) + J(t_{2g}, t_{2g}) + 2K(t_{1g}, t_{2g}) - K(t_{1g}, t_{2g}) - K(t_{2g}, t_{2g})$

Unfortunately, this approach leaves us with a number of energy terms which are quite difficult to evaluate, most notably the many center exchange and coulomb integrals. Additionally, we predict the occurrence of a large number of absorption bands,

which in many cases are not actually observed. One conclusion that can be drawn from this is that some of these many center electrostatic integrals are quite small. This is rather obvious for K(a, b) since the charge density $\psi_a \psi_b$ is the product of two orthogonal orbitals and since the squared overlap $\psi_a^2 \psi_b^2$ is anticipated to be small for orbitals on different centers.

Because the value of K(a, b) in a ligand to metal charge transfer process is expected to be small, Jorgensen[10] has proposed that one ignore this term. His approach is to once again use a one electron molecular orbital diagram as a visualization of the charge transfer process. Assuming all exchange integrals are zero, the energy required to make a transition from the configuration $\psi_a^2 \psi_b^2 \psi_c^2$ to the configuration $\psi_a^2 \psi_b^2 \psi_c \psi_d$ is

(5) I(c) - I(d) + J(d, d) - J(c, d)

where I(n) is the ionization energy of orbital n and J is the coulomb integral previously defined. Since the electron affinity of an orbital may be represented by I(n) - J(n, n), the transition energy of equation (5) becomes

(6) I(c) - A(d) - J(c, d)

where A(d) is the electron affinity of orbital d. Note that the transition costs us the ionization energy of the ligand π orbital, but in return we gain the energy due to the d orbital electron affinity

and a term that represents an attraction between the transferred electron and the hole left in the previously fully occupied ligand orbital by its transfer.

"Educated estimates" of the various terms in equation (5) can be made. J(c,d) for octahedral transition metal halides is approximately 30,000 cm^{-1}. J(d,d) for first row transition metal ions is β J(d,d) free ion where β is the nephelauxetic ratio $\frac{B \text{ complex}}{B \text{ free ion}}$ and B is the Racah interelectronic repulsion parameter.[11] In the free ion, J(d,d) is approximately 100,000 cm^{-1}. Note that the difference in ionization energies I(ligand π) - I(metal d) is much smaller than the observed energy transition since it is the sum of these terms in equation (5) that we measure spectroscopically.

In a different approach to charge transfer energies, one can express interelectronic repulsion in a configuration resulting from an electron transfer as a function of the number of electrons and their resultant spin angular momentum. Again, this method is attributed to Jorgensen,[10,12] who defines a parameter A (which is not the Racah A). The energy of a baricenter of a configuration of q electrons, which is the weighted average of the number of energy states in that configuration, is by this method

(7) $\frac{q(q-1)A}{2}$.

However, one must then relate terms of different spin multiplicity to the average energy of a configuration, and this is done by a correction to equation (7) called the "spin pairing energy". This energy term is

(8) $[\ \langle S(S+1)\rangle \ - \ S(S+1)\ ]\ D$

where S is the total spin quantum number and D is the "spin pairing energy parameter". $\langle S(S+1)\rangle$ is defined as follows.

(9) $\langle S(S+1)\rangle = \frac{q(q+2)}{4} - \frac{(2l+2)\cdot q(q-1)}{2(4l+1)}$

where q is the number of electrons in the configuration and l is the orbital quantum number. In addition, D is defined for d orbitals as

(10) $D = 7/6\ (5/2\ B + C)$

where B and C are Racah parameters. Finally, for d orbitals the parameter A in equation (7) is defined as

(11) $A = A\,(\text{Racah}) - 14/9\ B + 7/9\ C$

In summary, the energy of a configuration of q^{d} electrons with total spin quantum number S is

(12) $E = \frac{q(q-1)A}{2} + [\ \langle S(S+1)\rangle \ - \ S(S+1)\ ]\ D.$

With equation (12) we can attempt to represent some part

of the energy difference between various charge transfer states. For example we can calculate the energy difference between the $\pi^5 t_{2g}^4$ and $\pi^5 t_{2g}^3 e_g$ configurations using equation (12), although we must recognize that we are neglecting such difficult considerations as the difference between $J(\pi, t_{2g})$ and $J(\pi, e_g)$ and other similar energy terms.

Yet another approach is to rely on our chemical intuition and attempt to relate charge transfer energies to electronegativity differences between metal and ligand. Pauling[13] has presented a list of electronegativities, which can be used to predict, in effect, how ionic or covalent various compounds will be. Although the actual definition of electronegativity has not been universally agreed upon, the idea that some atoms or ions are more likely to attract electrons than others is quite reasonable. In general, an order of ligand electronegativities can be ascertained, and such an order is $F^- > O^{2-} > Cl^- > Br^- > I^-$. That is, the fluoride ion is the least likely to release its most weakly bond electron. In addition to an ordering of ligands, transition metal ions can also be placed in a hierarchy of electronegativity. As one goes across the first row transition metal ions, the ion electronegativity generally increases. As one increases the nuclear charge, the stability of

the d orbital increases, and in fact the d electrons begin the first series as weakly held and in quite diffuse orbitals, and end the series as core electrons. The ionization potentials follow a trend of increasing value, with a break at the d^5 configuration, and we are addressing ourselves in this concept of electronegativity to the negative value of ionization potential.

Based on electronegativity arguments, we can predict trends in charge transfer energies. A transition from a highly electronegative ligand to a certain metal ion is expected to be at higher energy than a similar transition from a ligand of low electronegativity.

Jorgensen has attempted to make this idea more quantitative and from a compilation of charge transfer data has assigned values related to electronegativity of various ligands and metals. He has found, that relative to a fluoride to metal charge transfer transition, the energy of a chloride to metal is approximately 28,000 cm^{-1} lower. Another 6,000 cm^{-1} separates chloride and bromide and 10,000 cm^{-1} separates bromide and iodide.

By selecting a series of compounds with one particular ligand and varying metal ions, one can also deduce energy trends and relate them to metal orbital electronegativities. Through the use of a multiplicative factor, one can relate Pauling's electro-

negativity values to expected charge transfer energy, and this gives

(13) E (charge transfer) = $30,000(\chi \text{ ligand} - \chi \text{ metal}) cm^{-1}$

where χ is the value of electronegativity.

Using this equation, corrected for spin pairing energies (equation (8)), one can predict in many cases the value of charge transfer energy. Unfortunately, the electronegativity values have a possible error of at least . 1 unit which corresponds to 3,000 cm^{-1}.

The previous approaches are those that have been proposed to explain the results of Jorgensen's pioneering work, and subsequent experiments along a similar vein. This is not to imply that different types of experiments and approaches have not been undertaken. Indeed, MCD (Magnetic Circular Dichroism) techniques have been used to determine the symmetry of involved orbitals,[6,7,14] temperature dependence of crystal spectra,[15] and systems of symmetry other than octahedral have been studied.[16,17] However, the approaches to the analysis of the energy of various charge transfer bands still depend on the types of assumptions presented previously. These approaches are especially interesting and important, because the bulk of data concerning charge transfer transitions are on the second and third row transition metal halides of octahedral symmetry.

One relatively recent investigation of electron transfer

spectra is quite important because it concerns first row transition metal ions as impurities in a wide band gap material, and the study was extended into the vacuum ultraviolet region. Tippins[1] obtained samples of corundum (Al_2O_3) doped with Ti^{+3}, V^{+3}, Cr^{+3}, Mn^{+4}, Fe^{+3}, and Ni^{+3}, and observed the room temperature and liquid nitrogen temperature absorption spectra of these systems. We found several high energy absorption bands which could not be assigned as d-d transitions. These bands were of high intensity, showed no temperature dependence, and the position of each band was dependent on the particular transition metal ion impurity. Tippins assigned these transitions as charge transfer in nature, and attempted to relate the energy of each band to a series of terms derived from a classical transfer of electrons between free ions. He postulated that the process was an electron transfer between the O^{2-} valence band ($p\pi$ orbitals) and the t_{2g} or e_g metal orbitals in these systems of almost octahedral (although actually C_3) symmetry. The energy of this transfer would be

$$(14)\quad E = \text{Madelung } (+) + \text{Madelung } (-) - \frac{e^2}{r_o} + \chi\ (O^{2-}) - I(M^{+2}) - \psi \text{ polarization} + \Delta E \text{ crystal field}$$

where Madelung represents the electrostatic lattice energy, $\frac{e^2}{r_o}$

is the exciton energy, or attraction of the valence band hole for the transferred electron, χ is the electron affinity, I is the ionization potential, γ polarization is the polarization energy of the dipole formed in this process, and ΔE crystal field is the change in d orbital energy caused by the different configurations and crystal field before and after the electron transfer. This equation has its origins in the von Hippel cycle[18] and is derived by considering the following sequence of events. The positive and negative ions between which the charge transfer will occur are removed from the crystal which costs Madelung energy. An electron is transferred from the ligand to the metal which requires χ (ligand) - I(metal). The ions are replaced in the crystal, however, the energy of this replacement seems to be ignored. Note that this replacement energy is zero when considering a lattice of charges +1 and -1, for which this equation was originally postulated. When returned to their original lattice sites, the electron pair returns $\frac{e^2}{r_o}$ to the system, and the lattice is polarized by this electron transfer, reducing the total energy by γ polarization. Finally, the crystal field energy correction is added as explained previously.

Equation (14) is then the sum of these terms, and if one believes that it is representative of the charge transfer process,

one can argue that, if an impurity ion is substituted into the lattice, nearly all of these terms will remain invariant in a ligand to impurity charge transfer. These invariant terms can be lumped into a constant C, and the charge transfer energy is then

(15) E (charge transfer) = C - I(metal) + Δ E crystal field

Ideally, then, in spite of the fact that all the terms of equation (14) cannot be accurately calculated (especially γ polarization which is in the range 20,000-50,000 cm^{-1}), energy trends can be correlated to ionization potential and crystal field energy, and this correlation could give us some insight into the charge transfer process.

Tippins obtained the parameter C in equation (15) by fitting that equation to the energy of the absorption bands in vanadium, chromium, and iron doped corundum, which gave the best resolved bands of the ions studied. He then used this value of C and equation (15) to predict the location of other charge transfer bands, with some success.

We will be utilizing an approach similar to that of equation (14) as an aid in the determination of the direction of electron transfer in our systems. Therefore it is appropriate to examine in a more critical manner several of the approximations made in a

simplification of this type, and their validity or shortcomings.

We would expect that, since the energy terms derived by this electron transfer process are all of electrostatic origin, equation (14) will be most applicable to the most ionic systems, namely the fluorides. Additionally, we should consider the effect of host crystal on the unknown term, γ polarization. It follows that the anion of lowest polarizibility (ease of distortion of electronic distribution), will be the most amenable to calculation by this method. Again, the fluoride ion is the most highly qualified ligand, its polarizability being approximately 1/3 that of O^{2-} and 1/4 that of Cl^-.

The energy term, $\frac{e^2}{r_o}$ in equation (14) seems to serve as a catch-all in Tippins' calculation. Specifically, it replaces the coulomb integral between the d orbital wavefunction and the ligand wavefunction, the exchange integral between the same functions, and the intra d orbital exchange integral. It is in reality, an average energy term, representing the interaction between the energy levels formed by a particular metal configuration and the energy levels corresponding to different linear combinations of the fluoride $p\pi$ orbitals. A rough estimaste of $\frac{e^2}{r}$ for our crystal systems indicates that, compared to most other terms in equation

(14), it contributes only a small correction ($\sim$ 3 ev) to the total energy. Because it is merely an average over all possible levels described above, it is probably constant within one particular host, fortunately permitting comparisons among various transition metal ions in that host.

There is one further quite important energy consideration related to the $\frac{e^2}{r}$ term before which has been simplified in Tippins' approach, and this is due to the fact that his method is a one electron method that neglects interelectronic repulsion. The transferred electron terminates on the transition metal ion, in either a t_{2g} or e_g orbital, and in this one electron scheme, the energy difference between the two possibilities is merely 10 Dq. Additionally, only one absorption band for each ion is predicted. In several cases, our data and Tippins' data consist of several absorption bands per ion, which can be rationalized only by a consideration of the spectroscopic terms arising from each electronic configuration. In effect, we are moving one step further in the direction of a more complete consideration of the charge transfer energy by taking into account electron-electron repulsion within a configuration and configuration interaction between like terms in different configurations. Our calculation should take into account

the fact that we are neither in the strong field regime nor the extremely weak crystal field area, but in some intermediate situation.

Recognizing the importance of interelectronic repulsion, we can determine the charge transfer energy by the following process. The metal ionization potential represents the energy absorbed or released in a transition from the ground state free ion term in one oxidation state to the ground state free ion term in a second oxidation state. However, we must correct this energy value for the difference between the lowest energy level in the crystal and the center of the configuration involved, both in the initial and final states. An example will clarify this approach.

Consider the transition

$$F^-(2p^6) + Mn^{+2}(d^5)\ {}^6S \rightarrow F^o(2p^5) + Mn^{+1}(d^6)\ {}^5D$$

The transition Mn^{+2} to Mn^{+1} (^6S to ^5D) releases the second ionization potential of manganese, 15.64 ev. In the crystal, the ground state of manganese is $^6A_{1g}$ which is at the same energy as the ^6S term. The Mn^{+1} ion is in the state $^5T_{2g}$ which is at an energy of 4 Dq below the center of the t^4e^2 configuration. Therefore the system returns 4 Dq units of energy in addition to the manganese ionization potential. We have neglected the energy required to remove the electron from the fluoride ion, since in a series of ions

in one particular host, this value should be a constant. Therefore a comparison of energy values among metal ions calculated in this manner should indicate the direction of electron transfer in any one particular host.

C. The Transition Metal as an Electron Donor

We will now concern ourselves with the possibilities that the absorption spectra result from an excitation in which the electron originates on the transition metal ion and terminates in the host metal ion s orbital or in which the electron originates on the transition metal ion and terminates on the ligand.

We can expeditiously dispose of this latter alternative for the transition metal fluorides on which we are reporting. The major requirement for the transition metal to ligand process is that the anion has available low lying unfilled antibonding orbitals. Examples of ligands that meet this criterion are dipyrazyl, orthophenanthroline, and pyrazine. Studies of transition metal ions in complexes involving similar ligands have been undertaken,[19,20] but in this area, as in the area of ligand to metal charge transfer transitions, our understanding of the data is limited. In any case, the fluoride ion does not have the appropriate orbitals available for such a transition.

In the previous section, in addition to conceptually presenting the molecular orbital approach, we were able to briefly review specific methods of data interpretation for ligand to metal transitions that have appeared in the literature. In this section, we will not have that option, for no previous transition metal halide or oxide

system has been interpreted as a transition metal ion to host metal ion excitation. Therefore, the remainder of this section will consist of what we believe to be valid conclusions or inferences, or expectations that can be derived from a careful consideration of the ramifications of this metal to metal charge transfer model.

Specifically, the process that we visualize for a metal to metal transition is such that the initial state is the ground energy level of the +2 transition metal ion in a crystal field of appropriate symmetry. The final state is composed of the transition metal ion in the +3 oxidation state and the transferred electron in a molecular orbital corresponding to some combination of nearest neighbor host metal ion s orbitals. An alternate viewpoint is that the electron has been excited into the crystal conduction band.

This model leads us to a number of rather interesting considerations, among which is an expectation of very little interaction between the transferred free or nearly free electron, and the transition metal ion-fluoride system from which the electron has come. This interaction should be quite weak because of the small overlap between the host metal ion s orbital and the transition metal ion d orbital. The transition metal-host metal distance in the three fluoride hosts extends over the range 3.4 to 4.0 Angstroms. A

small overlap indicates a number of further considerations, one of which is that we anticipate the observation of an absorption spectrum which correlates with the excited states of the +3 transition metal ion in a crystal field. We should observe transitions from the +2 transition metal ion to each level of the +3 ion and the nearly free electron will merely add a small perturbation to absorption spectra expected from this process. A logical conclusion based upon this model is that, if the metal metal wavefunction overlap is small, the oscillator strength will also be small. As we approach a limit of extremely weak interaction we might anticipate the necessity of a vibronic mechanism with its resultant oscillator strength temperature dependence. In effect we are saying that the gerade to ungerade transitions contribute very little to the integrated band intensities because of this lack of overlap.

It would be incorrect to completely neglect the final state electron since it will interact to some small but finite extent with the remainder of the system. Utilizing a molecular orbital approach, and assuming an electron localization on nearest neighbor host metal ion centers, we are able to predict the wavefunction symmetries and obtain some indication of the possible electron electron interactions. As a specific example, the Mg ions in the $KMgF_3$

lattice form an octahedron around the impurity ion. By a consideration of the properties of the host metal ion s orbitals under the symmetry operations of the O_h group, we find that these six orbitals transform as the A_{1g}, E_g and T_{1u} irreducible representations of that group. By obtaining direct products with the symmetry representations of the +3 transition metal ion (the excited state of our system) we are able to predict the number of anticipated absorption bands. In practice, because of the small wavefunction overlap, we expect these electron hole interactions to be of such a magnitude that they would only manifest themselves as a small absorption band broadening. In the D_{2h} point group which corresponds to the MgF_2:transition metal systems, this approach is quite useful in the prediction of the polarization properties of each absorption band.

Another contribution to the absorption bandwidth is the result of the changing of the formal oxidation state of the transition metal ion by one unit through this electron transfer process. This large change in electronic distribution will result in a relaxation of the lattice, and therefore in a large variation of the equilibrium position between the ground and excited states. In fact, each excited state will have its own particular equilibrium position and

shape of its potential curve. In some cases therefore, the transition will be to a steeply rising portion of the potential curve, generating high energy vibrations and a large bandwidth, while, in other cases, the vertical electronic transitions will be more nearly to the equilibrium position of the excited state. Because of these large shifts on a configuration coordinate diagram, the absorption bands are expected to remain broad upon cooling the crystals to liquid helium temperature.

This lattice relaxation mechanism will also have some effect on band energies. We stated previously our expectation of electronic transitions from the +2 transition metal ion ground state to levels of the +3 transition metal ion excited state. The absorption spectra should reflect these excitations by showing one band for each possible transition, and the band splittings should correlate to those observed in spectra of the +3 transition metal ion in the same lattice. The relaxation mechanism however, will cause a deviation from the anticipated band splittings. Because the actual process observed will be a transition from the equilibrium position of the +2 metal ion to some portion of the potential curve of the +3 metal ion, the energies observed spectroscopically will not coincide with those determined from a transition from the equilibrium position of the

+3 metal ion to its excited states. In fact, we might even anticipate in an extreme instance a change in the energy ordering of the excited state levels because of differing equilibrium positions and potential curves of these levels.

D. Considerations Common to Ligand to Metal and Metal to Metal Processes

We will now address ourselves to three distinct considerations, the results of which should remain valid for either direction of the charge transfer process.

First, we anticipate that the oscillator strength of the absorption bands should vary in a simple fashion with the transition metal ion involved. In the ligand to metal transition, the absorption intensity is dependent upon the fluoride p orbital-transition metal d orbital overlap. In the alternate transition under consideration, the absorption intensity will vary with the host metal ion s orbital-transition metal d orbital overlap. In either process within a given host crystal, the oscillator strength will therefore depend upon the extension of the transition metal d orbital in space. At the beginning of the transition series, the d orbitals are diffuse, and as the nuclear charge steadily increases across the first row, they become more and more contrascted until they eventually become core orbitals. The oscillator strength is expected to also follow this trend of decreasing with an increase in atomic number.

A second expectation that is based upon the same argument is that the absorption bandwidth should decrease along the transi-

tion series in any one particular host. A smaller d orbital will interact less strongly with the lattice than will a larger d orbital, and the data of Tippins confirm this statement.

Finally, low oscillator strength transitions are anticipated for each direction of electron transfer. In the ligand to metal process, the lowest energy absorption bands expected result from an excitation from a t_{1g} combination of fluoride p π orbitals to the g orbitals of the transition metal ion. In the metal to metal process, we also expect low intensity transitions because of the small overlap anticipated between the transition metal and host metal ions. For a purely Laporte forbidden transition we expect an oscillator strength range of 10^{-6} to 10^{-4}. For an allowed electronic transition, we expect oscillator strength values approaching unity. By considering the concept of "intensity stealing" from high energy fully allowed charge transfer bands, it is our expectation that the oscillator strengths measured in our systems will be intermediate to these two extremes.

The original attempt to make quantitative this intensity stealing concept in the area of charge transfer excitations was undertaken by Englman.[21] He utilized the only available data (which were the low energy band edges) to correlate the intensity

of forbidden transitions with the energy separation between these transitions and the fully allowed charge transfer transitions. Fenske[22] followed several years later with a more satisfying explanation, and proceeded to correlate measured oscillator strengths of d orbital to d orbital transitions with the energy of fully allowed ligand to metal charge transfer transitions based on the experimental data of Jorgensen.

Using a first order perturbation theory approach, and the metal to metal process as an example, an odd parity vibration mixes charge transfer states of odd character into the originally even transition metal d orbital wavefunction and even host metal ion wavefunction. Using these ideas, one has

$$(16)\qquad \left|\text{TMd (mixed)}\right\rangle = \left|\text{TMd}\right\rangle + \sum_{\substack{\text{odd CT}\\ \text{states}}} \frac{\left|\text{odd CT}\right\rangle\left\langle\text{TMd}\right|\frac{\partial H}{\partial Q}\left|\text{odd CT}\right\rangle}{E_{CT} - E_{TMd}}$$

$$(17)\qquad \left|\begin{matrix}\text{host}\\ \text{metal(mixed)}\end{matrix}\right\rangle = \left|\begin{matrix}\text{host}\\ \text{metal}\end{matrix}\right\rangle + \sum_{\substack{\text{odd CT}\\ \text{states}}} \frac{\left|\text{odd CT}\right\rangle\left\langle\begin{matrix}\text{host}\\ \text{metal}\end{matrix}\right|\frac{\partial H}{\partial Q}\left|\text{odd CT}\right\rangle}{E_{CT} - E_{\text{host metal}}}$$

where $\left|\text{TMd}\right\rangle$ represents the transition metal d orbital wave-

function and $\frac{\partial H}{\partial Q}$ represents the effective odd parity perturbing vibration.

The transition moment becomes

$$(18)\quad \langle \text{TMd (mixed)} \,|\, \text{er} \,|\, \text{host metal (mixed)} \rangle =$$

$$\sum_{\substack{\text{odd CT} \\ \text{states}}} \frac{\langle \text{TMd} \,|\, \text{er} \,|\, \text{odd CT} \rangle \langle \text{host metal} \,|\, \frac{\partial H}{\partial Q} \,|\, \text{odd CT} \rangle}{E_{CT} - E_{\text{host metal}}} +$$

$$\sum_{\substack{\text{odd} \\ \text{CT} \\ \text{states}}} \frac{\langle \text{host metal} \,|\, \text{er} \,|\, \text{odd CT} \rangle \langle \text{TMd} \,|\, \frac{\partial H}{\partial Q} \,|\, \text{odd CT} \rangle}{E_{CT} - E_{\text{TMd}}}$$

From the above expressions it is clear that the square of the transition moment (which is proportional to the oscillator strength) is quite sensitive to the energy denominators. Since the above denominators are smaller than those for a d to d transition, we expect the Laporte forbidden charge transfer bands to be of higher intensity than d to d transitions, irrespective of the direction of the charge transfer process.

REFERENCES TO CHAPTER III

1. H.H. Tippins, Phys. Rev. B 1 , 126 (1970)

2. L.F. Mattheiss, Phys. Rev. B 6, 4718 (1972)

3. C.J. Ballhausen and H.B. Gray, Molecular Orbital Theory, W. A. Benjamin, Inc., 1964

4. C.K. Jorgensen, Mol. Physics 2 , 309 (1959)

5. D.S. McClure, Solid State Phys. 9, 399 (1959)

6. F. Modine, Ph.D. thesis, University of Oregon, 1971

7. G.N. Henning, A.J. McCaffery, P.N. Schatz and P.J. Stephens, J. Chem. Phys. 48, 5656 (1968)

8. C.K. Jorgensen, Mol. Phys. 2, 309 (1959)

9. A.B.P. Lever, Inorganic Electronic Spectroscopy, Elsevier, 1968

10. C.K. Jorgensen, Orbitals in Atoms and Molecules, Academic Press, 1962

11. G. Racah, Phys. Rev. 62 , 438 (1942)

12. C.K. Jorgensen, Progr. Inorg. Chem. 12, 101 (1970)

13. L. Pauling, The Nature of the Chemical Bond, Cornell University Press, 1960

14. A.J. McCaffery, P.N. Schatz and T.E. Lester, J. Chem. Phys. 50, 379 (1969)

15. P. Day and E.A. Grant, Chem. Comm., 123 (1969)

16. B. Corain and A.J. Poe, J. Chem. Soc. (A), 1318 (1967)

17. G. DeMichelis, L. Olean, L. DiSipio and E. Tordello, Coordin. Chem. Rev. 2, 53 (1967)

18. N.F. Mott and R.W. Gurney, Electronic Processes in Ionic Crystals, Oxford University Press, 1940

19. R.J.P. Williams, J. Chem. Soc., 137 (1955)

20. A.B.P. Lever, J. Lewis and R.S. Nyholm, J. Chem. Soc., 5262 (1962)

21. R. Englman, Mol. Phys. 3, 48 (1960)

22. R.F. Fenske, J. Am. Chem. Soc. 2, 252 (1967)

CHAPTER IV

INTERPRETATION OF DATA

A. Direction of Electron Transfer

In the previous chapter we have delineated our expectations for each of the two possible directions of the charge transfer process. In this chapter we will present specific interpretations of the transition metal fluoride data obtained in the near and vacuum ultraviolet spectral regions.

Our original anticipation was that we would observe high energy absorption bands due to the fluoride orbital to transition metal d orbital process. However, our experimental results argue strongly against this interpretation. Note from Tables II, III, and IV of Chapter III that the integrated intensities of these transitions are much lower than that expected from a fully allowed ligand t_{1u} or t_{2u} to transition metal t_{2g} or e_g process. In addition, because of the observed oscillator strength dependence upon temperature, we conclude that we are dealing with Laporte forbidden transitions. Therefore the only reasonable ligand to metal assignment would be one in which the originating orbital would be the ligand t_{1g} com-

bination. This assignment leads to two major discrepencies. First, from an examination of previous transition metal halide charge transfer data, we would expect to observe the next higher energy transition, ligand t_{1u} to metal t_{2g} or e_g, at approximately 6000 cm^{-1} to higher energy than the t_{1g} to metal transition. For the $KMgF_3$ host, Figure 26 shows that the energy difference between the lowest energy absorption band and what could possibly be the low energy tail of an allowed transition is in excess of 30,000 cm^{-1} for vanadium, over 35,000 cm^{-1} for chromium, and over 35,000 cm^{-1} for iron, indicating that these relatively weak absorption bands are probably not of ligand t_{1g} origin.

There is a second and much more convincing approach that precludes the assignment of the ligand to metal direction for these transitions, and this approach is based on the fact that some ions are more readily oxidized or reduced than other ions. The charge transfer energy correlates rather well with ion electron affinity (or ionization potential) in the work of Jorgensen and Tippins previously discussed. Further illustration is found in the work of Day and Jorgensen[1] on $NiCl_4^{2-}$, $NiBr_4^{2-}$ and $CoCl_4^{2-}$, $CoBr_4^{2-}$, and CoI_4^{2-}. The energy of the transition increases for each positive ion as one goes from I^- to Br^- to Cl^-, exactly as predicted

by halide electron affinities. In addition, the cobalt halide transition is some 7000-8000 cm^{-1} higher in energy than the similar nickel halide band, again as predicted by ionization potential differences.

Without fear of overemphasizing the importance placed upon the concept of easily oxidizable and reducible ions and energy predictions based upon such a concept, we will quote here a reply by Jorgensen to the suggestion that perhaps some of his second and third row transition metal halide bands are not ligand to metal charge transfer bands, but are actually d to d transitions. His response is that the assignments are not based merely upon the value of extinction coefficient but

> "Rather, the regular variation (in energy) as a function of the constition of the chromophores, . . . is the fundamental basis for our confidence in the identification as electron transfer bands."[2]

With this strong reliance upon ionization potential trends firmly established in all previous successful charge transfer interpretations, we expect our data also to conform to such a pattern in some qualitative way. A first approach is to calculate the transition energy using equation (15) Chapter III (the method of Tippins).

His method should be quite applicable since the systems studied by himself and those studied by us are more similar than the work on second and third row transition metal halides of symmetry lower than octahedral. Visualizing the process in the $KMgF_3$ lattice as

$F^- 2p^6$ + transition metal^{+2} $\rightarrow$ $F^o 2p^5$ + transition metal^{+1}

we obtain the values of Table I through the use of equation (15).

Table I

Ligand to metal charge transfer energy as calculated by E $\propto$ - metal IP + $\Delta E_{\text{crystal field}}$, equation (15), for various ions in $KMgF_3$ lattice. A more negative value of E indicates that the transition should occur at a lower energy.

Ion	Second Ionization Potential (ev)	E Crystal Field (ev)	Calculated Energy (cm^{-1})
V^{+2}	-14.65	1.53	-106,000
Cr^{+2}	-16.49	1.49	-122,000
Mn^{+2}	-15.64	2.04	-109,500
Fe^{+2}	-16.18	0	-130,200
Co^{+2}	-17.05	0	-137,500
Ni^{+2}	-18.15	.90	-139,500

It is not the absolute value of the energy calculated, but the difference in energy between ions that is meaningful. In Figure 1, we have reproduced the $KMgF_3$:transition metal absorption spectra with the ligand to metal trends indicated. This figure demonstrates quite clearly that our data do not follow these trends.

In our previous discussion of equations (14) and (15), we noted that the effects of interelectronic repulsion within a configuration have been ignored, and that an improved calculation should consider the energy splittings of the levels with respect to the configuration center. An example of the energy terms involved is given for octahedral Mn (II) in Chapter III. In Table II we summarize the energy calculated for a fluoride to metal transition in $KMgF_3$, which includes the electron repulsion terms previously neglected. In Figure 2 we reproduce the absorption spectra and indicate the energy positions from Table II. The data still do not agree with the ligand to metal interpretation.

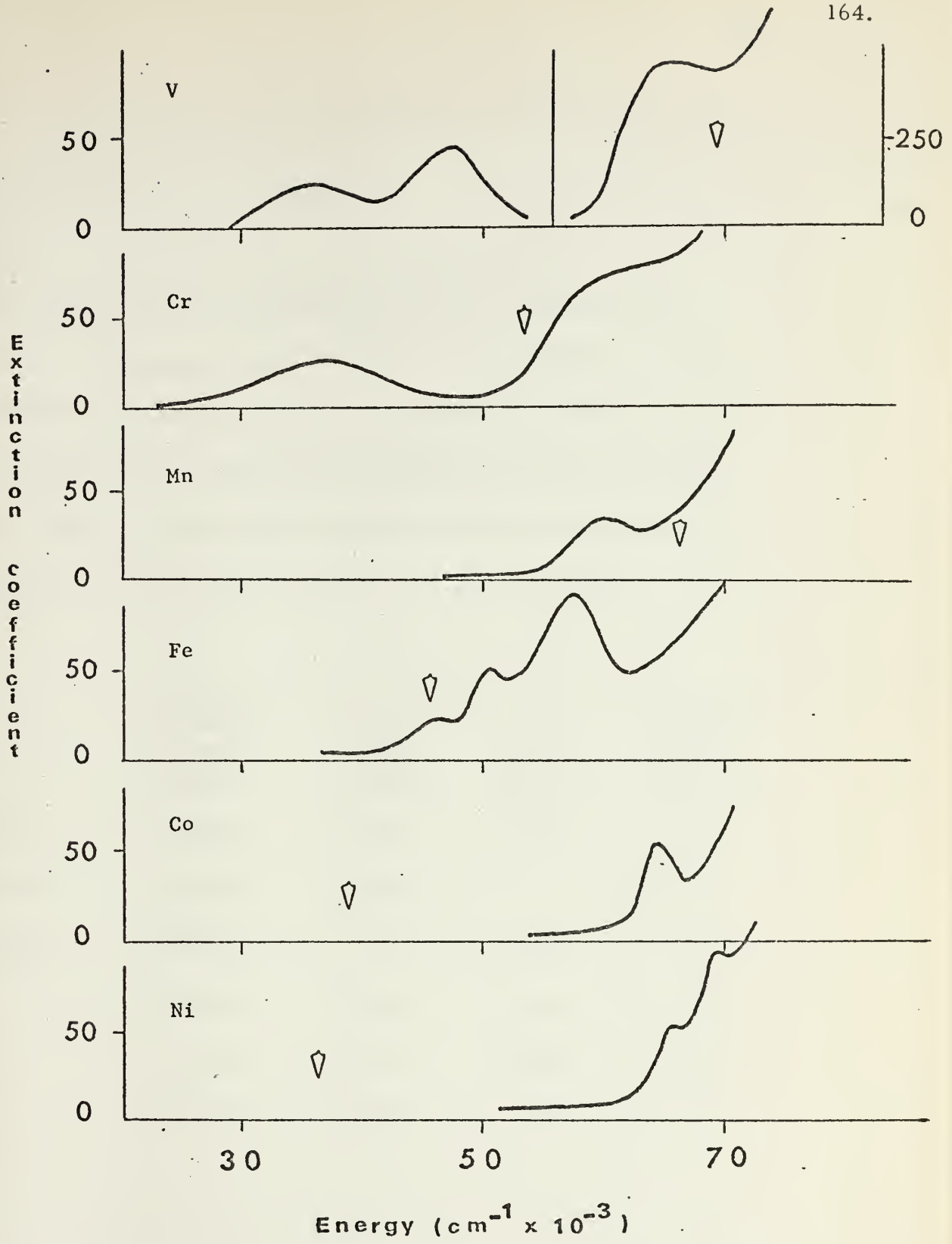

Figure 1. Low temperature absorption spectra of transition metal ions in $KMgF_3$. Arrows indicate position of lowest component of ligand to metal charge transfer transition as calculated by equation (15). The lowest energy absorption band in $KMgF_3$:Fe has arbitrarily been chosen as the zero of energy, since the relative and not the absolute energies are meaningful.

Table II

Ligand to metal charge transfer energy as calculated by E α - metal IP + $\Delta E_{\text{crystal field}}$ for metal ions in $KMgF_3$. ΔE is calculated by a consideration of the difference between the lowest energy level of a configuration and the lowest energy level in a crystal field. A more negative value of charge transfer energy indicates that the transition should be at a lower energy.

Metal Ion	Second Ionization Potential (cm^{-1})	E Ground State (cm^{-1})	E Final State (cm^{-1})	Charge Transfer Energy (cm^{-1})
Vanadium	-118,000	9600	-2400	-110,800
Chromium	-132,900	4800	0	-128,100
Manganese	-126,000	0	-1600	-127,600
Iron	-131,000	3200	-3400	-131,200
Cobalt	-137,200	5315	-4800	-137,685
Nickel	-146,200	8000	-1600	-138,200

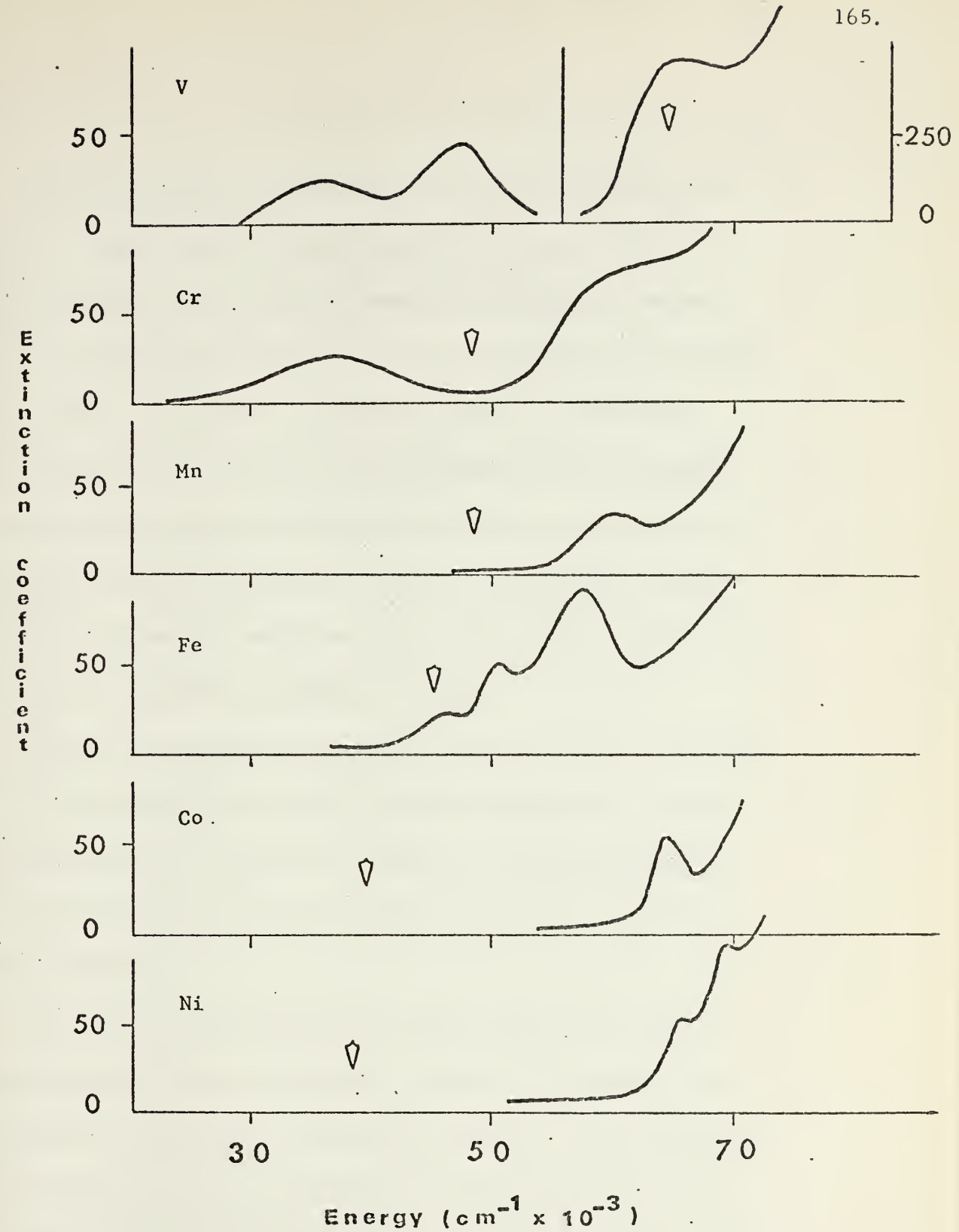

Figure 2. Low temperature absorption spectra of transition metal ions in $KMgF_3$. Arrows indicate position of lowest component of ligand to metal charge transfer transition as calculated by consideration of electron-electron repulsion terms. The lowest energy band in $KMgF_3$:Fe has arbitrarily been chosen as the zero of energy.

We now consider the possibility that the absorption bands observed in these transition metal fluoride systems are due to a transition metal d orbital to host metal ion s orbital excitation. We have calculated energy trends for this transition again including electron-electron repulsion, and the results are presented in Table III and shown in Figure 3. We anticipate that the energies calculated in this manner correlate with the lowest energy absorption band of each ion. In general, the fit is quite good, considering the fact that we have neglected many of the same energy terms (polarization energy for example) as Tippins.

There is one ion that does not fit well, and that is the nickel ion. With $KMgF_3$:Ni, it is highly probable that we have reached a "crossover point", and are in a situation in which the absoption bands of this system represent the ligand t_{1g} to metal e_g charge transfer transition.

There are several pieces of evidence that lead us to the present $KMgF_3$:Ni band assignments. We refer once again to the Mattheiss APW calculation on the $KNiF_3$ system. This calculation predicts that the lowest energy fluoride 2p to nickel 3d (e_g) transition should occur at .60 rydbergs, or 65,800 cm^{-1}. If we consider the number of absorption bands anticipated in a fluoride to

Table III

Transition metal to host metal s orbital charge transfer energy as calculated by $E \propto$ transition metal IP + $\Delta E_{crystal\ field}$ for metal ions in $KMgF_3$. ΔE is calculated by a consideration of the difference between the lowest energy level of a configuration and the lowest energy level in a crystal field. A lower value of charge transfer energy indicates that the transition should be observed at a lower energy.

Metal Ion	Third Ionization Potential (cm^{-1})	E Ground State (cm^{-1})	E Final State (cm^{-1})	Charge Transfer Energy (cm^{-1})
Vanadium	236,385	14,580	-12,443	238,522
Chromium	249,611	7,200	-21,800	235,011
Manganese	271,700	0	-11,940	259,760
Iron	247,111	3520	0	250,631
Cobalt	270,000	5300	- 7200	268,100
Nickel	291,630	8690	-17,490	282,830

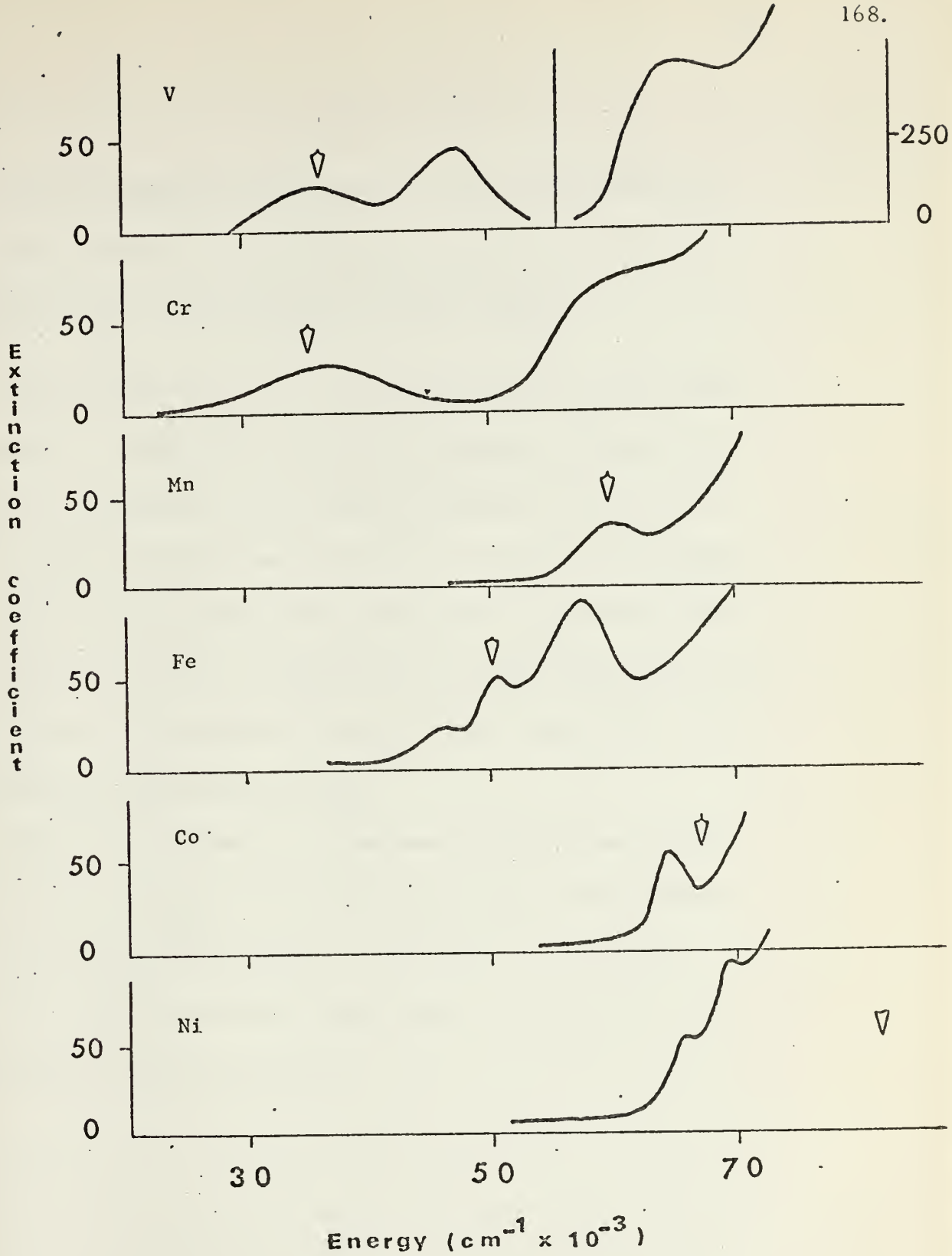

Figure 3. Low temperature absorption spectra of transition metal ions in $KMgF_3$. Arrows indicate position of lowest component of metal to host metal charge transfer transitions as calculated by consideration of electron-electron repulsion terms. Arrows have been moved to give best fit since the relative energy and not the absolute energy is meaningful.

metal transition, which the above one electron energy value does not consider, we get,

ligand hole $T_{1g} \times Ni^{+1}(d^9)\ E_g = T_{1g} + T_{2g}$

and a prediction of two bands. We observe two high energy bands at 64,000 cm^{-1} and 68,000 cm^{-1} in every sample of $KMgF_3$:Fe that we have investigated. Wet chemical analyses show that each of these samples contains the nickel ion as an impurity in addition to the iron ion. In the pure $KMgF_3$:Ni spectrum, we observe only the 64,000 cm^{-1} band as an inflection on a rising cutoff, and therefore it is quite conceivable that the 68,000 cm^{-1} band is obscured by this large background absorption.

On the basis of the poor agreement with the metal to host metal calculated energy, the excellent agreement with Mattheiss's energy calculation and agreement with number of absorption bands, we assign the two high energy bands to the fluoride to nickel charge transfer transitions.

B. Absorption Band Assignments

On the basis of our assignment of the majority of the transition metal fluoride absorption bands as resulting from metal to metal transitions, and recalling our expectations of small electron-transition metal interaction and the observation of +3 transition metal ion energy levels, we will now make specific band assignments.

Referring to the absorption spectra presented in Chapter II, our interpretation of the individual bands is as follows. For $KMgF_3$:V, the lowest energy band corresponds to the $^3T_{1g}$ level of the V^{+3} t_{2g}^2 configuration. Through the use of a Tanabe-Sugano diagram with a Dq/B value of 1.9, we predict three absorption bands with spacings of 12,800 cm^{-1} ($^3T_{2g}$) and of 25,000 cm^{-1} ($^3T_{1g}$) to higher energy than the lowest observed band. The measured absorption band peaks correspond to differences of 9400 cm^{-1} and 27,300 cm^{-1}. For the $KMgF_3$:Cr system, we anticipate two bands corresponding to the Cr^{+3} $^4A_{2g}$ (t_{2g}^3) level and the $^4T_{2g}$ (t_{2g}^2 e_g) level, which are separated by 10 Dq. This separation is predicted to be approximately 18,000 cm^{-1} and the observed peak to peak splitting is 22,700 cm^{-1}. The $KMgF_3$:Mn system is expected to exhibit one band corresponding to the Mn^{+3} ^5E_g

($t_{2g}^3 e_g$) level, and at 10 Dq higher in energy (18,000 cm^{-1}), the $^5T_{2g}$ ($t_{2g}^2 e_g^2$) level. The observed single band correlates in energy to the ^5E_g level, with the $^5T_{2g}$ level obscured by the rising absorption edge. In the MgF_2:Mn system, the same interpretation is made and the spectrum does exhibit a single absorption band.

The $KMgF_3$:Fe system is an enigma at this time and bears further study. The transition from the Fe^{+2} ($t_{2g}^4 e_g^2$) configuration to the Fe^{+3} ($t_{2g}^3 e_g^2$) configuration gives rise to several possible spin quartets ($^4A_1$, $^4A_2$, ^4E, $^4T_1$, $^4T_2$) and one spin sextet ($^6A_{1g}$) which is the normal d^5 high spin ground state. As an excited state configuration we might also expect the $^6A_{1g}$ level to be lowest in energy. The energy calculation of Table III shows that the best energy fit puts the $^6A_{1g}$ level directly on the 49,400 cm^{-1} absorption band which is not the lowest in energy. At this time we do not know the detailed ordering of these various levels, but it is certainly possible that a quartet term becomes the lowest in energy in the excited charge transfer state. We are successful however in the prediction of several absorption bands by this metal to metal model, and the absorption spectrum of MgF_2:Fe also consists of several bands, again as expected.

Returning to the series of transition metal ions in $KMgF_3$

and MgF_2, the systems $KMgF_3$:Co and MgF_2:Co are expected to give rise to one band which corresponds to the Co^{+3} $^5T_{2g}$ ($t_{2g}^4 e_g^2$) level and, at 10 Dq to the higher energy ^5E_g ($t_{2g}^3 e_g^3$) level which is obscured by the rising absorption edge. As described previously, the $KMgF_3$:Ni system is interpreted as a fluoride to metal system giving rise to two absorption bands.

An alternative interpretation can be presented for the $KMgF_3$:V system. The vanadium ion is the best reducing agent among the first row transition metal ions studied, and therefore, as an electron donor, lies closest in energy to the conduction band. Because of this case of oxidation, the two higher energy absorption bands might correspond to transitions well into the conduction band. This is postulated since, among the assignments for all the absorption bands presented above, only these two require a two electron transition in the extreme strong field scheme.

In view of the different geometry of the excited +3 transition metal ion state from the +2 ground state as discussed in Chapter III, the semiquantitative agreement between our expectations and the data is strong confirmation of these assignments.

C. Intrahost Comparisons

One interesting comparison that can be made based upon the data of Chapter II is a comparison of the spectra of one particular transition metal ion in three different hosts, which can be made in our case for the cobalt ion. There are a number of spectral similarities that reinforce the idea that we are observing the similar transition in all three hosts. Upon cooling the crystals from 300°K to 4.2°K, the band peaks shift 1100 cm^{-1} in the $KMgF_3$:Co and CaF_2:Co systems, and 800 cm^{-1} in MgF_2:Co. All three hosts give rise to only one observable absorption band in each, and this band is of much lower bandwidth than that found for other transition metal ions in the same host. The oscillator strength of these single bands varies with temperature, giving $\frac{f(300^{\circ}K)}{f(4.2^{\circ}K)}$ of 1.39 for $KMgF_3$:Co, 1.64 for MgF_2:Co and 1.94 for CaF_2:Co.

There are a number of energy terms that could possibly be of importance in contributing to the energy difference of the same transition among the three hosts, three of which will be considered here.

First, we would anticipate that the host that returns the most energy via the exciton term, $-\frac{e^2}{r}$, would show the lowest

energy absorption band. A crude estimate of this energy can be made by considering the transition metal - host metal distance R, and comparing $\frac{e^2}{R}$ value with the knowledge that $\frac{e^2}{r}$ = 109,737 cm^{-1} for r = .529 Å in the hydrogen atom. The values of $\frac{(109,737)\ (.529)}{R}$ and R for the three hosts are given in Table VI.

Table VI

Values of $-\frac{(109,737)\ (.529)}{R}$ for values of R (transition metal - host metal distance) appropriate for each fluoride host.

Host	R (Angstroms)	E (cm^{-1})
CaF_2	3.85	-15,020
MgF_2	3.58	-16,190
$KMgF_3$ (TM-K)	3.42	-16,920
$KMgF_3$ (TM-Mg)	3.97	-14,590

This exciton term indicates a maximum energy difference of only 1900 cm^{-1} in the extreme case.

Another consideration is lattice electron affinity, a measure of which is the F^- to host metal excitation energy, or crystal band

gap. A comparison of these three gives $KMgF_3$ lowest, CaF_2 higher, and MgF_2 highest in energy, however the maximum separation is approximately 7000 cm^{-1}.

A third factor is the crystal field splitting of the impurity ion. In the cubic CaF_2 lattice, we expect the transition metal ion levels to be inverted, and for the same interionic distance, acted upon by 8/9 of the strength of the octahedral crystal field. For completeness sake, the impurity fluoride distances are 2.36 Å for CaF_2, 1.98 Å for $KMgF_3$ and 1.99 Å for MgF_2.

The observed charge transfer energies in these cobalt doped hosts are CaF_2:Co lowest at 62,700 cm^{-1}, $KMgF_3$:Co at 63,800 cm^{-1}, and MgF_2:Co at 64,200 cm^{-1}, a maximum separation of only 1500 cm^{-1}. The three liquid helium temperature absorption bands are shown in Figure 4.

Obviously there are other energy terms in a many center excitation of this type, but it is rather interesting that the various terms balance out in the case of the cobalt impurity. A comparison of manganese impurity in $KMgF_3$ and MgF_2, and a comparison of the absorption spectra of iron in these two hosts again indicate that competing terms cancel to give similar transitions within several thousand reciprocal centimeters of each other. This fact

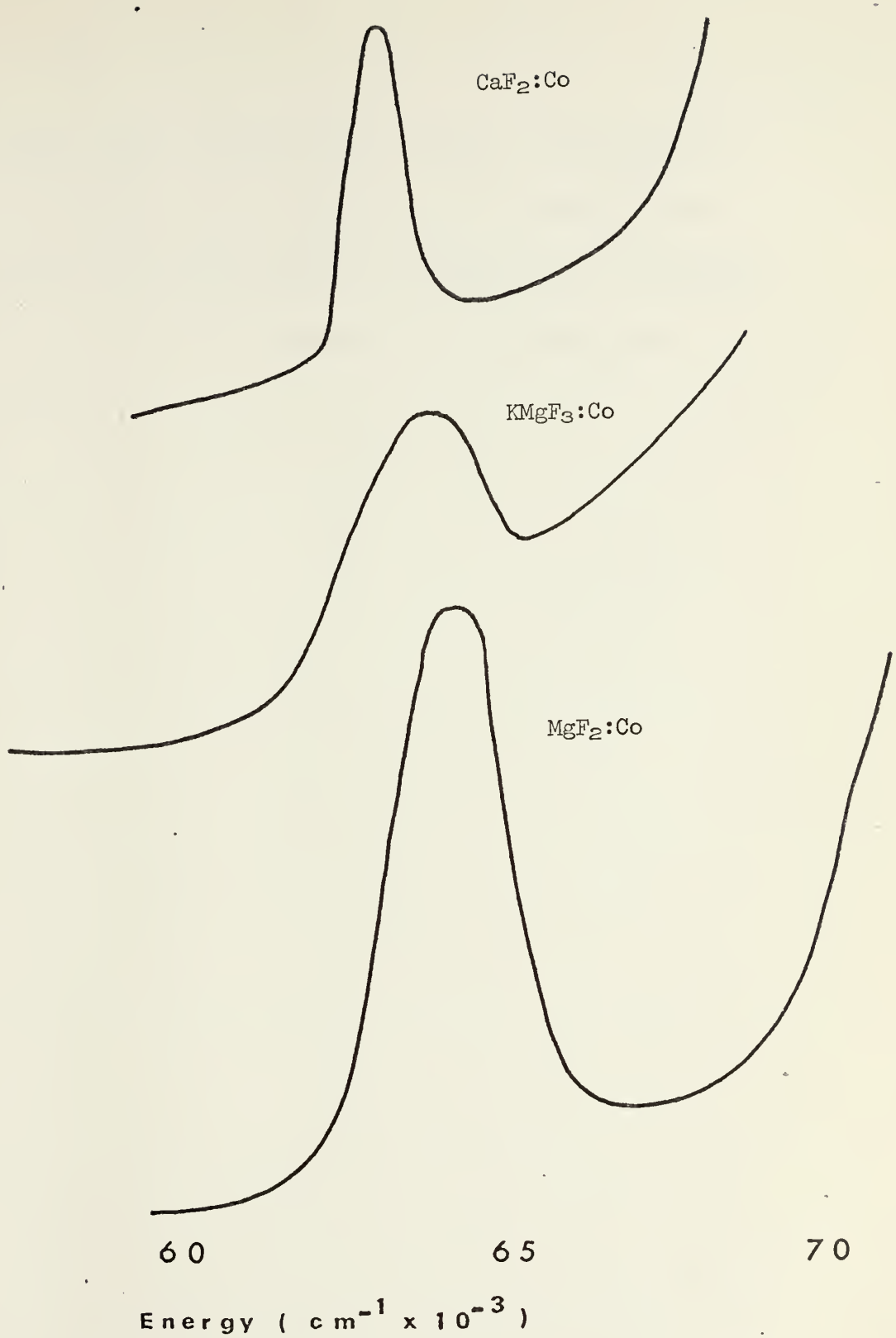

Figure 4. Energy comparison of three cobalt doped fluorides at 4.2°K.

could prove quite useful in a search for electronic transitions of impurity ions in similar hosts. For example, we might concentrate our efforts, in attempts to observe $Cr:MgF_2$, near the regions 36,000 cm^{-1} and 59,000 cm^{-1} which is where the $KMgF_3$:Cr transitions occur.

D. Miscellaneous

We noted in Chapter III that a visualization of the transferred electron as residing in a molecular orbital composed of nearest neighbor host metal ion s orbitals permits us to determine the symmetry of the electron wavefunctions, and that this would be useful in interpreting polarization data. Three of the systems that we have investigated have the potential for absorbing plane polarized light to a different extend along different crystallographic directions, and these three are MgF_2:Mn, MgF_2:Fe, and MgF_2:Co. However, the results of a polarized absorption experiment are that plane polarized light is absorbed equally with the electric vector parallel and perpendicular to the unique crystal direction.

The metal to metal charge transfer model adequately rationalizes this observed lack of polarization, and it does so by considering the nearly free electron wavefunction. In the D_{2h} symmetry appropriate to the MgF_2 lattice, the odd parity perturbing lattice vibrations span the A, B_1, and B_2 representations, the s orbital molecular orbitals span the A, B_1, B_2, and B_3 representations, and the dipole moment operators transform as B_3, B_2, and B_1 for the x, y, and z directions respectively. By obtaining the appropriate direct products among the ground state, final

state, dipole moment, and odd parity vibrations, it is determined that the totally symmetric representation occurs for each possible polarization direction.

The determination of direct products for the MgF_2:Co system is representative of the results for the other two impurity ion:MgF_2 systems and we will demonstrate the basics of that determination. The initial state is the Co^{+2} ion, whose lowest energy wavefunction transforms as the T_{1g} representation of the O_h symmetry group. Under the D_{2h} field of the MgF_2 lattice, this level becomes B_1, B_2, and B_3, neglecting the effects of spin orbit splitting which will be considered later.

The final state consists of the Co^{+3} ion, and including spin orbit effects, its levels are A, B_1, B_2, and B_3 in D_{2h} symmetry. The s type molecular orbitals are, as previously stated, of A, B_1, B_2, and B_3 symmetry also. By taking the direct product of any one spin orbit excited state with the ground state manifold and a lattice vibration, one obtains the B_1, B_2, and B_3 irreducible representations. Finally, the direct product of this result and each dipole moment operator (B_1, B_2 and B_3) is determined, and since $\Gamma_i \times \Gamma_i = \Gamma_1$ (A_1), we determine that the transition moment is predicted to have some finite value along

each of three orthogonal directions. By the inclusion of spin orbit effects in all states, we arrive at the same conclusion.

We will now consider why the transition moments, which we have indirectly measured along two directions, have the same value.

One explanation is that the observed absorption band corresponds to a summation of intensity of a large number of closely spaced energy levels. Since, as we have seen from group theoretical considerations, there are so many permitted transitions along each possible polarization direction, what we actually observe is little or no change in band intensity along each direction when we obtain an absorption spectrum using plane polarized light.

We submit that it is not unreasonable to expect that the energy levels of these charge transfer states will be quite closely spaced, and a brief listing of several interacting sources of these many levels will demonstrate the reasonableness of the line of thought. To begin with, Gladney[3] has reported that the maximum splitting of the twelve distinct energy levels of MgF_2:Co is only 1398 cm^{-1}, therefore several of these ground state levels will probably be populated at all times.

Secondly, the Co^{+3} excited state will itself be split into

fifteen spin orbit states of various symmetry. A third consideration is the result of the coulombic interaction between the nearly free electron and the remaining "hole", or Co^{+3} ion. Since the electron is shared by at least eight equivalent Mg ions in MgF_2, a description of this situation in terms of a Wannier exciton is probably accurate. If this is correct, the electron-hole energy levels can be described by a Rydberg equation, and these exciton states will be $A\frac{\mu}{n^2}$ units of energy below the lowest level of the conduction band. In this term, A is a constant dependent upon the crystal dielectric constant, μ is the electron hole reduced mass and n numbers the resultant levels. From this description we expect an infinite number of energy levels, one for each value of n. Finally, lattice vibrations generated by the electronic transition will interact with the many other levels described above, to give rise to an absorption band that represents the summation of a very large number of transitions along each possible polarization direction in the MgF_2 lattice. The result of a large number of vibronically allowed excitations will be no difference in absorption of plane polarized light in these charge transfer systmes.

Finally, we must comment upon an alternative intensity producing mechanism in these charge transfer systems. We have

previously predicted that, based upon d orbital-host ion s orbital overlap trends expected by a consideration of d orbital sizes, the absorption band oscillator strength will decrease along the first transition metal row in the periodic table. A scrutiny of Tables II and III of Chapter II show that this decrease is not observed. An examination of the crystal structures of these impurity doped fluoride systems indicates that a number of direct and indirect superexchange pathways exist. In the superexchange process, the electron transfer between metal ions occurs with the aid of the fluoride ion wavefunctions and this process might readily occur and even dominate the more conventional process that relies on metal-metal wavefunction overlap. This is obviously an area that should be investigated further.

E. Concluding Remarks

We have presented in this chapter a model that is unique in the brief history of the study of charge transfer transitions. In effect we are saying that the fluoride ion is so electronegative in nature that, in the case of wide band gap fluoride host materials doped with first row transition metal ions, a competing process, the transition metal to host metal ion transition actually occurs. It is not until we reach the nickel ion, with its extremely high value of ionization potential, that the fluoride to transition metal ion excitation becomes energetically more favorable.

Based on this model, we have presented explanations for charge transfer energies, oscillator strength temperature dependence, the number of absorption bands and their relative energies, the lack of polarization phenomena, absorption bandwidths, and absolute oscillator strengths. Much of the data interpretation in this work has been on a qualitative level, which is justified by the fact that so little data on similar systems are presently available. It is sincerely hoped that the success of our model in explaining the data of Chapter II and the limitations of our knowledge as evidenced by this work will in some way serve as an incentive for others to attempt to overcome the initial difficulties of data

collection in the vacuum ultraviolet spectral region. It is also hoped that within the next several years, the same originality and innovative experimental work that have characterized investigations of d-d orbital electronic transitions, will be directed toward the understanding of these charge transfer processes.

REFERENCES TO CHAPTER IV

1. P. Day and C.K. Jorgensen, J. Chem. Soc., 6226 (1964)

2. C.K. Jorgensen, Progr. Inorg. Chem. 12, 101 (1970)

3. H.M. Gladney, Phys. Rev. 1, 253 (1966)

ABSTRACT

The investigation of the electronic excitations of a number of first row transition metal ions as impurities in wide band gap fluoride host materials has been extended through the vacuum ultraviolet spectral region.

The technology associated with this work includes continuous mode rare gas light sources, a high resolution vacuum monochromator, photon counting detection, linear polarizers, and liquid helium temperature capabilities, all designed specifically for the vacuum ultraviolet region.

Broad, temperature dependent absorption bands of moderate intensity are observed in potassium magnesium fluoride doped with vanadium, chromium, manganese, iron, cobalt, and nickel, magnesium fluoride doped with manganese, iron, and cobalt, and calcium fluoride doped with manganese, iron, and cobalt. These bands are interpreted as arising from a transition metal orbital to host metal ion orbital electronic transition, a process that has not previously been observed in similar systems. The $KMgF_3$:Ni system is the only exception, its absorption spectrum resulting from the more conventional fluoride 2p to nickel 3d charge

transfer excitation.

Based on these models, explanations have been offered for spectral details such as bandwidths, oscillator strength temperature dependence, absolute oscillator strength, lack of polarization phenomena, number of bands, and relative band energy.

Thesis
S12 Sabatini
Near and vacuum ultra-
violet study of metal
donor and metal acceptor
charge transfer transi-
tions in transition metal
doped fluoride host mate-
rials.
146598